NASA CR 135151

(NASA-CR-135151) EVALUATION OF DIRECTIONALLY SOLIDIFIED EUTECTIC SUPERALLOYS FOR TURBINE BLADE APPLICATIONS Final Report (General Electric Co.) 107 p HC A06/MF A01 CSCL 11F G3/26

N79-16948

Unclas 14064

EVALUATION OF DIRECTIONALLY SOLIDIFIED EUTECTIC SUPERALLOYS FOR TURBINE BLADE APPLICATIONS

April 1978

GENERAL ELECTRIC COMPANY
Corporate Research and Development
Schenectady, New York 12301

Prepared for

NATIONAL AERONAUTICS AND SPACE ADMINISTRATION
Lewis Research Center
Cleveland, Ohio 44135

Contract No. NAS3-19711
Final Report

TABLE OF CONTENTS

TABLE OF CONTENTS (Cont'd)

LIST OF ILLUSTRATIONS

LIST OF ILLUSTRATIONS (Cont'd)

LIST OF ILLUSTRATIONS (Cont'd)

LIST OF TABLES

LIST OF TABLES (Cont'd)

1. SUMMARY

This program's objective was to identify at least one new, high temperature eutectic superalloy for potential use in jet engine turbine blades. The γ/γ'-Mo eutectic alloys satisfy this objective.

Thirty-two alloys were considered in six different eutectics systems:

1. γ/γ'-Mo (Ni-base, rods of αMo)
2. γ-β (Ni-base, lamellae or rods of (Ni, Fe/Co)Al)
3. α-β (α Cr, Fe, Ni-base, rods of (Ni, Fe)Al)
4. γ-M_2Ta (Ni-base, rods of M_2Ta)
5. Co MC (Co-base, rods of TaC)
6. γ/γ' (Ni-base, rods of Ni_3Al γ')

The six systems were evaluated in terms of microstructural control, tensile and rupture strength as a function of temperature, resistance to thermal cyclic degradation, and density. Based on these results, alloys from the γ/γ'-Mo, γ-β and γ-γ' systems were selected for more detailed evaluation.

The alloys from the three systems were subjected to longitudinal and transverse tensile and rupture tests over a temperature range of 750 °C to 1100 °C. Longitudinal shear strength was measured at several temperatures, and resistance to thermal cyclic degradation after prolonged exposure at 1150 °C was determined. Each of the alloys was further subjected to cyclic oxidation exposures at 750 °C and 1100 °C. To evaluate processability, the selected alloys were directionally solidified in an alumina shell mold for a turbine blade shape.

The three major conclusions of this study are:

1. The γ/γ'-Mo system has potential as a high-pressure turbine blade material. Research on this system should continue and should expand from the exploratory nature of this contract to encompass serious alloy development and engineering evaluation.

2. The γ-β system has potential as a vane material. Research on this system should address the critical question of thermal fatique resistance.

3. The γ-γ' system shows promise for developing into a potential turbine blade material. Exploratory research to evaluate that potential should continue.

2. INTRODUCTION

Advancement in turbine blade materials technology has been fundamental to the evolution of the jet engine for its entire history. The desire for improved turbine blade materials has been continuous, and the result has been an increase in metal capability of about 15 °F per year. Since the early 1950's this growth in capability has depended on improvements of gamma prime strengthened nickel superalloys. These in turn required the development of the vacuum melting process to achieve control and consistency of increasingly complex alloy compositions. Significant improvements in conventional, vacuum-cast superalloys beyond René 120 is considered unlikely. It is apparent that another major innovation is needed. The innovation discussed here is directional microstructures achieved by directional solidification.

Directional Solidification (DS) of superalloys provides three important advantages over conventional, randomly oriented microstructures:

- Virtual elimination of strength-limiting grain boundaries perpendicular to the solidification direction, which in turbine blades is also the major stress axis. This enhances rupture strength.
- A substantial reduction in elastic modulus in the growth direction, which greatly reduces stresses generated by thermal gradients and thus increases resistance to thermal fatigue.
- A large increase in ductility in the growth direction which allows the addition of substantially greater amounts of alloying elements for strength improvement, while still maintaining adequate ductility.

Turbine blades and vanes in the hotter sections of the modern jet engine are subjected to gas stream temperatures above the melting point of the metal and far above the temperature where strength is limiting. The problem is solved by cooling blades and vanes with air bled from the compressor. The first turbine stage aft of the combustor is the worst case, because it requires the greatest amount of cooling air. The later stages experience cooler gas temperatures because work is extracted from the cycle upstream and, depending on the design, require either reduced amounts or no cooling air. An improved, higher temperature turbine blade alloy can be used either to reduce the amount of cooling air or to increase the turbine inlet gas temperature, or a combination of both.

Many laboratories are seeking to improve turbine blade materials through various approaches, including: synthesized composites using strong filamentary reinforcements, directional eutectics (in situ composites), and ceramics. Of these, the most promising candidates for the next generation of blade alloys are judged to be the directional eutectics. The goals for this program on new eutectic systems are:

1. Longitudinal tensile strength at 750 °C of 1050 MN/m² (150, 000 psi) and at 1100 °C of 700 MN/m² (100, 000 psi).
2. Elongation of at least 5% in longitudinal tensile tests at all temperatures.
3. A 1000 hour longitudinal rupture life at 750 °C under 700 MN/m² (100, 000 psi) stress and at 1100 °C under 140 MN/m² (20, 000 psi) stress.
4. Ability to withstand 500 hours (@ 1 cycle/hr) of cycling between 425 °C, or less, and 1150 °C with less than 10% decrease in stress rupture resistance.
5. Longitudinal shear strength of not less than 35% of the longitudinal tensile strength.
6. Oxidation resistance equal to that of Hastelloy X at 750 °C and 1100 °C.
7. Aligned structure when solidified at a rate of 20 mm/hr or greater for a thermal gradient of 100 °C/cm or less with a 12.5 mm diameter bar.
8. A melting point of not less than 1250 °C.
9. A density of not over 9.15 g/cm³ (0.330 lb/in³).
10. A transverse tensile elongation of >1% at room temperature.

These goals are extremely challenging for new systems and, thus, must be treated as goals, not as a measure of success or failure in a program of limited time and resources.

This program's objective was to produce at least one new directionally solidified eutectic alloy for potential use in jet aircraft engine turbine blades. The property goals for this alloy were superior to those of directionally solidified eutectic alloys currently undergoing extensive study for potential use in engines. This program consisted of two portions, alloy development and detailed evaluation. The first portion consisted of development of six eutectic alloy system bases, each having at least one ductile phase. Composition and/or processing parameter variations were made for each system base. Alloys achieving well aligned structure were tested for high temperature tensile strength, stress rupture resistance, and thermal cycling resistance.

The systems studied follow below:

1) The γ/γ' -Mo System (M. F. Henry)

This system consists of a matrix of γ/γ', primarily of Ni and Al, and body centered cubic fibers, primarily of Mo. The primary reasons for

studying this system were the ductility of both phases, low density, high temperature strength, and ease of processing. Two primary methods of altering properties in the γ/γ' -Mo system would appear fruitful: alloying of the matrix and alloying of the Mo fibers. Elements like Ta and Ti, which are good γ' formers, also have total solid solubility in Mo at 1300 °C. Chromium, which also forms a continuous series of solid solutions with Mo, might give enhanced fiber volume fraction and oxidation resistance. Additions of rhenium would be expected to partition both to the γ and to Mo and could enhance fiber ductility.

2) The γ-β System (M. R. Jackson)

This system consists of γ, a face centered cubic solid solution of Ni, Cr, Fe, and Al, and, β, a CsCl structured substoichiometric (Ni, Fe) Al. The primary reasons for studying this system were its expected oxidation/hot corrosion resistance, low density, low cost melt stock, high probability of alloying for strengthening, and ease of processing. Several methods of altering properties are possible for γ-β eutectics. For Fe-rich γ matrices, conventional Fe-base superalloy metallurgy can be used to strengthen the eutectic. For Ni-rich matrices, elements favoring γ' can be added. For either case, certain elements are potent β strengtheners. Alloys based on Ni, Co, Al and W γ-β composites also are considered.

3) The γ-γ' System (M. R. Jackson)

This system consists of γ, an austenitic matrix of Ni, Co, Re, W and V, and fibers of γ', an ordered $L1_2$ phase based on Ni_3Al but which substitutes Ta for some Al. The primary reasons for studying this system were a high probability of alloying for strengthening, large volume fraction of the second phase, and high temperature phase stability.

4) The γ-M_2Ta System (M. R. Jackson)

The system consists of an austenitic γ matrix of Ni, Fe, Cr and Ta, and a hexagonal intermetallic M_2Ta phase, with Cr, Fe and Ni "M" sites. The primary reasons for studying this system are its expected oxidation resistance, a high probability of alloying for strengthening, high temperature phase stability, and large volume fraction of the second phase.

5) The Co-MC System (J. L. Walter)

The eutectic system consists of an fcc cobalt base alloy matrix with dispersed fibers of fcc TaC. These alloys are of interest because they have relatively good resistance to oxidation and, when directionally solidified, have strengths at high temperatures in excess of any cobalt or nickel base superalloy. It has been shown that the use of a high temperature solution treatment, followed by a precipitation treatment, increases stress

rupture life. The alloy to be so treated was one containing 20wt% W, 10wt% Ni, 20wt% TaC, and balance cobalt, the strongest of all of the cobalt base-TaC eutectic alloys when directionally solidified at rates of 2 cm/hr or higher. The microstructure of the alloy consists of about 10% by volume of TaC single crystal fibers in the cobalt alloy matrix.

6) The α-β System (J. L. Walter)

The DS eutectic NiAl-Cr consists of Cr rods or fibers in a matrix of NiAl. While the NiAl imparts excellent resistance to oxidation and corrosion, it lacks ductility at room temperature. The chromium phase, on the other hand, is quite ductile since the fibers are of the order of 2 μm in diameter. It was discovered that the replacement of 5 atom % Cr by an equal amount of Fe caused the eutectic to "turn inside out"; i.e., the CrFe phase became the matrix and the NiAl phase became the dispersed rod phase. The ductile CrFe alloy matrix should provide both improved ductility at room temperature and greater strength at elevated temperatures. The latter occurs because the CrFe alloy is stronger than NiAl at elevated temperatures.

The second portion of the program consisted of detailed evaluation of the three most promising alloys developed. Properties evaluated were longitudinal and transverse tensile strength and ductility, stress rupture resistance before and after exposure to high temperature thermal cycling, longitudinal shear strength, cyclic oxidation resistance, and reactivity of the molten alloy with an appropriate shell mold material. The completion of this phase included a ranking of all the systems studied and a comparison of the best alloys to other eutectic alloys and superalloys.

3. MATERIALS AND PROCEDURES

3.1 Melting

For this initial research on new eutectics, starting materials were of reasonably high purity. Typical material purities were:

Element	Maximum Total Impurities %	Major Non-Volatile Impurity
Al	0.01	60 ppm Si
C	0.002	5 ppm Al, Si, Cu
Co	0.06	0.036% Ni
Cr	0.5	0.35% Fe
Fe	0.06	40 ppm Cu
Mo	0.3	0.01% Fe
Ni	0.02	0.01% C
Re	0.02	100 ppm W
Ta	0.02	40 ppm W
Ti	0.3	0.03% Fe
W	0.5	0.05% Mo, Si

Raw metal charges were melted in alumina crucibles in an argon atmosphere, using a motor-generator induction heater at approximately 10 kHz. Elements such as Al and C were added after initial melting. Melts were superheated about 300 °C, cooled to measure a thermal arrest temperature, remelted, and then poured into copper chill molds.

3.2 Directional Solidification

Directional solidification was performed in modified Bridgman furnaces. The smaller ingots were directionally solidified by in situ melting 2 cm diameter melt stock in 2 cm diameter recrystallized Al_2O_3 crucibles in an argon atmosphere. The furnace had a graphite susceptor which was inductively heated by a radio frequency (approximately 450 kHz) induction power supply. The ingot sat on a water-cooled copper side chill during directional solidification. The smaller 2 cm diameter ingots were generally 9 to 11 cm long.

The larger ingots were produced by melting the alloy master melt in an upper melting chamber with a motor-generator set and then pouring the molten charge into 4 cm diameter, recrystallized Al_2O_3 crucibles. The

source in this apparatus was a resistance-heated, wire-wound furnace tube. Turbine blade shapes were directionally solidified in this same apparatus.

3.3 Structure Evaluation

Initial evaluation of structure of directionally solidified ingots was performed by grinding a longitudinal flat along the entire length of the ingot and polishing it to a metallographic finish for microscopic examination. Ingots were then documented for lengths of chill cast structure, hyper- or hypo-eutectic structure, aligned structure, and/or cellular structure. From this evaluation the ingot was scheduled for machining into test specimens, or a modification was performed on chemistry or solidification rate.

3.4 Density Determination

Densities were determined on coupons from the aligned sections of directionally solidified ingots. The density was calculated from weights of coupons in air and in glycol.

3.5 Tensile Tests

Figure 3-1 shows the specimen design used for longitudinal and transverse tensile tests. The specimens were tested in split grips in a screw-driven Instron tensile machine. The specimens were tested either in air or in a capsule at an approximate pressure vacuum level of 5 μm as designated. The crosshead rate used was 0.05 cm/min. The effective gage length was taken as 1.14 cm, yielding a plastic strain rate of 0.045 min^{-1}. Load versus time was recorded.

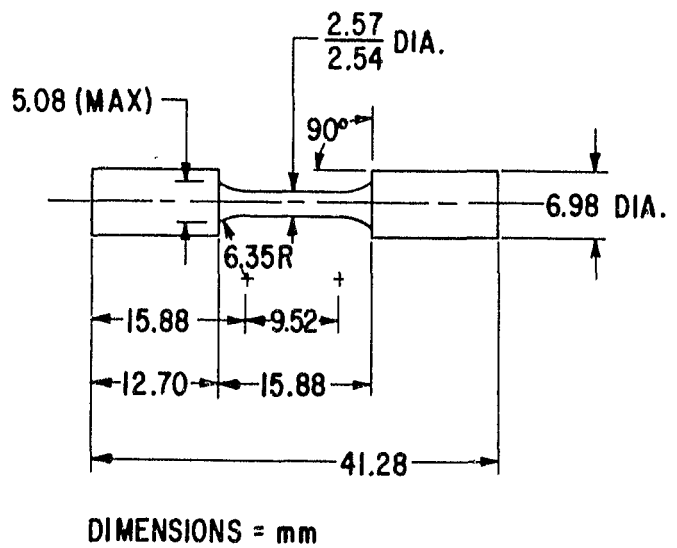

Figure 3-1. Specimen Used for Tensile and Creep Rupture Tests

3.6 Longitudinal Shear Tests

For longitudinal shear strength, a specimen was designed with a shear area equal to the minimum area perpendicular to the principal stress. Figure 3-2 shows the specimen design, which consists of a uniform section of diameter 0.41 cm and one button head of length 0.10 cm. The shear area is then (π) (0.41) (0.10) or approximately 0.13 cm^2. The specimens were tested in split grips at a crosshead rate of 0.05 cm/min and load versus time was recorded.

This test, while not an academically pure shear test, was a good evaluation of in-service loading conditions.

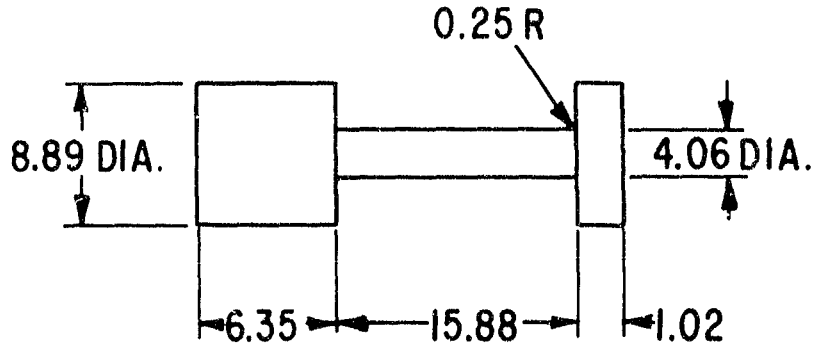

Figure 3-2. Specimen Used for Longitudinal Shear Tests

3.7 Stress Rupture Tests

The specimen design used for longitudinal and transverse stress rupture tests was the same as that used for tensile tests (Figure 3-1). Tests were run as constant load tests in air or 5 psig argon, as designated.

3.8 Thermal Cycling

Specimen blanks 0.7 cm in diameter by 4.4 cm long were used for thermal cycling. The specimen blanks were cycled bare or sealed within an evacuated quartz tube in a static air, resistance-wound furnace tube. The thermal cycle consisted of a one hour period, with 50 minutes in the furnace and 10 minutes outside the furnace which was automated for continuous operation. A thermocouple recorded temperature on a strip chart recorder. The specimens cooled to approximately 200 °C and spent approximately 40 minutes at the furnace temperature of 1150 °C during each cycle. A thermocouple and a continuously monitoring proportional controller maintained furnace temperature.

After thermal cycling, a short piece was cut off the end of each blank for metallographic examination. The remainder was machined into a stress rupture specimen.

3.9 Cyclic Oxidation

The apparatus and cycle used for the static air cyclic oxidation tests were the same as those used for the thermal cycling. Test specimens were 0.25 cm in diameter by 4.13 cm long. Maximum temperatures of 1100 and 750 °C were used as designated. Periodic weight change measurements were made.

3.10 Mold/Metal Reactivity

A mold/metal reactivity test evaluated the reactivity of a candidate shell mold material for directional solidification of turbine blades. Because eutectics are cast at maximum melt temperatures in excess of those currently in use for conventional superalloys, it was decided to use an Al_2O_3 shell mold with a SiO_2 base binder. The molds consisted of inner layers of fine flour coats and several outer layers of a heavier Al_2O_3 sand. The blade castings were grown with a superheat of approximately 250 °C in a Bridgman apparatus having an upper pouring chamber.

4. THE γ/γ'-Mo SYSTEM (M.F. HENRY)

4.1 Background

This system base consists of an ordered face centered cubic alloy of a (Ni, Al) matrix of γ/γ' and a body centered cubic Mo reinforcing phase. The primary reasons for studying this system are the ductility of both phases, low density, high temperature strength, and ease of processing.

There is a eutectic in the Ni-Al system at 24.4 a/o Al and 1385 °C[1] and a eutectic in the Ni-Mo system at 35 a/o Mo and 1315 °C.[1] The presence of the high congruent point of NiAl at 1638 °C and the high melting point of Mo at 2610 °C means there must be a liquidus isotherm in the Ni-Al-Mo system at 1315 °C which winds its way from the Ni-Mo eutectic to the Ni-Al line at about 70 a/o Al. The ternary Ni-Al-Mo diagram at 1175 °C[2] shows a two-phase solid state region γ'+Mo. This suggests the presence of a γ'-Mo eutectic where the low melting trough crosses over the γ'+Mo regime. Such a eutectic has been reported[3, 4] at Ni-17.6 a/o Al-16.7 a/o Mo. Work at the General Electric Corporate Research and Development Center has revealed a very flat thermal arrest in the cooling curve at Ni-17.68 a/o Al-16.30 a/o Mo at 1302 °C. At the eutectic temperature, there is about 1.1 a/o solubility of Ni in Mo, and about 6.5 a/o solubility of Al in Mo.[1]

Literature on the reported γ'-Mo eutectic was very limited. Thompson and Lemkey[4], in a table, report a Ni_3Al-Mo eutectic with 26 v/o fibers, a melting point of 1306 °C, a density of 8.18 g/cm^3, a Young's Modulus of 138 GN/m^2 (19.7 x 10^6 psi), and room temperature tensile properties of 1120 MN/m^2 (160 ksi) ultimate strength with 21% elongation. The composition reported by Ashbrook[3] was Ni-8 w/o Al-27 w/o Mo.

Prior to this contract the General Electric Research and Development Center performed a considerable amount of study on the γ/γ'-Mo system. Two alloys had received mechanical testing. The alloys are designated AG8 and AG15 and their compositions are:

	Atom Percents			Weight Percents		
Alloy	Ni	Al	Mo	Ni	Al	Mo
AG8	65.7	17.6	16.7	65.0	8.0	27.0
AG15	66.0	17.7	16.3	65.5	8.1	26.4

The AG8 appears to be very close to a pure γ' matrix in the as-DS'ed state while the AG15 contains a low volume fraction of γ in the matrix. The AG8 was grown at 2.5 and 5.1 cm/hr and the AG15 was grown at 2.5 and 15.2 cm/hr. The ingots were approximately 2.2 cm in diameter and 10 cm in length and were grown in a thermal gradient of 70-80 °C/cm. The AG8 was

aligned at 2.5 cm/hr and incipient cellular at 5.1 cm/hr. AG15 was aligned at 2.5 cm/hr and cellular at 15.2 cm/hr. The density of AG8 was measured at 8.26 g/cm^3 and an electronic gating technique on the SEM gave a fiber volume fraction of 0.19.

The values of room temperature ultimate strength were significantly higher than that reported by Thompson and Lemkey.[4] The reasons are not clear, but possible explanations could be the degree of alignment or the level of impurities. Also, Thompson and Lemkey do not report a solidification rate. The hot tensile tests were quite encouraging. The strengths were below the goals set for this contract effort, but the strengths and ductilities were respectable for a simple three element system.

These two alloys were also stress rupture tested in argon, and results were considered very promising for a simple three element system. They provided hope that alloying additions could bring this system up to the stress rupture goal.

During the course of this contract, a separate General Electric study on Ni-Al-Mo phase diagram[5] determined that all the alloys studied here were γ-Mo eutectics. Lemkey[6] had reported that above 5 w/o Al, the alloys were γ'-Mo eutectics which subsequently precipitated γ. This study[5] shows that even at 8 w/o Al, which yields a fully γ' matrix at room temperature, that the alloy froze as a γ-Mo eutectic and precipitated γ'. Reference 5 shows the work in detail.

4.2 Alloys

The alloys studied on this contract cover a range of 10.0 to 17.7 atom percent aluminum and include a preliminary study of the effects of Ta, Ti, and Re as fourth element additions. Table 4-1 lists the compositions examined as atomic percents, and Table 4-2, as weight percents. The compositions are listed in the order that they were examined.

An ingot of each alloy was directionally solidified as a 2.2 cm diameter bar at 2 cm/hr using a thermal gradient of approximately 100 °C/cm. The ingots were examined for microstructure by grinding a longitudinal flat the entire length of the bar. This flat was then metallographically polished and examined microscopically. If a given composition resulted in 5 cm of aligned structure at 2 cm/hr, a second bar was grown at 2 cm/hr and the alloy was scheduled for mechanical testing. If an alloy did not yield aligned structure at 2 cm/hr, a second bar was grown at 0.64 cm/hr and that bar was scheduled for mechanical testing. Table 4-3 gives the metallographic results and densities.

Table 4-1

Melt Compositions in the γ/γ'-Mo System

Atomic Percents

Alloy	Ni	Al	Mo	Ta	Ti	Re
1	66.0	17.7	16.3	--	--	--
2	65.6	14.4	20.0	--	--	--
3	65.3	11.7	20.0	3.0	--	--
4	64.8	16.2	16.0	--	3.0	--
5	66.8	16.7	16.0	--	--	0.5
6	64.0	15.8	20.2	--	--	--
7	65.8	13.2	21.0	--	--	--
8	67.2	11.8	19.0	--	3.0	--
9	65.5	10.0	24.5	--	--	--

Table 4-2

Melt Compositions in the γ/γ'-Mo System

Weight Percents

Alloy	Ni	Al	Mo	Ta	Ti	Re
1	65.5	8.1	26.4	--	--	--
2	62.5	6.3	31.2	--	--	--
3	58.0	4.8	29.0	8.2	--	--
4	64.3	7.4	25.9	--	2.4	--
5	65.3	7.5	25.6	--	--	1.6
6	61.4	6.9	31.7	--	--	--
7	62.0	5.7	32.3	--	--	--
8	67.3	5.2	28.2	--	2.3	--
9	59.4	4.2	36.4	--	--	--

Table 4-3

Characterization of Directionally Solidified γ/γ'-Mo Ingots

Alloy	DS Rate (cm/hr)	Length of Aligned Structure (cm)	Density (g/cm^3)
1	2	8.9	--
1	2	8.2	8.34
2	2	7.4	--
2	2	8.2	8.56
3	2	0	--
3	0.64	9.4	9.09
4	2	0	--
4	0.64	8.1	8.20
4	0.64	5.7	--
5	2	0.9	--
5	0.64	6.5	8.40
6	2	5.9	--
6	0.64	7.5	8.42
7	2	8.9	--
7	2	8.7	8.65
8	2	0	--
8	0.64	8.0	8.57
9	2	0.9	--
9	0.64	6.1	8.93

There were three exceptions to this procedure. On examination of its longitudinal stripe alloy 6 appeared to be incipient cellular, so a second bar was grown at 0.64 cm/hr and both rates were scheduled for mechanical testing. Detailed transverse metallography of the 2 cm/hr bar of alloy 6 later classified the bar as aligned. Alloy 8, grown at 2 cm/hr, was cellular and the second bar was grown at 0.64 cm/hr. Both rates were mechanically tested, specifically to evaluate the effect of this degree of cellularity on mechanical properties. Electro-discharge-machining (EDM) of the first 0.64 cm/hr ingot of alloy 4 revealed numerous casting defects in the form of "folds" and/or "laps" extending into the interior of the ingot. After the stress rupture specimens gave unexpectedly short lives, a second ingot was grown at 0.64 cm/hr. Examination after EDM revealed a high density of "folds" or "laps" in this ingot also. It appears that 3 a/o Ti added to Ni-Al-Mo of such a high Al content (16.2 a/o) will not be very castable. Alloy 8 with 3 a/o Ti and only 11.8 a/o Al did not display the same problem.

Figure 4-1 shows the structure of alloy 1. The matrix has been deep etched to reveal the morphology of the Mo reinforcing fibers. The fibers are predominantly square, with a side dimension of 0.5 to 8.0 μm when grown at 2 cm/hr. As the Al content is lowered in the three element Ni-Al-Mo system, the amount of γ' precipitate decreases.

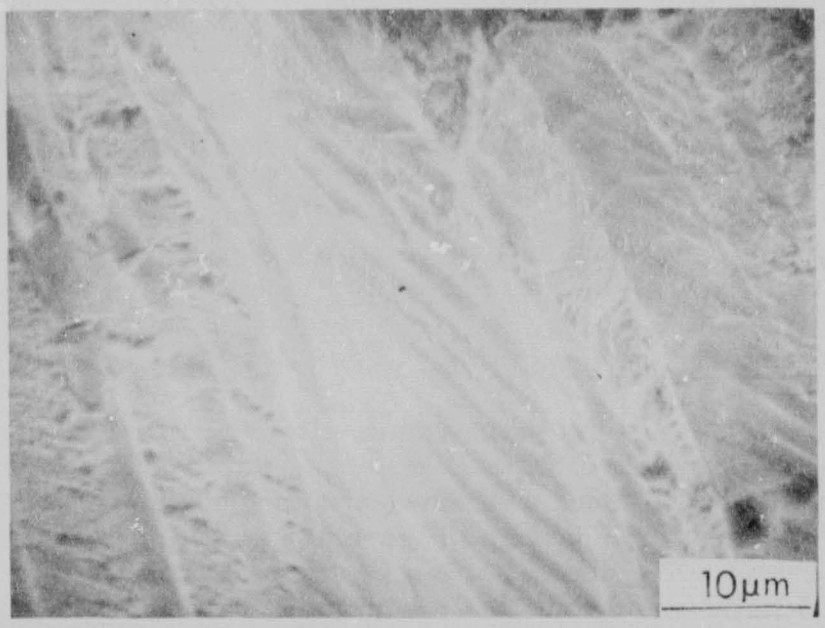

Figure 4-1. Scanning Electron Micrograph of a Transverse Section of Deep Etched Alloy 1 (γ/γ'-Mo)

A transverse section of alloy 1 grown at 2 cm/hr was thinned and examined in transmission electron microscopy (TEM). Electron diffraction was performed to determine crystallographic orientations. The Mo-fibers and γ' matrix both have a <100> growth direction. The square sides of the Mo-fibers are (110) planes and mate with (100) planes in the γ' matrix.

Electron diffraction of alloy 2 also clearly revealed the presence of diffracting planes with a spacing 3.9 Å. Dark field pictures on that spot show those planes to be present in a precipitate phase within the gamma. A search of the x-ray card files and the ternary phase diagram has identified that phase as Ni_4Mo. Re-examination of alloy 1 diffraction patterns also revealed a spot at 3.9 Å, thus the Ni_4Mo is also present in that alloy.

4.3 Tensile Properties

Table 4-4 presents the initial tensile data gathered on 2.2 cm diameter ingots of the nine γ/γ'-Mo alloys studied here. Ultimate tensile strengths at 750 and 1100 °C are plotted versus atomic percent aluminum in Figure 4-2 for the 3 element alloys. For optimum tensile strength in the Ni-Al-Mo system, Figure 4-2 shows that an alloy should have 13-14 a/o Al. The strengths for the Ta, Re, and Ti additions fall in the same regime, except for alloy 4 which had "folds" and/or "laps."

Alloy 7 (at 13.2 a/o Al) grown at 2 cm/hr was selected for a more detailed mechanical property evaluation than the screening tests used for the other 8 γ/γ'-Mo alloys. Table 4-5 presents all the tensile results for alloy 7, and Figure 4-3 plots the ultimate strengths. The transverse strength is above 60% of the longitudinal from 100 to 1100 °C and above 70% from 400 to 1050 °C. The longitudinal ductility of alloy 7 is in excess of 15% at all temperatures and is above 2.5% in transverse ductility for the 3 temperatures measured. Alloy 7 meets the ductility goals of this program.

4.4 Longitudinal Shear Strength

Longitudinal shear tests were run on alloy 7 grown at 2 cm/hr at room temperature, 750 and 1100 °C. All the shear failures were along the gauge section as designed. Figure 4-4 shows a macrograph of a failed 750 °C specimen, Table 4-6 gives the data and Figure 4-5 plots it. The original goal for this program was a longitudinal shear strength of not less than 35% of the longitudinal tensile strength. The preliminary data show this ratio to be greater than 35% for the temperature range of 300 to 1100 °C. For 650 °C, which is a typical critical dovetail temperature, the ratio is approximately 52%.

4.5 Stress Rupture Resistance

Table 4-7 presents the initial stress rupture data gathered on 2.2 cm diameter ingots of the nine γ/γ'-Mo ingots studied here. The table shows

Table 4-4

Tensile Data on γ/γ'-Mo Alloys

Alloy	DS Rate (cm/hr)	Temp. (°C)	0.2% Y.S. (MN/m^2)	U.T.S. (MN/m^2)	% Elong.	% R.A.
1	2	25	652	1311	17	16
		750	982	1048	17	33
		1100	429	434	66	88
		1100	414	424	34	55
2	2	750	998	1084	19	32
		1100	539	544	49	80
		1100	504	517	60	83
3	0.64	750	772	934	46	42
		1100	338	347	34	44
4	0.64	750	645	855	42	51
		1100	260	261	41	38
5	0.64	750	834	862	17	41
		1100	410	410	59	55
6	2	750	1007	1055	17	39
	2	1100	485	485	70	66
	0.64	750	924	979	17	49
	0.64	1100	383	383	85	74
7	2	750	965	1103	18	32
		1100	449	457	40	87
		1100	432	441	41	87
8	2	750	979	1062	29	47
	2	1100	368	385	36	47
	0.64	750	934	1041	19	32
	0.64	1100	410	419	58	96
9	0.64	750	848	1027	25	34
	0.64	1100	236	268	39	94

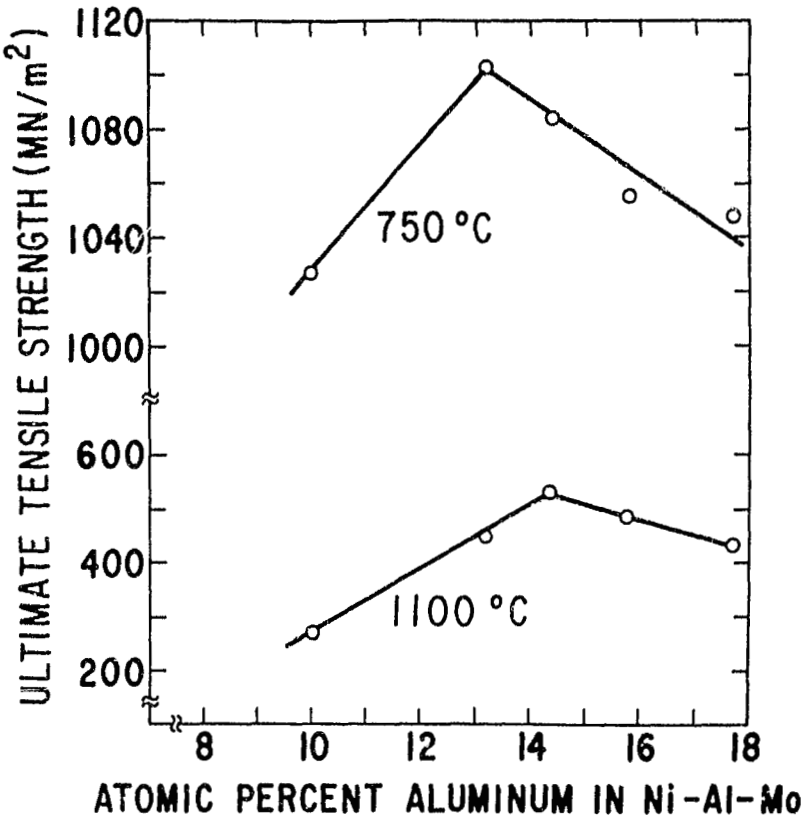

Figure 4-2. Ultimate Tensile Strength Versus Atomic Percent Aluminum for Three-Element γ/γ'-Mo Eutectics

why alloy 7 was selected for detailed property evaluation on this contract. Alloy 7 had the best balance of critical gradient to rate ratio and 750 and 1100 °C stress rupture resistance.

Figure 4-6 displays stress rupture resistance for the three element alloys as a function of aluminum content. As with the tensile strengths discussed in Section 4.3, stress rupture resistance is maximized for the three element system in the vicinity of 15 a/o Al.

Alloy 8 (11.8 a/o Al with 3.0 a/o Ti) was grown and tested at two rates in the initial property evaluation to evaluate the effect of cellular material. The microstructure of alloy 8 grown at 2 cm/hr is considered to be severely cellular. The stress rupture comparison is as follows (from Table 4-7):

Temp. (°C)	Stress (MN/m^2)	Time to Failure (hr)	
		Cellular (2 cm/hr)	Aligned (0.64 cm/hr)
750	700	124.4	104.5
1100	110	42.6	256.2

Table 4-5

Tensile Results on Alloy 7 (γ/γ'-Mo) Solidified at 2 cm/hr

Temp. (°C)	0.2% Y.S. (MN/m^2)	U.T.S. (MN/m^2)	% Elong.	% R.A.
		Longitudinal		
25	814	1593	18	20
25	821	1600	18	17
550	903	1214	20	22
750	965	1103	18	32
750	986	1110	15	27
750	972	1083	18	34
850	1020	1020	22	47
900	883	889	26	59
1000	605	634	34	64
1100	449	457	40	87
1100	432	441	41	87
		Transverse		
25	772	917	2.8	4.7
750	889	924	5.4	17
1100	266	281	61	[illegible]

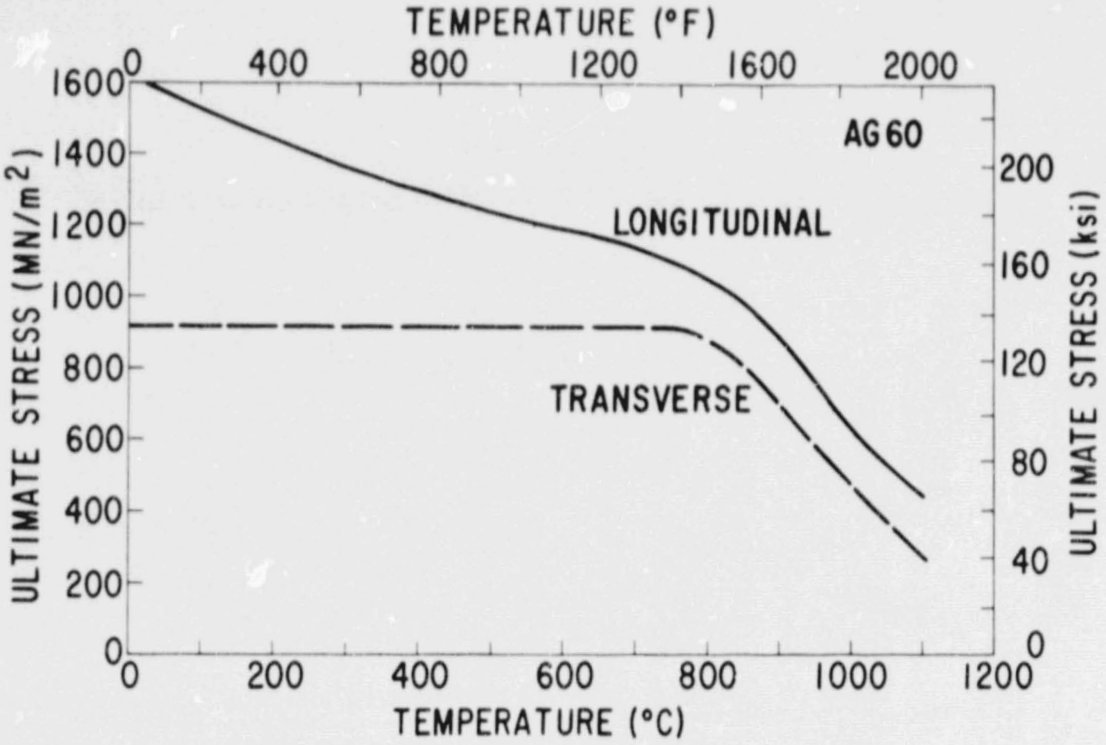

Figure 4-3. Transverse and Longitudinal Ultimate Tensile Stress Versus Temperature for Alloy 7 (γ/γ'-Mo)

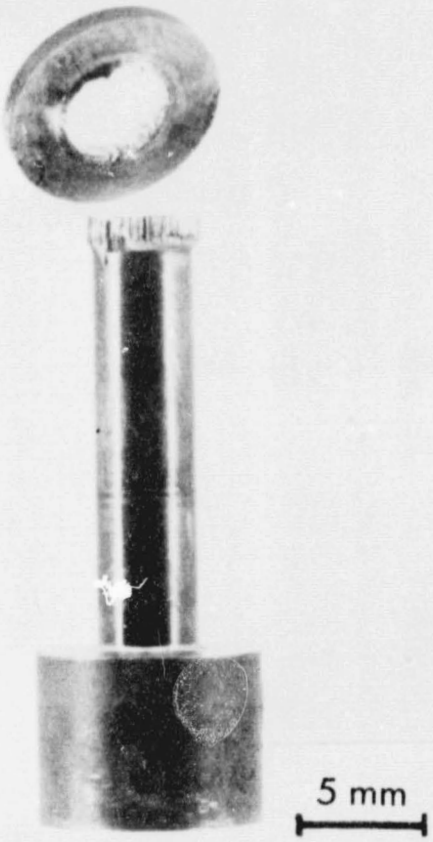

Figure 4-4. Macrograph of γ/γ'-Mo Longitudinal Shear Specimen Tested at 750 °C

Table 4-6

Longitudinal Shear Strength of γ-γ'-Mo

Alloy 7 at 2 cm/hr

Temp. (°C)	Long. Shear Strength (MN/m^2)
25	350
75[illegible]	618
1100	193

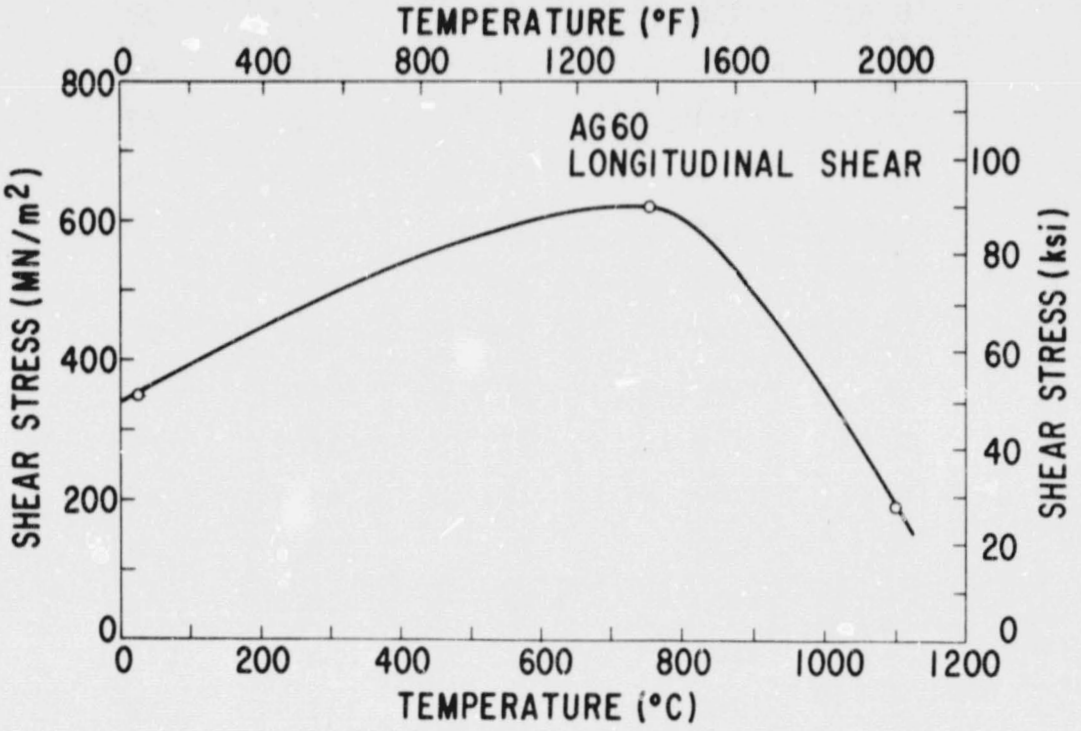

Figure 4-5. Longitudinal Shear Stress Versus Temperature for Alloy 7 (γ/γ'-Mo)

Table 4-7

Stress Rupture Data on γ/γ'-Mo Alloys

Alloy	DS Rate (cm/hr)	Temp. (°C)	Stress (MN/m^2)	Time to Failure (hr)	% Elong.	% R.A.
1	2	1100	83	375.4	44	92
	2	1100	110	128.2	39	88
2	2	750	700	116.9	32	42
		1100	125	64.3	20	79
		1100	110	157.3	24	74
3	0.64	750	700	46.6	9	19
	0.64	1100	110	56.0	19	37
4	0.64	750	700	1.0	43	66
		1100	110	11.0	40	85
		750	700	1.0	27	30
		1100	110	30.5	34	80
5	0.64	750	700	17.4	30	75
	0.64	1100	110	80.7	41	90
6	2	750	700	50.2	21	28
	2	1100	110	132.9	32	82
	0.64	750	700	16.8	20	17
	0.64	1100	110	54.7	44	82
7	2	750	700	510.0	24	42
		1100	110	178.3	14	27
		1100	110	155.3	17	65
8	2	750	700	124.4	18	36
	2	1100	110	42.6	10	21
	0.64	750	700	104.5	12	24
	0.64	1100	110	256.2	36	80
9	0.64	750	700	267.0	12	15
	0.64	1100	110	41.9	14	64

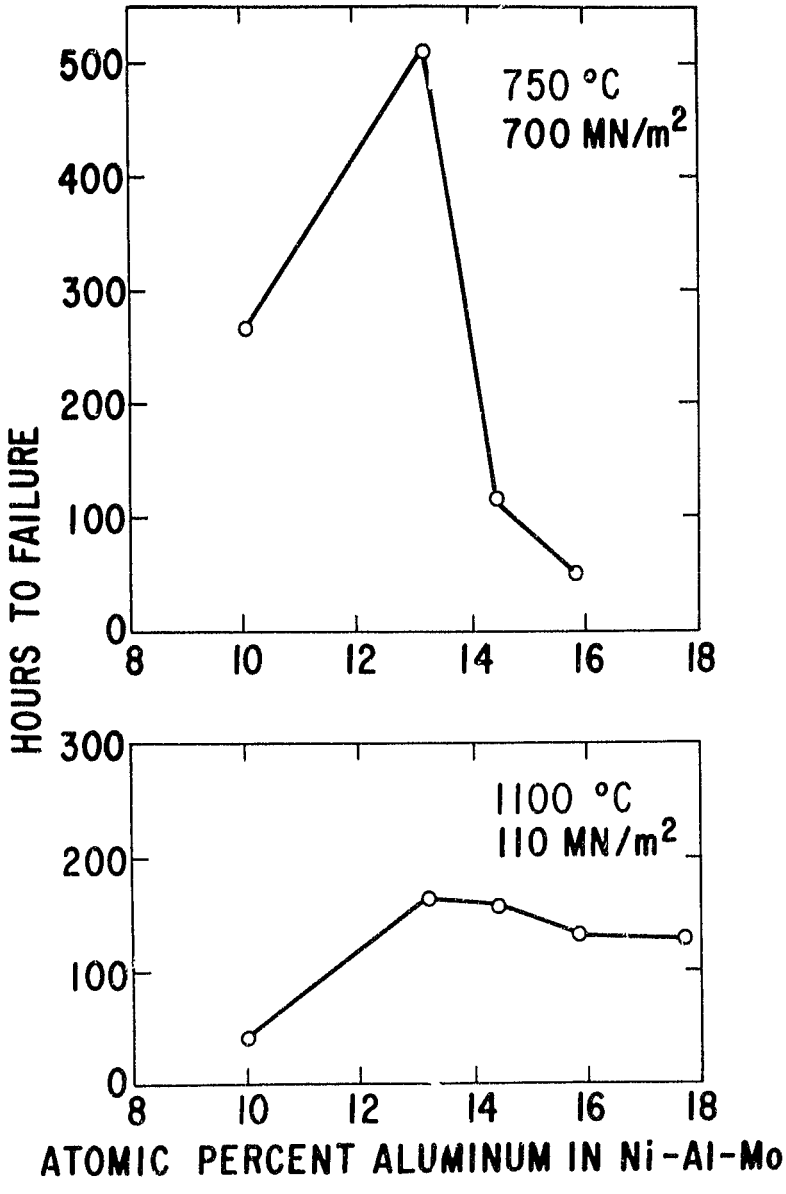

Figure 4-6. Hours to Failure in Stress Rupture Versus Atomic Percent Aluminum for Three-Element γ/γ'-Mo Eutectics

The cellular material is seen to be much less creep resistant at 1100 °C and about the same as aligned material at 750 °C.

Alloy 7 (at 13.2 a/o Al was selected for more detailed tests. Table 4-8 gives the results. Note that for the condition where four tests were run (1100 °C and 110 MN/m^2), the scatter about the mean life is only ±15% or ±0.15 × 10^3 on Larson-Miller parameter.

Figure 4-7 is a plot of longitudinal and transverse stress rupture resistance of alloy 7 grown at 2 cm/hr and tested in argon. The transverse stress rupture resistance is excellent and is essentially parallel to the longitudinal, even down to test temperatures of 750 °C.

Two rupture tests on alloy 7 were run in an air atmosphere to quantify the degree of degradation in life caused by the hostile environment. From Table 4-8 the air atmosphere caused a 15% loss in life or 0.15 parameter loss at 750 °C and a 30% loss in life or 0.35 parameter loss at 1100 °C.

Alloy 7 was aligned at 2 cm/hr in a gradient of 100 °C/cm. To look at the effect of solidification rate, an ingot of alloy 7 was grown at 3 cm/hr in a gradient of 130 to 150 °C/cm. The ingot was 14 cm long. Metallographic

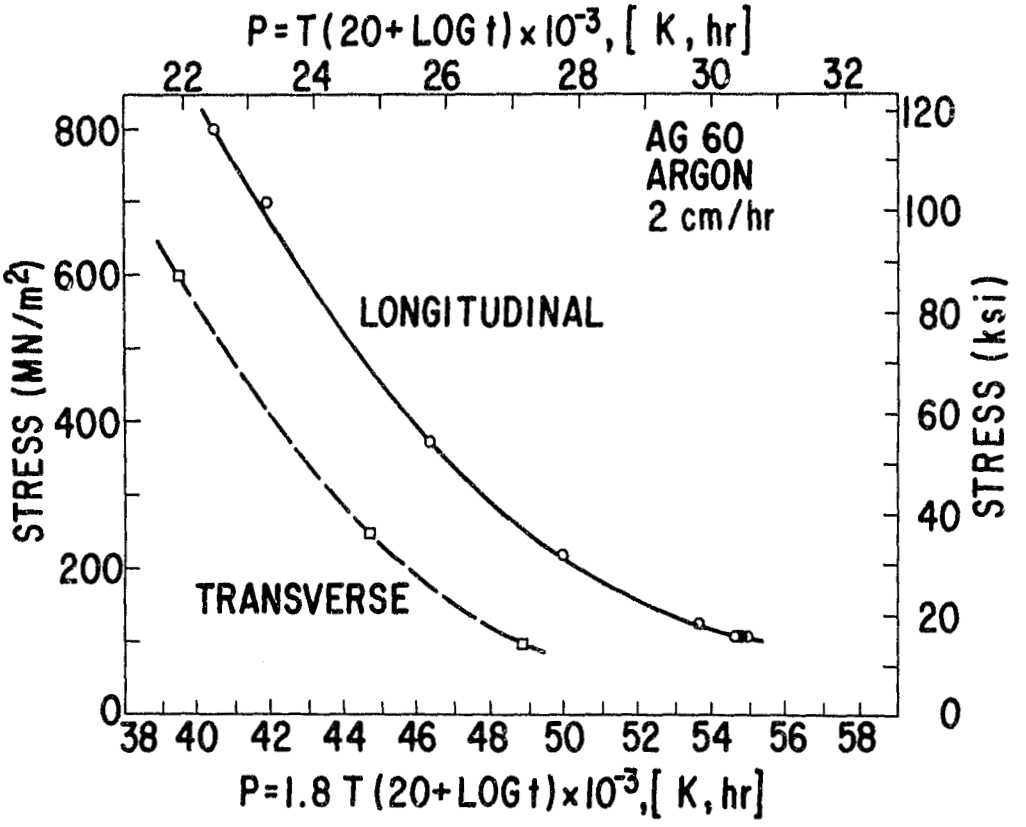

Figure 4-7. Longitudinal and Transverse Stress Rupture Resistance of Alloy 7 (γ/γ'-Mo) Grown at 2 cm/hr and Tested in Argon

Table 4-8

Stress Rupture Results for Alloy 7 (γ/γ'-Mo)

DS Rate (cm/hr)	Test Atmos.	Temp. (°C)	Stress (MN/m^2)	Life (hr)	P_{20}*	% Elong.	% R.A.
			Longitudinal				
2	Argon	750	700	510.0	41.83	24	42
		750	800	85.3	40.40	14	35
		750	800	83.3	40.38	17	39
		900	375	87.6	46.34	47	65
		1000	220	62.8	49.96	25	64
		1100	110	178.3	55.00	14	27
		1100	110	155.3	54.86	17	65
		1100	110	148.2	54.81	17	56
		1100	110	133.3	54.69	21	63
		1100	125	49.8	53.63	18	66
	Air	750	800	70.0	40.24	16	26
		1100	110	110.3	54.49	26	72
3	Argon	750	800	159.5	40.90	21	42
		750	800	121.2	40.68	19	41
		1100	125	98.8	54.37	18	69
		1100	125	88.2	54.25	24	75
			Transverse				
2	Argon	750	600	25.8	39.44	2	3
		900	250	13.5	44.63	6	12
		1000	100	20.3	48.84	2	1

*$P_{20} = T(1.8)(20 + \log t) \times 10^{-3}$, [K, hr]

examination of a polished longitudinal stripe revealed 1.4 cm of chill cast structure, 5.2 cm of aligned structure, a zone of 4.1 cm with the edges of the stripe cellular and the center aligned, and the remaining 3.3 cm cellular. Both structures were tested at 750 and 1100 °C in stress rupture. The data from Table 4-8 are summarized here:

DS Rate (cm/hr)	Microstructure	Life (hr) at 750 °C and 800 MN/m²	Life (hr) at 1100 °C and 125 MN/m²
2	Aligned	84.6	49.8
3	Aligned	159.5	98.8
3	Incipient Cellular	121.2	88.2

The 3 cm/hr stress rupture life is approximately twice that of the 2 cm/hr material, which is 0.5 parameters at 750 °C and 0.75 parameters at 1100 °C. The incipient cellular material showed a 10 to 15% loss in life over aligned material at the same rate. The indications are that even a small fraction of cellular cross-section will degrade rupture resistance.

4.6 Thermal Cycling Resistance

Thermal cycling resistance was evaluated by prior thermal cycling to 1150 °C and subsequent rupture testing at 1100 °C. Section 3 describes the procedure. Alloys 1, 2, and 7 were thermally cycled for approximately 150 hours or cycles, and alloy 7 was also cycled for 500 hours or cycles.

The microstructural effect of thermal cycling in all three alloys was to agglomerate the γ phase in the matrix. In the as-directionally solidified state, the γ phase was essentially between, and not touching, the Mo fibers. After thermal cycling to 1150 °C, the γ phase was clumped and touching the Mo-fibers. Figure 4-8 shows a comparison of uncycled and cycled material for alloy 1

Table 4-9 gives the subsequent stress-rupture results on thermally cycled specimens. Two specimens of alloy 7 which were thermally cycled saw an overshoot on temperature of approximately 75 °C (135 °F) for about 80 cycles. These specimens showed about a 70% loss in life as opposed to the 55% loss exhibited by the specimens cycled for 160 cycles to 1150 °C.

The tentative conclusion is that the lower aluminum content alloys undergo more thermal cycling degradation. It must be noted, however, that the maximum temperature used in the cycling was 1150 °C. Previous studies on thermal cycling have examined maximum temperatures of 870 to 1100 °C and shown that the effect is very sensitive to maximum cycle temperature, with the degree of degradation decreasing maximum temperature. It is necessary, therefore, to evaluate these alloys at a more realistic maximum temperature like

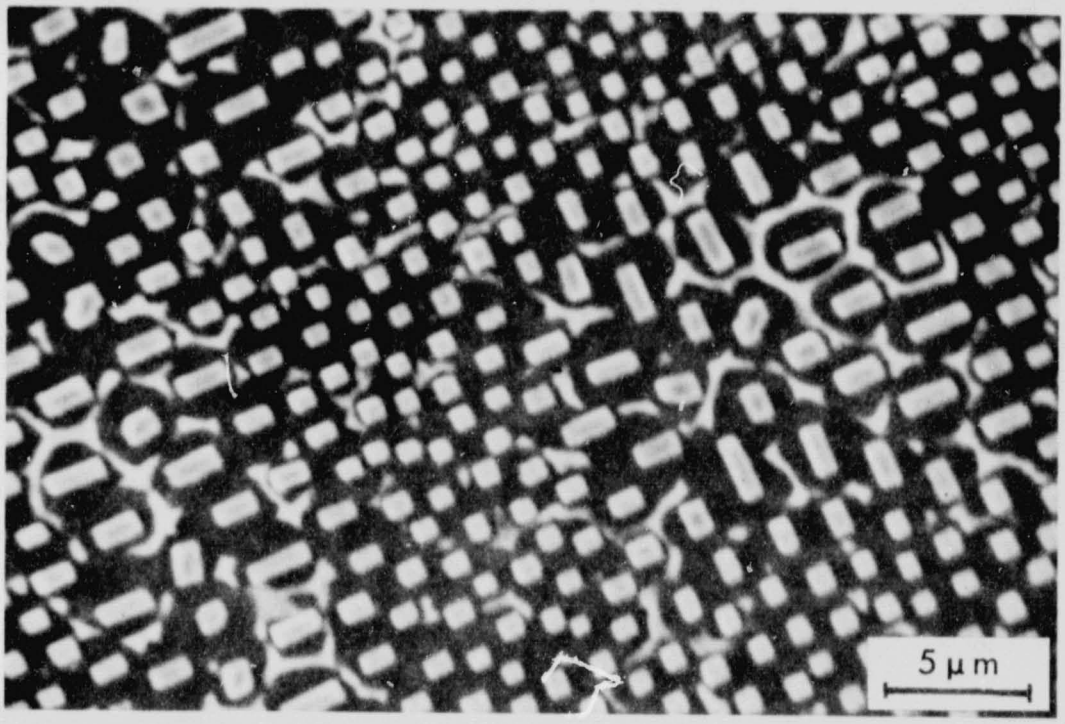

(a)

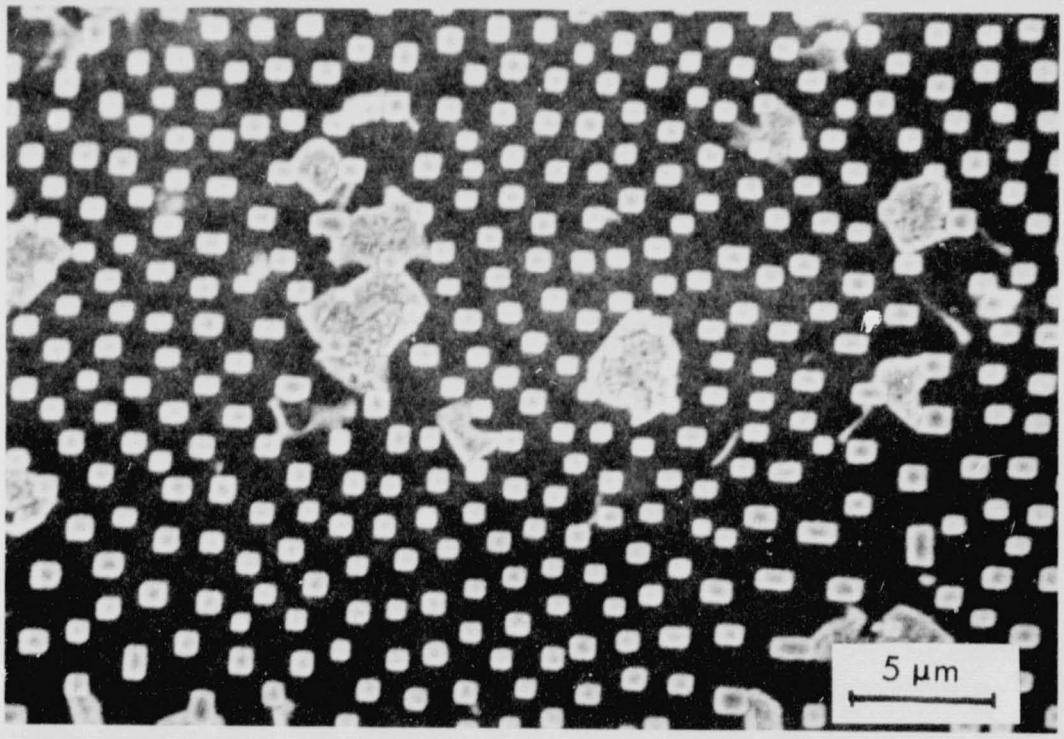

(b)

Figure 4-8. Scanning Electron Micrographs of Transverse Sections of Alloy 1 (γ/γ-Mo): a) Uncycled, b) After 150 Hours Cycling to 1150 °C

Table 4-9

Results of Prior Thermal Cycling and Subsequent Stress Rupture for γ/γ'-Mo Alloys Cycled to 1150 °C

Alloy	No. of Thermal Cycles	Life in Hours at 1100 °C and 1100 MN/m^2 after Cycling	Ratio of Cycled Life to Uncycled Life
1	150	90.0	0.70
1	150	82.4	0.64
2	166	94.9	0.60
2	166	97.0	0.62
7	163*	52.8	0.34
7	163*	39.8	0.26
7	160	72.9	0.47
7	160	61.9	0.40
7	500	28.9	0.19
7	500	21.8	0.14

*Due to equipment malfunction, these cycles consisted of approximately 80 cycles to 1225 °C and 83 cycles to 1150 °C

1100 °C in order to fairly assess the degree of their thermal cycling problem. Cyclic oxidation pins cycled to 1100 °C showed far less agglomeration of γ phase than the specimens cycled to 1150 °C.

4.7 Cyclic Oxidation

Cyclic oxidation tests were performed in a static air furnace at 750 and 1100 °C. Section 3 gives details. Tables 4-10 and 4-11 present the data on the alloy, 7, receiving detailed evaluation under this contract.

The 21 mg/cm^2 weight loss in 1000 hours cycling to 750 °C represents a penetration of approximately 25 μ m or 0.001 inch. Metallography was performed on both specimens and no preferential attack of matrix or fibers was observed.

The 260 mg/cm^2 weight loss of 170 hours cycling to 1100 °C represents a penetration of approximately 300 μm or 0.012 inch. Metallography was performed on both specimens and no preferential attach of matrix or fibers was observed.

Table 4-10

Cyclic Oxidation of Alloy 7 (γ/γ'-Mo) at 750 °C

Hours of Cycling	Weight Change (mg/cm^2)	
	Specimen No. 1	Specimen No. 2
0	0	0
9	-1.74	-1.66
32	-1.96	-1.97
52	-2.10	-2.17
87	-3.44	-3.18
182	-6.84	-6.46
347	-10.73	-10.31
418	-12.71	-12.30
512	-13.73	-13.47
583	-15.21	-14.88
679	-16.79	-16.18
871	-20.01	-19.63
1007	-21.00	-21.03

Table 4-11

Cyclic Oxidation of Alloy 7 (γ/γ'-Mo) at 1100 °C

Hours of Cycling	Weight Change (mg/cm^2)	
	Specimen No. 1	Specimen No. 2
0	0	0
26	-17.80	-23.14
49	-67.52	-69.53
101	-149.18	-150.63
122	-185.59	-187.59
169	-260.77	-265.03

4.8 Mold/Metal Reactivity

Alloy 7 was used to evaluate potential mold/metal reactivity problems in the γ/γ'-Mo system. The casting trial was on a GE CF6 blade grown at 1cm/hr. Figure 4-9 shows the blade. Because of the silica core, the maximum melt temperature was limited to 1565 °C (2850 °F). The blade was grown at 1 cm/hr to allow for more time for reaction of the molten metal and ceramic. The mold was a multilayer, silica-bonded alumina shell produced at the General Electric Corporate Research and Development Center, and the core was a commercially purchased silica body.

The blade surface after the mold was broken off showed no serious surface defects. The blade was then sectioned longitudinally, mounted, and metallographically polished. There was little or no evidence of interaction with the mold. In general, the performance of this alloy in the mold is good.

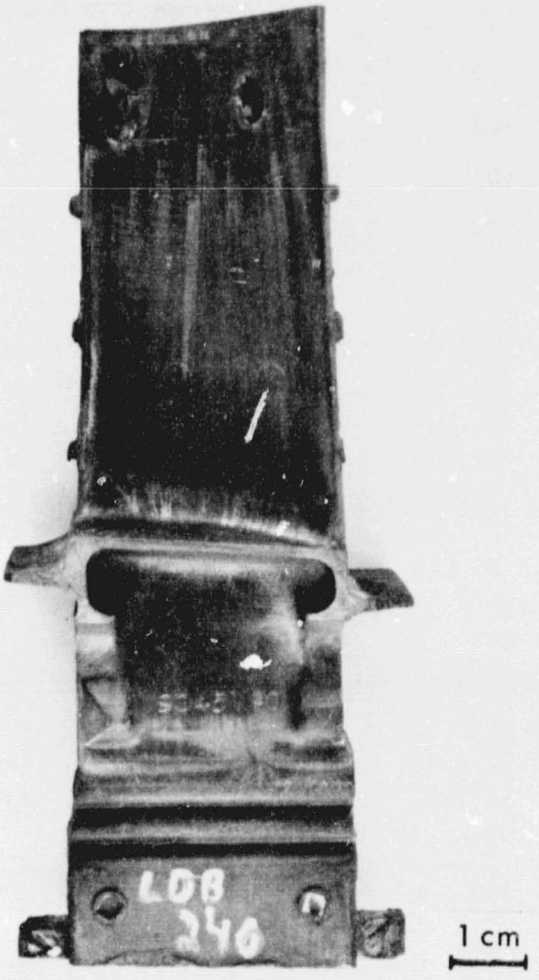

Figure 4-9. Macrograph of CF6 Blade of Alloy 7 (γ/γ'-Mo) Grown at 1 cm/hr

5. THE γ-β SYSTEM (M.R. JACKSON)

5.1 Background

The system consists of a face centered cubic solid solution (γ) of Ni, Al, and other elements, and a CsCl structured (β) substoichiometric (Ni, M)Al, where M is generally Fe or Co. The primary reasons for studying this system were its expected oxidation/hot corrosion resistance, low density, low cost melt stock, high probability of alloying for strengthening, and ease of processing.

Unlike the Co-Al binary system,[7-9] the Ni-Al system does not exhibit a γ-β eutectic. In the binary Ni-Al system,[1] a eutectic forms at 24 a/o Al and 1385 °C, between γ and γ'. However, Cr additions tend to suppress the stability of the γ' phase[10-12] and a liquidus trough is expected between γ and β. Below about 1000 °C, the $\gamma+\beta$ phase field is eliminated from the NiCrAl ternary phase diagram by the presence of a $\gamma'+\alpha$ (bcc Cr) field.[11] Simple NiCrAl γ-β alloys are expected to be microstructurally unstable for service that includes temperature cycling through the $\gamma+\beta \rightleftarrows \gamma'+\alpha$ transition.[13] Another ternary system that has been studied in detail is the NiFeAl system. Fe suppresses the stability of γ', and because of the large compositional range for β-(Ni, Fe)Al and the narrow range for γ', the $\gamma+\beta$ phase field is not eliminated at lower temperatures. Eutectics in this ternary system are expected to be microstructurally stable.

The interest in the γ-β quarternary Ni-Cr-Fe-Al system arises from the exceptional high temperature oxidation resistance of Ni-Cr-Al alloys. These materials are being considered as coatings for hot section jet engine turbine components.[14-16] The goal of studying the γ-β alloys is to couple the expected oxidation resistance with the useful high temperature mechanical behavior that may result from an aligned eutectic structure.

A considerable amount of research was performed at General Electric on the γ-β NiFeCrAl system prior to the beginning of the present contract.[17] A 10 a/o addition of Fe or Cr results in 1.5 a/o less Al in the eutectic alloy. Eutectic trough Al compositions were determined as a function of Cr and Fe contents, and partial or complete suppression of γ' solid state precipitation was controlled through composition adjustment. Cyclic oxidation exposures to 1100 °C showed the Cr-containing alloys formed a protective scale, while the Ni-Fe-Al alloys spalled rapidly. Room temperature strength was excellent, due to the β phase, but high temperature strength was poor as β weakens rapidly as temperature increases above 650 °C.

After the beginning of the present program, additional studies at the General Electric Company indicated another class of γ-β alloys, based on the Ni-Al-W system, might have greater flexibility in alloying to improve properties. Compositions in this class constituted a major portion of the present study. The experimental ternary Ni-Al-W diagram of Budberg[18] and that

calculated by Kaufman and Nesor[19] were in significant disagreement. An experimental redetermination showed the form of the diagram to be the same as Budberg's analysis, but the γ and β compositions were close to Kaufman and Nesor's calculations. The $\gamma+\beta$ eutectic phase compositions do not change significantly from the eutectic temperature range down to 800 °C, suggesting cyclic thermal stability for these alloys. No $\gamma'+\alpha$ field was observed, and it is concluded that the calculated diagram of Kaufman and Nesor is incorrect.

5.2 Alloys

Tables 5-1 and 5-2 list the compositions studied for the γ-β system. Alloys 10 and 11 are in the Ni-Fe-Cr-Al system, with alloy 11 containing 1 a/o W to attempt solid solution strengthening. The remaining alloys are in the Ni-Co-Al-W system with iterations aimed at determining microstructure/composition/property relationships. Alloys 12-15 consider different Co levels, alloy 17 considers partial replacement of W by Mo, and alloy 18 attempts to change the morphology of the γ-β eutectic from lamellar to fibers of β.

Table 5-1

Melt Compositions in the γ-β System

Atomic Percent

Alloy	Ni	Al	Fe	Cr	W	Co	Other
10	53	17	10	20	-	-	-
11	52.	17	10	20	1	-	-
12	58.9	23	-	-	3.1	15	-
13	49.3	22.9	-	-	2.8	25	-
14	67.7	23.9	-	-	3.4	5	-
15	64.7	23.2	-	-	2.8	10	-
16	64.5	23.2	-	-	2.3	10	-
17	64.2	23	-	-	2.3	10	.5Mo
18	64.5	20	-	-	1	10	.5Re 2V 2Ta

Table 5-3 lists the densities measured in aligned regions and the length of aligned structure observed on longitudinal polished stripes of the directionally solidified ingots. Bars were approximately 2 cm in diameter. In addition, a bar 4.1 cm in diameter was grown for alloy 15. For many of the alloys, the sort-out zone was less than 0.1 cm in length. This is an indication that the nominal melt composition is very close to the eutectic liquidus trough. A large change in volume fraction of β and of lamellar spacing was

Table 5-2

Melt Compositions in the γ-β System

Weight Percent

Alloy	Ni	Al	Fe	Cr	W	Co	Other
10	60.2	8.9	10.8	20.1	-	-	-
11	57.7	8.7	10.5	19.6	3.5	-	-
12	62.5	11.2	-	-	10.3	16.0	-
13	52.6	11.2	-	-	9.4	26.8	-
14	71.7	11.6	-	-	11.3	5.4	-
15	68.5	11.4	-	-	9.4	10.7	-
16	69.8	11.5	-	-	7.8	10.9	-
17	69.2	11.4	-	-	7.7	10.8	0.9Mo
18	66.9	9.6	-	-	3.3	10.4	1.6Re 1.8V 6.4Ta

noted as Co content increased. Figure 5-1 compares the structures for lamellar and fibrous Ni-Co-Al-W alloys. Although the longitudinal stripe of alloy 16 showed fully eutectic structure, the transverse sections indicated only a rim of eutectic, with the remainder being a mixture of γ dendrites and interdendritic eutectic. For alloy 18 the nominal melt composition was very Al poor, but aligned eutectic was produced at the tops of both ingots.

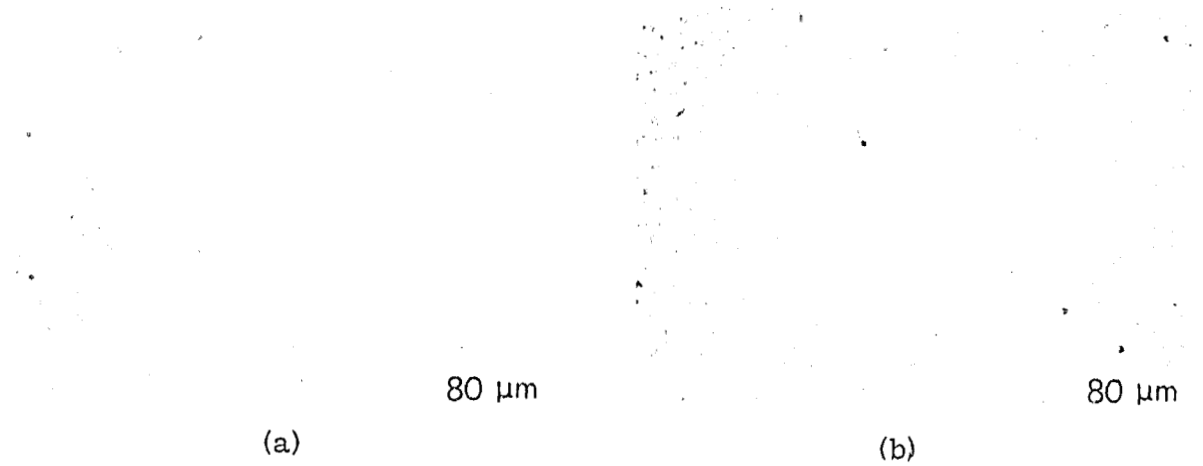

Figure 5-1. Transverse Microstructures for the Ni-Co-Al-W γ-β Eutectic Alloys: a) Lamellar (Alloy 17), b) Fibrous (Alloy 18)

Table 5-3

Characterization of Directionally Solidified γ-β Ingots

Alloy	DS Rate (cm/hr)	Length of Aligned Structure (cm)	Density** (g/cm^3)
10	2	7.4	7.46/--
	2	6.5	--
11	2	5.7	7.60/--
	2	5.9	7.60/--
12	2	8.1	8.06/8.08
	2	8.4	8.09/9.03
13	2	9.0	8.03/8.02
	2	9.3	8.01/7.99
14	2	6.1	7.97/7.96
	2	6.9	7.93/7.96
15	2	8.1	7.93/8.01
	2	8.1	7.90/8.03
	2*	13.6	--
16	2	5.8	7.95/7.82
	2	5.6	7.97/7.80
17	2	7.5	7.94/7.96
	2	7.9	7.93/7.93
18	1	6.8	8.13/8.20
	2	3.5	--

*4.1 cm diameter, all others 2.2 cm diameter
**Multiple determinations are separated by a /

For alloy 10, qualitative electron beam microanalysis was performed on the individual phases using a scanning electron microscope and solid state detectors. The analysis showed γ to be 45 a/o Ni, 26 a/o Cr, 12 a/o Fe, 17 a/o Al, and β to be 47 a/o Ni, 5 a/o Cr, 15 a/o Fe, 33 a/o Al. The composition of β in equilibrium with γ at 1250 °C should be near 35 a/o Al.

X-ray fluorescent analysis was performed on transverse sections from aligned regions of a number of Ni-Al-W γ-β eutectics (Table 5-4). The standard for the analysis was the chill-cast region of alloy 12. For analysis, the composition of this alloy was assumed to be the exact nominal melt composition, but this assumption may lead to errors in analysis. Also, the use of a single standard technique[20] can introduce further error. However, the data appear to be extremely consistent and reproducible. Trends in the data for Al and W correlate well with density data and with strength data. The fluorescence analysis shows that the addition of Co tends to lower the Al content of the eutectic. The W level increases slightly from 0 to 15 a/o Co, and then decreases at 25 a/o Co. Density of the alloys follows the same trend as do the W contents. The Al solubility in the γ phase decreases with increasing Co.

For the γ-β eutectics, variations in lamellar spacings observed along the length of an ingot are quite small and x-ray fluorescent analysis reveals that there is no significant segregation along the length of the ingot, as the density measurements confirmed.

5.3 Tensile Properties

Table 5-5 lists the results of tensile tests for the γ-β alloys. For the Ni-Cr-Fe-Al-base alloys, the 1 a/o W addition of alloy 11 produced significant improvements in strength at all temperatures, without appreciable degradation of ductility. Tensile properties at 750 °C and 1100 °C were low compared to turbine application requirements. Ductility for longitudinal specimens was adequate at room temperature and excellent at 750 °C and 1100 °C. Table 5-5 shows the results of longitudinal tests for the Ni-Co-Al-W base alloys whose ultimate strengths at room temperature are below those of the Ni-Fe-Cr-Al alloys. However, at both 750 °C and 1100 °C these alloys have tensile strengths that may be adequate for certain high temperature applications. The differences between the two classes of alloys at room temperature are probably due to the higher volume fraction of β for the Ni-Fe-Cr-Al alloys. At higher temperatures where the β phase exhibits greater ductility and less strengthening behavior, the high W concentration of the γ phase in the Ni-Co-Al-W alloys is probably responsible for improved performance. Elongations for the Ni-Co-Al-W alloys are comparable to those of the Ni-Fe-Cr-Al alloys over the temperature range studied.

Table 5-4

Fluorescent Analysis of Transverse Sections of Y-8

		Weight Percent				
Alloy	*	Ni	Co	Al	W	
14	CC	72.0	5.1	13.2	9.7	
14	B	72.2	5.2	12.7	10 0	
14	T	73.0	4.8	13.8	8.4	
15	B	64.6	10.7	12.0	12.7	
15	T	66.2	10.6	10.6	12.6	
15	CC	65.5	10.6	12.5	11.4	
15	B	66.0	10.7	12.3	11.1	
15	T	65.9	10.6	12.2	11.2	
12	CC	61.9	15.8	12.8	9.8	
12	B	62.9	16.0	11.4	9.7	
12	T	60.5	16.2	12.1	11.2	
12	CC	62.5	16.0	11.2	10.3	STANDARD
12	B	59.7	16.4	10.9	13.0	
12	T	62.3	15.8	11.0	10.8	
13	CC	50.7	28.8	11.0	9.4	
13	B	51.4	28.8	11.2	8.7	
13	T	51.4	29.0	10.5	9.1	
13	B	50.4	29.2	11.0	9.4	
13	T	50.7	29.3	9.6	10.4	

*Location in ingot:
CC-Chill cast, unremelted during directional solidification.
B-Bottom, in eutectic region, near beginning of aligned structure.
T-Top, in eutectic region, 4 cm above bottom section.

Table 5-5

Tensile Test Results for γ-β Alloys

Longitudinal Tests

Alloy	Temp. (°C)	0.2% Y.S. (MN/m^2)	U.T.S. (MN/m^2)	%Elong	%R.A.
10	23	885	1117	8	-
	750	482	497	49	-
	1100	64	64	112	-
	1100	58	58	107	-
11	23	945	1283	12	-
	750	583	596	34	-
	1100	66	66	68	-
	1100	69	69	61	-
12	750	772	779	10	28
	1100	218	225	59	-
	1100	246	255	52	24
13	750	593	593	12	34
	1100	141	143	42	5
	1100	184	184	55	16
14	1100	238	238	58	97
	1100	258	258	57	40
15	23	346	938	35	27
	23	304	965	36	23
	750	862	862	12	32
	750	834	834	13	35
	900	556	578	26	41
	1000	378	387	40	54
	1100	265	272	70	54
	1100	260	272	52	44
16	1100	247	250	70	62
	1100	260	263	65	58
17	750	710	786	28	-
	1100	226	231	70	66
	1100	234	238	73	70
18	750	917	924	12	46
	1100	292	313	23	26

Transverse Tests

15	23	216	216	0	0.4
	750	225	225	0	0
	1100	152	155	3.2	0.8

Typically, the yield strength of Ni-Co-Al-W alloys at room temperature is much less than the ultimate strength, but at higher temperatures the yield and ultimate strengths are nearly identical. Transverse strength is nearly independent of temperature and is much lower than the yield strength of the longitudinal tests. Transverse ductilities at room temperature and 750 °C are nearly zero, while there is slight ductility at 1100 °C testing.

Fracture surfaces were viewed by scanning electron microscopic techniques. At room temperature and 750 °C the fracture surfaces of all the lamellar alloys showed longitudinal delamination along γ-β interfaces and through the β platelets (Figure 5-2). The β exhibited a flat fracture, while the adjacent γ platelets necked to a knife-edge shape. At higher temperatures, considerable necking and deformation of the γ matrix occurred around segments of broken β platelets. Localized shearing of the matrix happened at high temperatures and in the heavily deformed shear bands, some recrystallization of the matrix was seen.

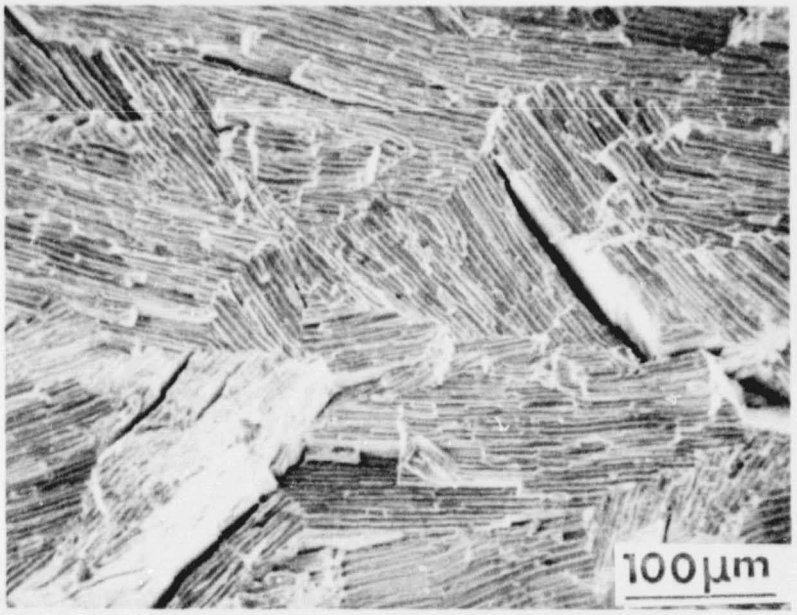

Figure 5-2. Scanning Electron Fractograph of Room Temperature Tensile Test of γ-β, Alloy 10

Figure 5-3 shows the microstructure observed for longitudinal sections through the fracture surfaces of specimens tensile tested at 750 °C and 1100 °C for the fibrous alloy 18. Figure 5-4 shows a SEM micrograph of the fracture. At 1100 °C, localized shear bands deformed, rather than fractured, the ductile β fibers. Recrystallization of the matrix was observed in the shear bands. At 750 °C a 46% reduction in area was noted and some grain boundary delamination was observed.

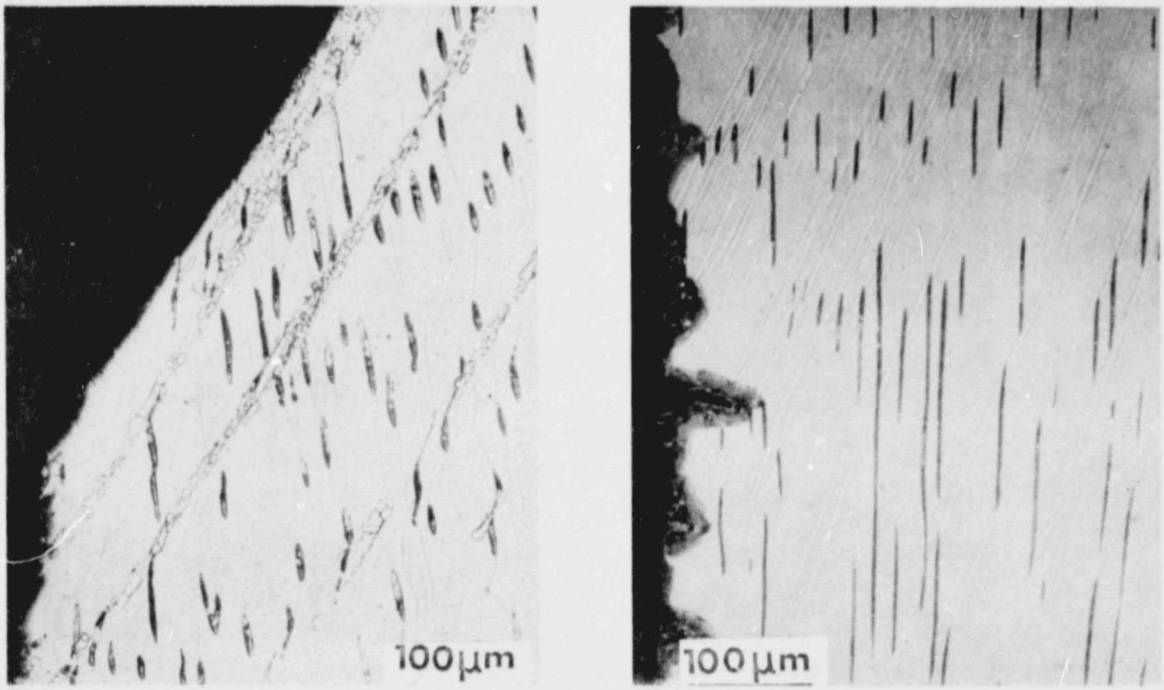

(a) (b)

Figure 5-3. Longitudinal Sections Through Tensile Fracture Specimens of Fibrous γ-β (Alloy 18) After Testing at a) 1100 °C and b) 750 °C

5.4 Longitudinal Shear Strength

Shear bars of alloy 15 were prepared to determine the longitudinal shear strength behavior of the lamellar γ-β structures. Table 5-6 gives properties. Figure 5-5 shows that the fracture in shear is completely grain boundary in nature. On the fracture surface one can see the scalloped grain boundary produced by intersections of the β platelets with the grain boundary.

Table 5-6

Longitudinal Shear Strength
of γ-β Alloy 15

Temperature	Longitudinal Shear Strength (MN/m^2)
23 °C	185
750 °C	223
750 °C	183
1100 °C	72

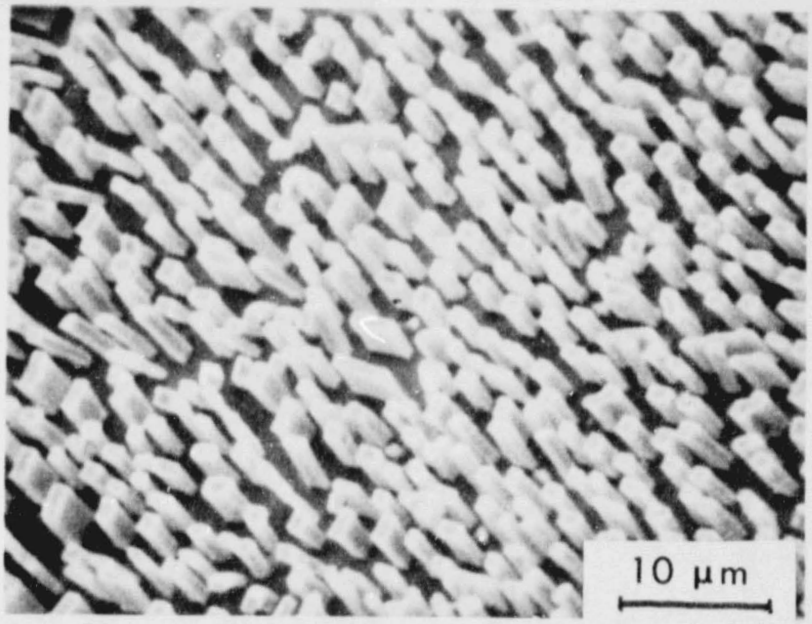

Figure 5-4. SEM Micrograph of the 750 °C Tensile Fracture of Alloy 18

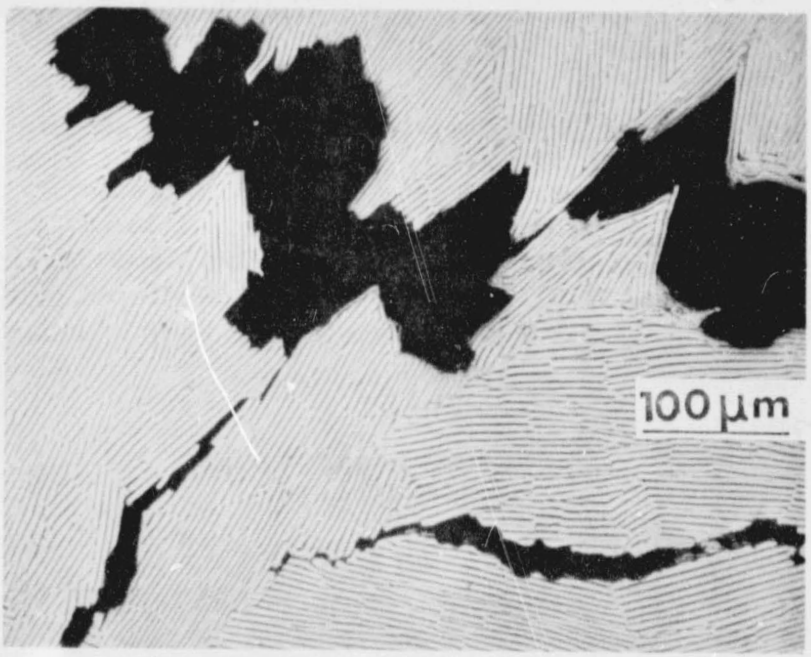

Figure 5-5. Micrograph Perpendicular to Stress Axis of a Longitudinal Shear Bar Showing Grain Boundary Crack Propagation in γ-β (Alloy 15)

5.5 Stress Rupture Resistance

Table 5-7 summarizes the results of stress rupture testing. The Ni-Co-Al-W alloys are considerably stronger than the Ni-Fe-Cr-Al γ-β alloys. The γ-dendritic structure of alloy 16 exhibits the same longitudinal rupture behavior at 1100 °C as do the eutectic structures of the same alloy. Apparently, the β phase does not provide substantial strengthening of the alloys at 1100 °C. At 750 °C and below the β phase provides significant strengthening of the alloy. Figure 5-6 plots the rupture strength versus parameter for alloys 13 and 15. The 10 a/o Co alloy (alloy 15) appears to be superior to the 25 a/o Co alloy (alloy 13), just as was the case for tensile strengths.

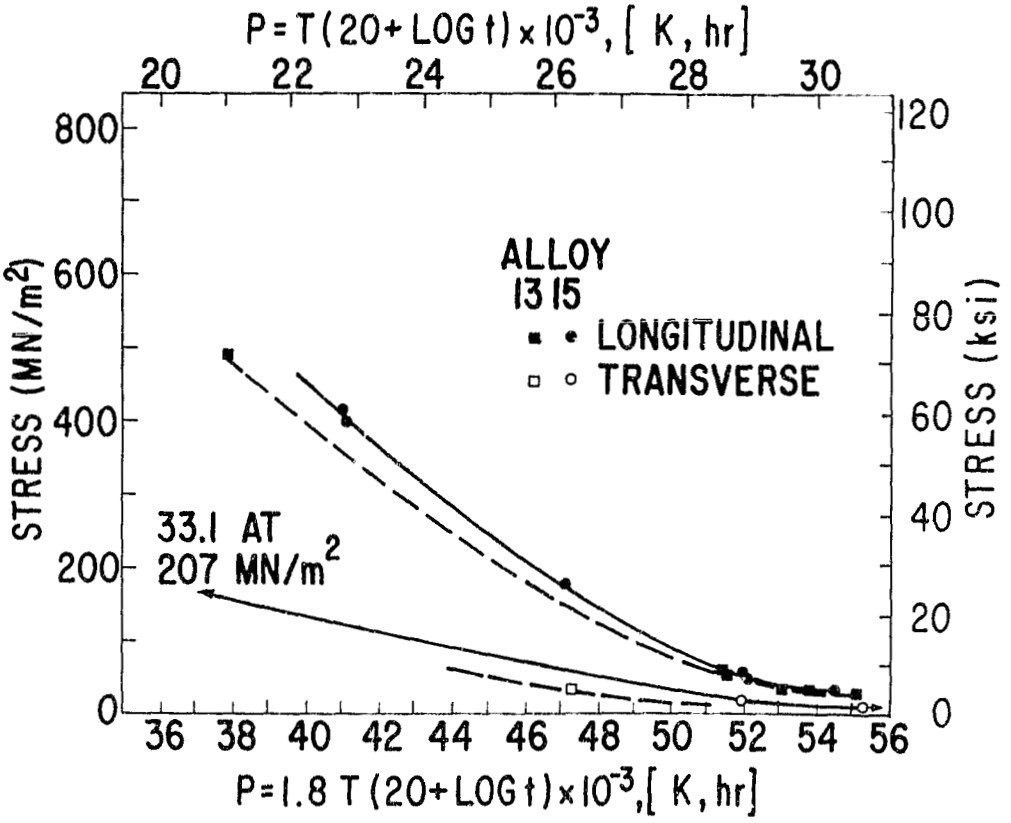

Figure 5-6. Larson-Miller Rupture Parametric Behavior for the Longitudinal and Transverse Orientations of Lamellar γ-β Alloys

Alloy 18 contains Re, V and Ta, and its rupture properties are far superior to any of the lamellar γ-β structures because of its composition. For the 750 °C tests, stress had to be increased twice (see Table 5-7) in order to produce rupture within a reasonable time. After some initial period, the creep rate approached zero for a load of 483 MN/m^2. The stress was increased to 586 MN/m^2, and again a near-zero creep rate was reached. The stress was increased to 690 MN/m^2 (100 ksi) and failure occurred in an additional 80 hours.

Table 5-7

Stress Rupture Behavior of γ-β Alloys

Longitudinal Stress Rupture*

Alloy	Temp. (°C)	Stress (MN/m^2)	Life (hrs.)
10	1100	24	10.3
	1100	14	172.7
11	1100	28	4.9
	1100	14	573.1
12	1100	76	7.7
	1100	62	11.1
13	750	483	3.3
	1100	62	7.0
	1100	56	7.8
	1100	34	31.0
	1100	34	64.1
	1100	28	206.6
14	1100	41	53.9
	1100	34	67.9
15	750	414	176.1
	750	400	200.9
	950	179	25.4
	1100	55	10.7
	1100	48	13.5
	1100	34	125.1
16	1100	48	21.6
	1100	41	28.4
17	750	379	179.6
	1100	34	74.2
	1100	41	42.2
18	750	690**	80.04**
	1100	97	12.36

Transverse Stress Rupture

13	1100	34	0.14
	1100	10	Unloaded after 234.8
15	750	207	0.01
	1100	17	11.0

*Argon at 1100 °C (except as noted), all other tests in air.

**Step-loaded, 120 hrs at 483 MN/m^2, 115 hrs at 585 $MN/^2$, and 80 hrs at 690 MN/m^2.

Figure 5-6 plots transverse rupture. Both alloy 13 and 16 are much weaker in the transverse orientation. Only the 1100 °C tests were under load for a time great enough to accumulate much creep damage. A transverse test of alloy 13 was terminated prior to failure, and Figure 5-7 shows macrographs of this bar. Although transverse tensile tests showed almost no strain, the creep bar had accumulated 50% strain when the test was stopped. Although the microstructure in the unstressed portion of the bar showed the grains to be randomly oriented, the platelet structure in the most heavily deformed regions was essentially parallel to the applied stress axis. The minimum thickness of the gage was approximately 24% as thick as the initial diameter. Along the original diameter perpendicular to the minimum thickness direction, there was no reduction in cross section, as seen in Figure 5-7. Away from the most heavily deformed region, very little platelet fracture occurred but grain boundaries and triple points were opened.

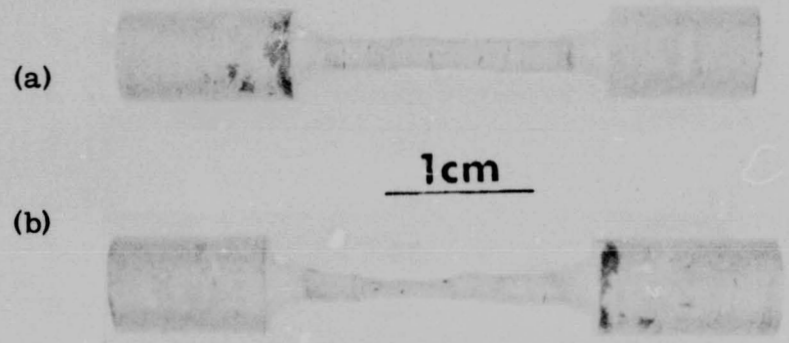

Figure 5-7. Macrographs of a Transverse 1100 °C Rupture Bar of γ-β (Alloy 13) Showing a) Growth Axis in the Plane of the Photograph, and b) Growth Axis Perpendicular to the Plane of the Photograph

5.6 Thermal Cycling Resistance

After approximately 150 hours of thermal cyclic exposure to 1150 °C in air, little microstructural change from as-solidified structures occurred. As expected, high energy sites, such as lamellar fault terminations and subgrain boundaries, showed agglomeration to reach a lower energy configuration, but overall alignment was retained. Loss of Al to oxide scale formation was most notable for the Ni-Co-Al-W alloys. Alloy 16, which was γ dendritic with interdendritic eutectic before cycling, was completely γ grains after cycling due to Al loss depleting the structure of β.

Table 5-8 lists rupture data for 1100 °C argon tests of the cycled materials. Although alloy 10 showed about 60% loss in rupture life, the remaining alloys showed no degradation due to cyclic exposure. No rupture data following thermal cyclic exposure were generated for alloy 18 because there was insufficient eutectic structure.

Table 5-8

Stress Rupture Behavior at 1100 °C in Argon
After Thermal Cyclic Exposure to 1150 °C

Alloy	Stress (MN/m^2)	Life (hrs)
10	14	76.1
	14	131.1
11	21	74.4
	21	40.1
12	62	13.8
	56	25.8
13	62	2.4
	56	11.7
14	41	59.2
	34	67.8
15	55	19.0
	48	11.6
16	41	16.9
	48	30.3
17	41	41.8
	34	78.4
15*	41	42.32
	34	122.79

*500 hours of cyclic exposure, all others 150-166 hours.

Bars of alloy 15 were cycled to 1150 °C for 500 hours in order to determine the effects of extended cycling. Table 5-8 includes the data for this condition in which no degradation occurred.

5.7 Cyclic Oxidation

Table 5-9 lists weight change for each γ-β alloy as a function of the number of one hour cycles of 1100 °C oxidation. For reference, a loss of ~8 mg/cm^2 corresponds to a 10 μm loss in pin radius. The behavior of the lamellar alloys varied very little with composition, and all alloys showed exceptional oxidation resistance. Although alloys 10 and 11 contain 20 a/o Cr, and the others contain

Table 5-9

1100 °C Cyclic Oxidation Weight Change for γ-β Alloys

Alloy	10		11		12		13		14		15	16		17		18	
hrs	Δ*		hrs	Δ	hrs	Δ	Δ		hrs	Δ	Δ	Δ		hrs	Δ	hrs	Δ
3	+ .1		7	0	6	+ .7	.7		43	+ .5	+ .4	+ .6		23	+ .7	22	-3.8
15	+ .3		14	+.1	12	+1.1	.6		66	+ .4	- .1	- .2		42	+1.1	85	- 8.2
121	- .8		29	+.1	20	+1.7	1.4		137	+ .4	- .3	- .3		75	+ .6	102	-12.6
218	-1.1		37	+.1	23	+1.5	1.0		233	0	-1.1	-1.0		98	+ .6	133	-13.0
287	-1.6		53	0	34	+ .4	0		400	-1.1	-2.4	--		151	0	157	-15.9
381	-1.9		61	0	108	0	- .4		496	-1.6	-3.2	-3.6		172	- .1	172	-21.5
481	-1.9		69	-.1	169	- .6	- .9		567	-2.0	-3.7	-4.2		236	- .2	293	-28.7
574	-1.9		84	-.2	240	-1.3	-1.6		662	-2.8	-4.7	-5.6		308	-1.2		
642	-2.3		117	-.2	437	-3.2	-2.7		820	-2.9	-4.9	-6.0		402	-2.4		
693	-2.3		189	-.4					891	-3.0	-5.2	-6.4		473	-3.6		
734	-2.7		284	-.7					985	-3.2	-5.5	-6.6		567	-3.1		
752	-2.7													621	-3.7		
968	-3.0																
1107	-3.1																
1199	-3.2																
1342	-3.2																
1561	-3.1																

*Δ = weight change in mg/cm^2

no Cr, the oxidation data for the two types of γ-β alloys showed no significant difference. Alloys 10 and 11 appeared to be marginally better than the Ni-Co-Al-W alloys at long cyclic exposure. For the Ni-Co-Al-W alloys, the approximate ranking of alloys followed the Al concentration of the aligned structures. The oxidation of alloy 18 proceeded more rapidly because of the presence of V and Re.

Table 5-10 lists the results of cyclic oxidation to 750 °C for two specimens of alloy 15. After 679 hours of cycling the pins still had a metallic sheen, with no evidence of thick oxide formation. The maximum change noted represented a loss of about 1 μm on the specimen radius. Very little oxidation or spallation occurred at 750 °C, as might be expected from the high Al content. Metallography revealed no structural changes at the specimen-atmosphere interface.

Table 5-10

750 °C Cyclic Oxidation Weight Change for γ-β Alloy 15

	Weight Change (mg/cm^2)	
Hrs	Specimen 1	Specimen 2
9	-.1	-1.2
32	-.9	-1.2
52	-.6	- .8
87	-.5	- .8
182	-.5	- .4
347	-.2	- .7
418	-.6	-1.0
512	-.3	- .6
583	-.2	- .5
679	0	- .3

After cyclic oxidation microstructures of the pins of γ-β were similar in nature for both the Ni-Fe-Cr-Al and Ni-Co-Al-W alloys. At the oxidizing surface a region of γ was produced. As Al diffused to the outer surface to form protective oxides, the composition of the region immediately below the oxide was depleted in Al, thereby transforming the γ+β phase field into the single-phase γ phase field. Alloy 16 was Al-deficient and had a γ-dendritic structure in the as-directionally solidified condition. After 100 hours of cyclic oxidation the pin of this alloy contained no β phase and began to show signs of internal oxidation and grain boundary attack.

5.8 Mold/Metal Reactivity

Reactivity of the molten 10 a/o Co γ-β eutectic alloy (alloy 15) with an alumina shell mold was tested by growing turbine blade shapes of the alloy at 2 cm/hr. A tandem casting was made of a solid and a cored TF-34 shape, with the blades grown in the tip-down configuration. There was appreciable interaction between the melt and the silica core which resulted in contamination of the entire melt and a matrix dendritic structure in both blades. However, no interaction between the melt and the mold system was observed. Solid blades of the 25 a/o Co alloy (alloy 13) were grown at 2 cm/hr in the TF-34 shape, fully aligned in the airfoil, and showed no interaction with the mold. Some breakdown in alignment occurred in the root.

6. THE γ-γ' SYSTEM (M.R. JACKSON)

6.1 Background

The system consists of γ, an austenitic matrix of Ni, Co, Re, W and V, and fibers of γ', an ordered $L1_2$ phase based on Ni_3Al, but with Ta substituting for some Al. The primary reasons for studying this system were a high probability of alloying for strengthening, large volume fraction of the second phase, and high temperature phase stability. Densities were expected to be substantially the same as present-day superalloys.

Studies on Ni-TaC alloys at the General Electric Company have included some zero and low Cr alloys. The decreased Cr was hoped to produce greater thermal stability through a decreased tendency for sigma phase formation, and also to cause greater maximum growth rates by minimizing G/R constraints. In the course of these alloy studies, it was found that Al and Ta levels were quite high in the last liquid to be directionally solidified due to segregation during solidification. The levels were great enough in some ingots to allow for the formation of nodules of γ-γ' eutectic. X-ray fluorescent analysis of regions that were primarily γ-γ' led to the determination of the eutectic compositions. Several attempts at alloy modification yielded alloys whose high temperature rupture properties were essentially equivalent to those of γ/γ'-δ and NiTaC-13 eutectics. Because the γ-γ' eutectics contained considerable Al, they were expected to resist oxidation better than γ/γ'-δ and NiTaC-13. Also, the possibility of higher maximum growth rates and of lower sensitivity to cellular microstructures were potential benefits of the γ-γ' system. Smashey of General Electric had earlier developed a class of γ-γ' eutectics, but these alloys were not based on Ni-Ni_3(Al, Ta) and they contained none of the potent strengtheners W or Re. Another study of γ-γ' eutectics considered the Ni-Ta-Al system, but no indication of mechanical properties was given.[21]

Studies at the General Electric Company have also involved a number of compositions aimed at producing γ-γ' eutectic structures. On a weight percent basis, the range of compositions investigated was 6-9 Al, 5-17 Ta, 0-10 Co, 0-6 V, 0-6 Re, 2-6 W, and the balance Ni. Eutectic structures could be formed when the total amount of Al and Ta, in atom percents, was in the range of approximately 19-22 a/o. For small additions of the other alloying elements, Al and Ta together could sum to the upper limit of about 22 a/o. However, as the amount of the other additions was increased, Ta and Al had to be decreased to avoid a microstructure containing the β phase. In general, alloys with a ratio of Ta/(Ta+Al) in the range of 0.12 to 0.23, on an atom percent basis, had the best balance of strength, oxidation resistance and density. For 1100 °C stress rupture in argon, a stress of 96 MN/m^2 resulted in failure after about 280 hours. This result is comparable to the present best high temperature eutectics, NiTaC-13 and γ-γ'-δ.

6.2 Alloys

Tables 6-1 and 6-2 list the compositions of alloys, and Table 6-3 lists microstructural analyses and densities. Densities were measured in the aligned portion of the ingots and ranged from 8.3 g/cm^3 to 9.0 g/cm^3. The Co level of the alloys had no noticeable effect on density. No alignment was achieved in alloy 23.

Figure 6-1 shows the longitudinal microstructure for alloy 19. Alloys 19 and 21 generally contained large regions of dendritic γ, within which was precipitated the γ' phase. The interdendritic regions contain aligned γ-γ' eutectic consisting of rods of γ' in a thin network of γ. At the melting point, it is presumed that the γ' phase is the minority component, but that the shape of the $\gamma/\gamma+\gamma'$ solvus is such that large amounts of γ' are precipitated from the γ matrix. This precipitation probably occurs close to the melting point, since the additional γ' forms on the original γ' fibers rather than as a particulate precipitate within the γ. Microstructural evidence from the 1150 °C thermally cycled material also suggests the γ' precipitation occurs at very high temperature. This will be discussed later. The high volume fraction of the rods of the γ' phase is analogous to the behavior observed by Cline for Co-CoAl.[7] The microstructures of alloys 20 and 22 were fully aligned structures. Again, the volume fraction of the γ' rods was very high.

Table 6-1

Melt Compositions in the γ-γ' System

	Atomic Percent							
Alloy	Ni	Al	Ta	Co	V	Re	W	Other
19	72	17	2.5	5	1.75	.75	1	--
20	72	15	4.5	5	1.75	.75	1	--
21	65.5	18.4	2.6	10	1.75	.75	1	--
22	67	16	4.5	10	1.75	.75	1	--
23	59.4	16.5	2.5	10	3	1.0	1.5	0.6Mo 5Cr 0.5HF
24	72.8	14.35	4.35	5	1.75	.75	1	--

Alloy 20 was chosen for more complete properties determination which required large diameter bars for transverse tensile and stress rupture specimen preparation. The first 4.1 cm diameter bar showed a largely γ' dendritic structure, with little aligned eutectic. A second ingot was grown from the same heat, and poor structure again resulted. Two more heats of this composition were made, and a 4.1 cm diameter by 15 cm long bar was produced from each. Approximately 5 cm of aligned eutectic resulted in one,

Table 6-2

Melt Compositions in the γ-γ' System

Weight Percent

Alloy	Ni	Al	Ta	Co	V	Re	W	Other
19	72.3	7.9	7.7	5.0	1.5	2.4	3.1	--
20	68.7	6.6	13.2	4.8	1.4	2.3	3.0	--
21	66.2	8.5	8.1	10.1	1.5	2.4	3.2	--
22	63.2	7.1	13.3	9.6	1.5	2.3	3.0	--
23	58.3	7.4	7.5	9.8	2.5	3.1	4.6	1 Mo 4.3Cr 1.5Hf
24	69.4	6.3	12.8	4.8	1.4	2.3	3.0	--

Table 6-3

Characterization of Directionally Solidified γ-γ' Ingots

Alloy	DS Rate (cm/hr)	Aligned (cm)	Density* (g/cm^3)
19	2	2.1	8.51/8.53
20	0.68	4.9	9.00/8.89
	2	7.8	8.94/8.92
	2	4.9**	--
	2	1.4**	--
21	1	2.9	8.55/8.34
	2	1.1	--
22	2	6.2	8.88/8.86
23	2	0	--
24	2	8.2	--

*Duplicate determinations are separated by a "/."
**4.1 cm diameter bars; others were 2.2 cm diameter.

and 4 cm in the second (1.4 cm well aligned). The microstructures that resulted suggest that the eutectic composition is extremely sensitive to small variations in chemistry and/or growth rate.

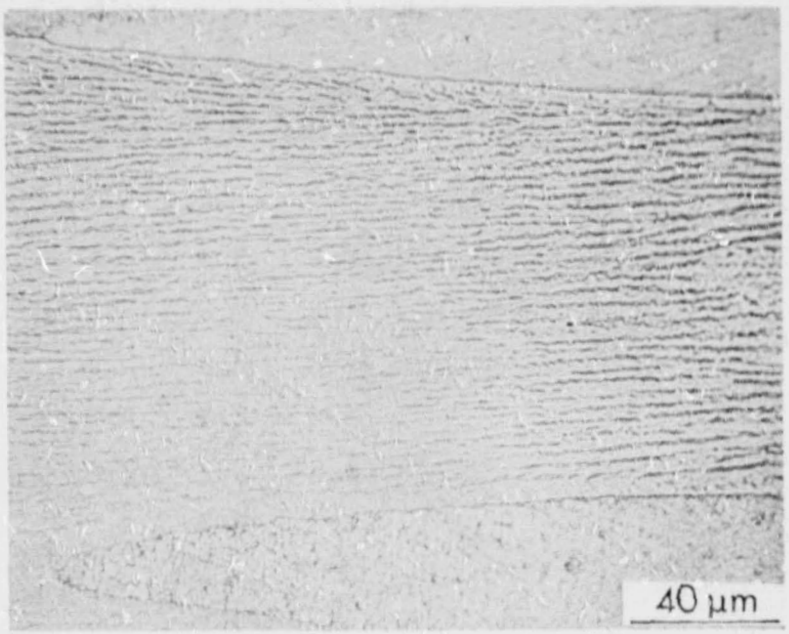

Figure 6-1. Longitudinal Microstructure of γ-γ' Alloy 19

6.3 Tensile Properties

Table 6-4 lists the tensile properties of the γ-γ' eutectic alloys. The most obvious feature in the data is the large amount of scatter in both strength and ductility, with ductility measured by percent elongation and reduction in area. With this degree of scatter, no differentiation between alloys could be made. The strengths in the range of 750-1100 °C are significantly greater than conventional superalloys.

The table also notes transverse properties. Ductility in the transverse direction is nil, and strengths are also much lower than the longitudinal orientation. The approximate ratio of transverse to longitudinal strength is 0.7 at 23 °C, 0.3 at 750 °C, and 0.3 at 1100 °C.

Figure 6-2 shows representative fractographs of the tensile test specimens for longitudinally and transversely oriented bars. Although some of the longitudinal bars showed in excess of 10% elongation, the fracture surfaces always had a characteristic non-ductile appearance. The fracture surfaces indicate a grain-boundary related failure, possibly in γ' films. Eutectic grain boundary failures were seen in longitudinally and transversely oriented samples when polished through the fracture surface.

6.4 Longitudinal Shear Strength

Shear bars of alloy 20 were prepared to determine the longitudinal shear strength behavior of the γ-γ' eutectic structure. Table 6-5 lists properties.

Table 6-4

Tensile Behavior of γ-γ' Alloys

Alloy	Temp. (°C)	0.2% Y.S. (MN/m^2)	U.T.S. (MN/m^2)	%Elong.	% R.A.
		Longitudinal Tests			
19	750	637	821	29	25
	1100	310	329	24	47
20	23	454	558	11	17
	23	512	678	8	5
	600	696	821	8	7
	700	814	821	21	28
	750	710	786	28	--
	750	717	724	3	0
	750	672	672	0	0.6
	850	703	710	22	28
	925	687	696	6	10
	925	504	504	32	37
	1000	239	239	0	0
	1100	428	466	37	50
	1100	352	406	36	39
	1100	269	269	17	1.2
	1100	412	412	18	12
21	750	976	986	1.2	5
	1100	351	361	10	8
	1100	345	390	26	38
22	750	632	667	23	11
	1100	311	371	34	6
24	1100	346	378	16	13
		Transverse Tests			
20	23	432	432	0	1.2
	750	231	231	0	0
	1100	114	114	0	1.6

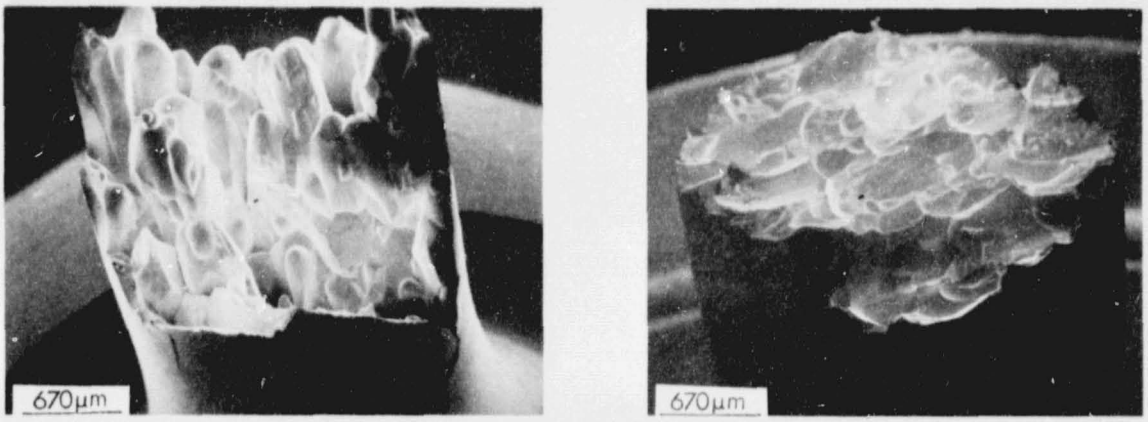

(a) (b)

Figure 6-2. Macrographs of Fracture Surfaces in γ-γ' Alloy 20 After Room Temperature Tensile Testing: a) Longitudinal and b) Transverse

These values are much less than the longitudinal tensile strengths of the γ-γ' alloys at all temperatures. However, at 750 and 1100 °C, the shear values are equivalent to transverse tensile strength, which was noted as being primarily a grain boundary strength test for this alloy.

Figure 6-3 illustrates the macroscopic appearance of the shear surface. The grain boundary nature of the fracture surface is apparent, and this appearance is typical of failures at all temperatures tested.

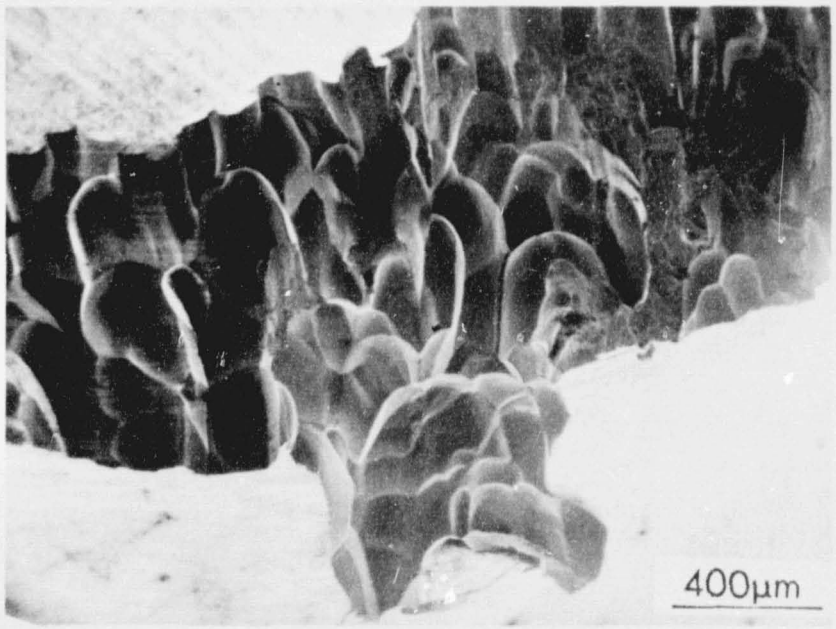

Figure 6-3. Fracture Surfaces of Longitudinal Shear Test Specimens of γ-γ' Alloy 20 Tested at 1100 °C

Table 6-5

Longitudinal Shear Strength of γ-γ' Alloy 20

Temperature	Shear Strength (MN/m^2)
23 °C	263
750 °C	272
750 °C	256
1100 °C	123

6.5 Stress Rupture Resistance

Table 6-6 lists and Figure 6-4 plots stress rupture data for the γ-γ' eutectic alloys. The table shows that there is a large variation in lifetime at any one stress, which made it extremely difficult to choose stresses to produce failure in reasonable times. For example, one bar of alloy 20 tested at 750 °C and 483 MN/m^2 failed in 0.01 hours. Tested under the same conditions, a second bar from the same ingot lasted 164.47 hours, with essentially a zero creep rate. The stress was increased to 586 MN/m^2 and the test lasted 8.84 hours before failure.

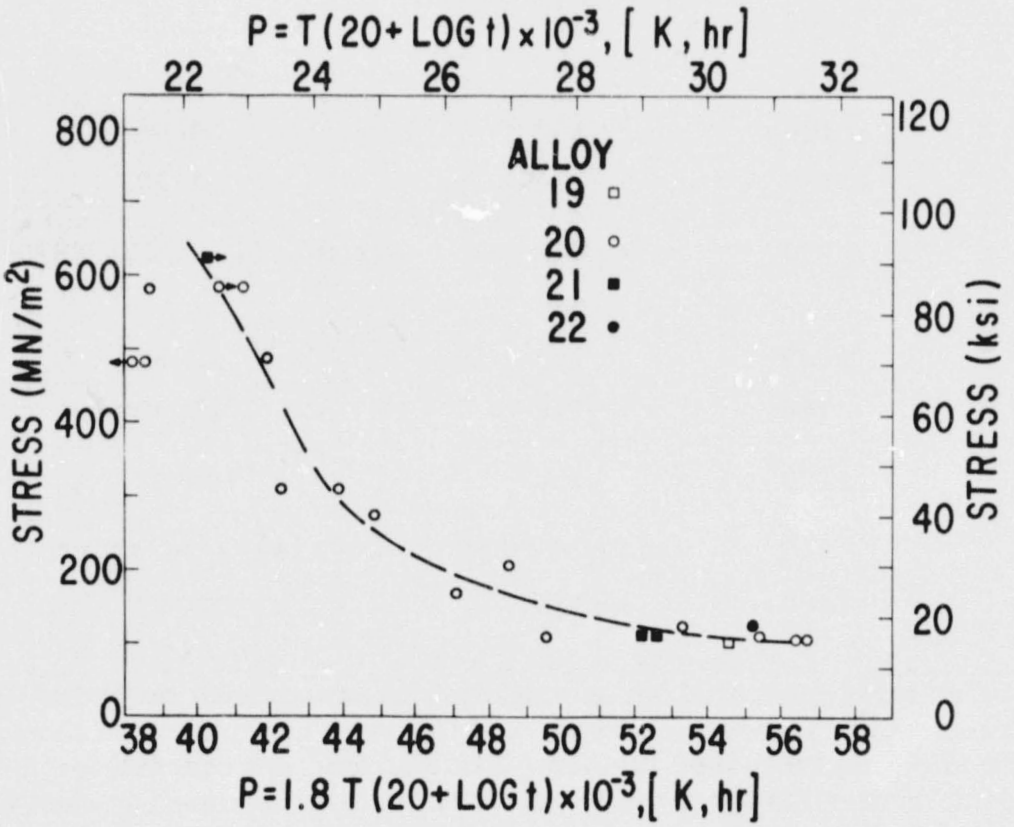

Figure 6-4. Larson-Miller Rupture Parametric Behavior of γ-γ' Alloys

Table 6-6

Stress Rupture Behavior of γ-γ' Alloys

Alloy	Temp.** (°C)	Stress* (MN/m^2)	Time to* Rupture (hrs)
19	1100	103	121.72
20	750	483	5.70
	750	483	0.01
	750	483/586	164.47/8.84
	750	586/655	234.58/0.03
	800	414/483	166.71/48.16
	900	310	On loading
	950	276	2.20
	950	310	0.77
	1000	207	15.03
	1000	172	3.68
	1100	103	538.69
	1100	103	772.92
	1100	124	34.94
	1100	110	1.12
21	750	448/483/586 621	312.04/189.13/151.83/66.82
	1100	110	12.93
	1100	110	18.40
22	1100	124	199.27
24	750	483/586/690	186.4/95.4/.17
	1100	110	216.93

*In five tests the initial stress resulted in an extended period of zero creep. Loads were increased, and if a zero creep rate was reached, the load was increased further. Time at load is recorded for these tests, rather than just total time to failure. The times at each load for these tests are separated by "/".

**Tests at ≥1000 °C in argon, others in air.

Figure 6-4 plots, in Larson-Miller parametric form, the data for samples with two or more stress levels before failure, with arrows pointing toward higher parameter values. Only one parameter value is plotted, the one with the highest combination of stress and parameter. The high stress portion of the stress parameter relation for the γ-γ' eutectics is very steep, while the slope is very shallow for stresses below approximately 200 MN/m^2.

Many of the low temperature tests showed severe grain boundary delamination. Although tests at 750 °C exhibited a non-ductile fracture appearance, failure did not occur until 5-10% elongation had occurred. For tests in the 950 °C range, 30% elongation was measured, and again the fracture surface was non-ductile in appearance. At 1100 °C, more than 50% elongation was measured in some samples, and the fracture surfaces were similar to those of tensile tests described in Section 6-3. Metallographic examination showed failures to be grain boundary related, just as in tensile testing.

6.6 Thermal Cycling Resistance

Bars of alloy 20 were cycled for 150 and 500 hours between 400 °C and 1150 °C in evacuated quartz tubes. Figure 6-5 shows the microstructure after cycling; it has changed considerably. Instead of a γ network ringing the γ' fibers, the matrix is now γ', with γ particles contained within the γ'. The particles are aligned along the growth direction, but are nearly spherical, rather than cylindrical and encircling the γ' rods. Despite the large microstructural changes, the mechanical properties do not degrade (Table 6-7). In fact, the tests for the 150 hour and 500 hour cycled material fall well above the line of stress versus parameter plotted in Figure 6-4.

Figure 6-5. Longitudinal Microstructure of γ-γ' Alloy 20 After Thermal Cyclic Exposure to 1150 °C for 500 Hours

Table 6-7

Stress Rupture Behavior at 1100 °C in Argon
After Thermal Cyclic Exposure to 1150 °C for Alloy 20

Number of Cycles	Stress (MN/m^2)	Life (Hrs)
150	117	250.3
500	117/138*	571/132*

*Zero creep rate at 117 MN/m^2 after 571 hours, so without unloading, stress was increased to 138 MN/m^2 and the test continued to specimen failure.

6.7 Cyclic Oxidation

Pins of alloys 19-22 were cycled to 1100 °C or 750 °C in a static air oxidation furnace. Table 6-8 lists the weight change measured at different increments of time for each alloy in 1100 °C cyclic oxidation, and Table 6-9 lists the data for 750 °C cyclic oxidation of alloy 20. Little occurs at 750 °C. At 1100 °C, alloys 20 and 22 (low Al alloys) lose weight more rapidly than do alloys 19 and 21 (high Al alloys). The weight change behavior of the high Al alloys is quite good, particularly in view of the absence of Cr in these alloys and the presence of vanadium.

6-8 Mold/Metal Reactivity

Reactivity of the molten γ-γ' eutectic alloy with an alumina shell mold was tested by growing turbine blade shapes of alloy 20 at 1 cm/hr. The slower rate allowed more reaction time. A tandem casting was made of a TF-34 and a J101 LPT shape, with the blades grown in the tip-down configuration. Figure 6-6 shows the tandem casting and the macroetched surface of the TF-34 blade. The airfoil and the major portion of the blade were well-aligned, but cellular structure was evident in the tang and platform regions. Matrix dendrites were noted on the flat side of the platform. The J101 LPT blade shape was cut up for microstructural investigation. No mold/metal reaction could be found.

Table 6-8

1100 °C Cyclic Oxidation Weight
Change Measurements for γ-γ' Alloys

Alloy	19	20	20		21		21	22
Rate (cm/hr)	2	0.68	2		1		2	2
Hrs	Δ*	Δ	Δ	Hrs	Δ	Hrs	Δ	Δ
23	+ .8	+ 3.6	+ 5.1	23	- 1.5	23	+ 1.1	+ 4.4
47	+ .8	+ 5.6	+ 7.1	64	- 3.4	42	+ 2.0	+ 7.5
71	+ .7	+ 7.2	+ 8.0	136	- 8.6	75	+ .7	+ 7.6
166	- .1	-25.7	-39.9	230	- 9.4	98	- 2.6	+ 4.8
228	+ .6	-27.5	-42.4	301	-10.4	151	- 1.3	- 31.1
324	+ .2	-49.4	-74.9	395	-11.0	172	- .9	- 30.7
395	+ .3	-54.2	-80.0	449	-11.4	236	- 3.1	- 47.5
499	+ .4			544	-12.2	308	- 9.0	- 66.2
714	-1.2					402	-16.6	- 90.8
961	-5.6					473	-22.3	- 98.4
*weight change in mg/cm^2						567	-29.9	-111.3

Table 6-9

750 °C Cyclic Oxidation
Weight Change Measurements
for γ-γ' Alloy 20 Grown at 2 cm/hr

	Weight Change (mg/cm^2)	
Time (hrs)	Pin 1	Pin 2
66	+ .9	+1.3
92	+1.2	+1.7
116	+1.6	+2.2
138	+1.7	+2.3
161	+1.5	+2.2
275	+2.2	+3.0

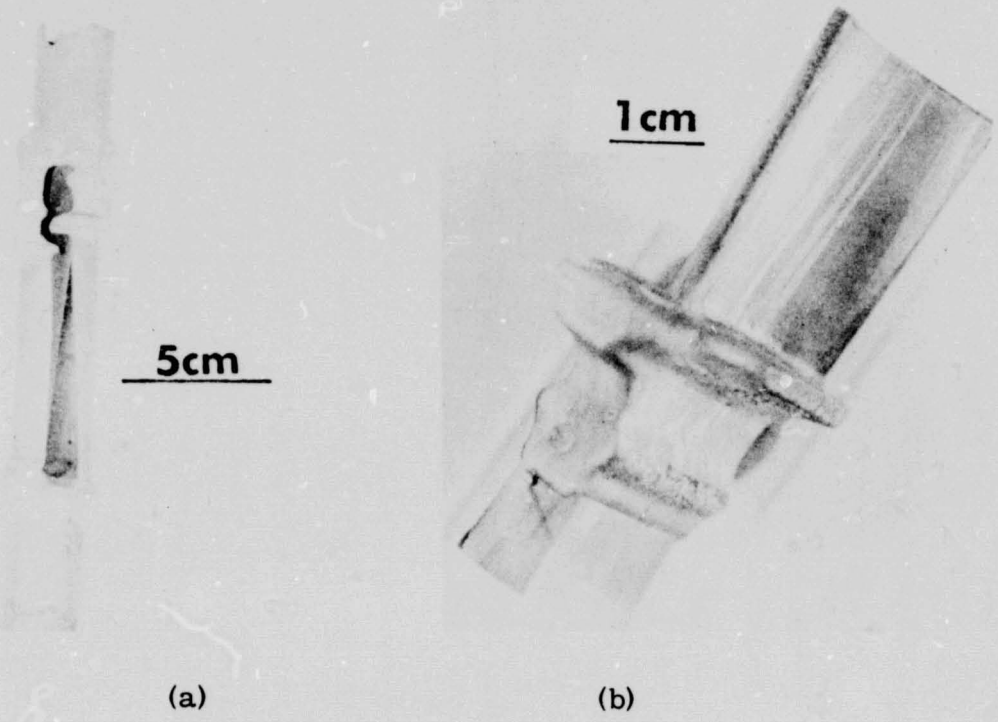

Figure 6-6. Macrographs of Mold-Metal Reactivity Tests of γ-γ' Alloy 20 Alumina Shell Mold, a) Tandem Casting and b) Etched TF34 Shape

7. THE γ-M_2Ta SYSTEM (M.R. JACKSON)

7.1 Background

This system consists of γ, an austenitic matrix of Ni, Fe, Cr and Ta, and M_2Ta, an hexagonal intermetallic phase, with Cr, Fe, and Ni on "M" sites. The primary reasons for studying this system were its expected oxidation/hot corrosion resistance, a high probability of alloying for strengthening, high temperature phase stability, and large volume fraction of the second phase. Density may decrease as Fe and Cr replace Ni. Higher Cr content may improve oxidation resistance. However, a matrix rich in Ni may offer more potential for precipitation hardening by Al additions to form γ', or for solid solution strengthening by elements like W or Mo. Replacement of Ta with either Nb or Ti would result in a decrease in density, but no expected loss of oxidation resistance. These additions may alter the matrix by precipitation of Ni_3 phases.

The oxidation resistance of Cr_2Ta (and Cr_2Nb) is excellent at 1250 °C.[22] Studies in the Ni-Cr-Ta ternary indicate very good oxidation resistance at 1250 °C in a regime around 67 a/o Ni, 25 a/o Cr, 8 a/o Ta.[23] In the Ni-Cr-Nb system, an α + Ni_3Nb phase field is present, indicating γ + M_2Nb is unstable. However, the liquidus slopes for the Ni-Cr and Ni-Ta binary diagrams [1] suggest that a eutectic of γ + Cr_2Ta is possible. To insure an M_2Ta rather than a Ni_3Ta structure, the addition of Fe makes the M_2Ta structure the energetically preferred phase. The Fe-Ta, Fe-Cr, and Fe-Ni binary diagrams[1] also point to a possible γ-M_2Ta eutectic. Further evidence is the presence of a eutectic in the Fe-Cr-Nb system studied by Jaffrey and Marich.[24] It is possible that Jaffrey and Marich were incorrect in hypothesizing that the phase was not an M_2Nb type, but a new ternary phase. The reported lattice parameters suggest the phase is an M_2Nb type. The existence of an α-M_2R eutectic would suggest that a γ-M_2R eutectic may also form, based on Fe-Ni binary diagram.[1]

In previous studies conducted by General Electric other alloys were melted and directionally solidified, with the Cr and Ta contents held constant (25 a/o and 8 a/o, respectively), the Fe content varied (0, 34, and 67 a/o), and the balance was Ni. The 67 a/o Fe alloy's composition was equivalent to that of Jaffrey and Marich,[24] with Ta replacing Nb. For the Fe-Cr-Ta alloy, there was excess M_2Ta which grew dendritically, with interdendritic regions being a rod eutectic. The 0 and 34 a/o Fe alloys had austenitic matrices. The 34 a/o composition was nearly on the rod eutectic composition, with a very slight amount of γ dendrites. For the 0 a/o Fe alloy a single eutectic structure was not obtained. Two possible eutectics, one of which is likely to be the γ-Ni_3Ta eutectic and another which is similar to the Fe-containing γ-M_2Ta eutectics, were observed.

7.2 Alloys

Tables 7-1 and 7-2 list three alloys studied in the γ-M_2Ta system. The microstructures of the as-cast bars of alloy 25 indicated that the alloy was slightly M_2Ta rich. Two ingots were directionally solidified at 2 cm/hr. Metallography of a longitudinal polished stripe on one bar showed <0.1 cm of M_2Ta sort-out, 8.9 cm aligned cellular, and on the second bar, 0.1 cm M_2Ta sort-out and 9.7 cm aligned cellular. Density was 9.26g/cm^3. The short sort-out region in the directionally solidified bars was evidence that the base composition was near the liquid $\rightarrow \gamma + M_2Ta$ eutectic trough. Fibrous cell centers and lamellar edges were evident. This is the same behavior as Jaffrey and Marich observed in Fe-Cr-Nb. Immediately above the M_2Ta sort-out zone, there was a short length of structure which was colonied rather than cellular.

Table 7-1

Melt Compositions in the γ-M_2Ta System
Atomic Percent

Alloy	Ni	Cr	Ta	Fe	Al
25	33	25	9	33	0
26	43.5	27	9	15	5.5
27	39.7	28.6	10.5	16.5	4.7

Table 7-2

Melt Compositions in the γ-M_2Ta System
Weight Percent

Alloy	Ni	Cr	Ta	Fe	Al
25	28.8	19.4	24.3	27.5	0
26	38.8	21.4	24.8	12.7	2.3
27	34.5	22.0	28.0	13.6	1.9

A second heat of alloy 25 was melted and directionally solidified at 0.64 cm/hr to determine if the solidified structure would improve with a decreased growth rate. After solidification, the bar had 0.1 cm sort-out of M_2Ta, 8.1 cm of banded but aligned structure (colonied). The initial portion of the aligned region was only very slightly colonied. The remainder of the region was more heavily colonied.

One ingot of alloy 26 was directionally solidified at 2 cm/hr. The solidified bar had 8.8 cm of colonied aligned structure. The density measured of a sample taken from the aligned region was 9.14 g/cm^3. Because the structure in the aligned portion of the ingot was quite colonied, the second ingot of the heat

was directionally solidified at 0.64 cm/hr, but the structure was again cellular. In the aligned region, the first 0.5 cm was fully aligned structure. In the fully aligned region of the structure formed at 0.64 cm/hr (Figure 7-1), the high volume fraction of the intermetallic phase was apparent. The nearly-square cross-section fibers appear to have been enlarged by additional solid-state precipitation of M_2Ta during the cooling period of the directional solidification process, so that many of the fibers impinge on their neighbors. The impingement has in some regions produced an almost lamellar morphology of the adjoing fibers. At the transition from fully aligned to colonied microstructure, many trifoil particles were present. Electron microprobe analysis of the fibers and the trifoils indicated no difference in composition. A competition between two different matrix and/or intermetallic preferred growth directions may account for the presence of the trifoil particles.

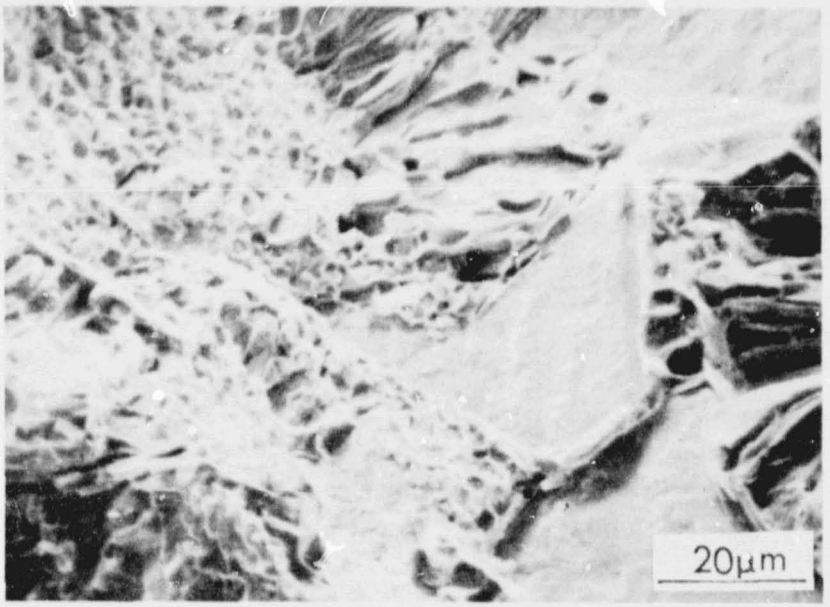

Figure 7-1. Transverse Micrograph Through Aligned Region of the γ-M_2Ta Alloy 26 Grown at 0.64 cm/hr

X-ray fluorescence analysis of transverse sections from alloy 26 was performed using the chill-cast section of the same ingot as the standard for analysis. Analysis indicated a substantial enrichment of Al in the liquid ahead of the growing aligned structure, and a high Ta concentration in the fibrous region. The composition of alloy 27 was that of the aligned region of alloy 26 analyzed by fluorescence. No completely eutectic structure was observed anywhere along the length of the directionally solidified ingot and the alloy was grossly Ta-rich.

Qualitative electron beam microanalysis of the phases in alloy 25 indicated γ to be 37 a/o Ni, 27 a/o Cr, 34 a/o Fe and 2 a/o Ta, and the fibers to be 27 a/o Ni, 22 a/o Cr, 31 a/o Fe and 20 a/o Ta, or M_4Ta. Using these compositions and measured volume fraction of 0.36 for the fibers, the eutectic composition is calculated to be 33.3 Ni, 25.2 Cr, 33.0 Fe, and 8.5 Ta. This is in substantial agreement with the melt composition, indicating the phase analysis is reasonable. Stoichmetric M_2Ta is 33 a/o Ta, and very little deviation from stoichiometry is expected, based on Cr-Ta and Fe-Ta binary diagrams.[1, 25]

A sample of intermetallic phase extracted from alloy 26 was analyzed to determine crystal structure and lattice parameters. The major phase was hexagonal, with a_o = 4.81Å and c_o = 7.855Å, essentially identical to Fe_2Ta parameters. It is likely that Cr and Ni both are on the Fe superlattice. A second (minor) phase was indexed as hexagonal with parameters of a_o = 5.30Å C_o = 8.70Å. The pattern was of the $MgZn_2$ type and the parameters are close to those of the phase Al_2Zr. A phase Al_2Ta has been reported in the literature, but with an orthorhombic crystal structure. In microprobe analyses of particles noted above, less than 10 a/o Al has been observed, so that Al_2Ta is not likely. What is surprising is that no evidence of an M_4Ta was seen, even though all particles analyzed have contained approximately 20 a/o Ta. Apparently, substantial substitution of the other constituents for Ta occurs on the Ta lattice to maintain an M_2Ta crystal structure.

7.3 Tensile Properties

Tensile testing at room temperature, 750 °C and 1100 °C, has been performed for alloys 25 and 26. The tests at room temperature were in air, while the other tests were in vacuum. Table 7-3 lists properties. In general, a slower growth rate improves strength because it causes an improved alignment in these compositions. The addition of Al causes a substantial improvement in strength at 23 °C and 750 °C, causes no change in strength at 1100 °C.

Figure 7-2 shows a fractograph of a room temperature tensile sample. Large flat regions appear due to the cleavage of the larger M_2Ta particles present in cell boundaries. This same feature is seen in the 750 °C fracture surface. In cell centers, the M_2Ta fibers show flat fracture, and the γ phase exhibits substantial necking. A better aligned structure may result in much higher strength, and possibly greater ductility, as the large cell boundary cleavage sites may act to nucleate tensile failure.

7.4 Stress Rupture Resistance

Table 7-4 lists stress rupture results at 1100 °C in argon for γ-M_2Ta alloys 25 and 26. Alloy 25 grown at 0.64 cm/hr lasted for 1545.5 hours at 20.7 MN/m^2 and showed no elongation; stress was increased to 27.6 MN/m^2 and failure occurred in an additional 224 hours. These results are plotted in Figure 7-3 using the Larson-Miller parameter for comparison. Both

Table 7-3

Tensile Data on γ-M_2Ta Alloys

Alloy	DS Rate (cm/hr)	Temperature (°C)	.2% Y.S. (MN/m^2)	U.T.S. (MN/m^2)	% Elong
25	2	23	960	960	0
	2	750	670	703	2
	2	1100	63	74	115
	2	1100	62	70	66
	.64	23	938	938	0
	.64	750	724	724	.11
	.64	1100	100	105	27
26	2	23	1214	1214	0
	2	1100	62	66	92
	.64	23	1729	1729	0
	.64	750	1158	1192	2.3
	.64	1100	97	101	58

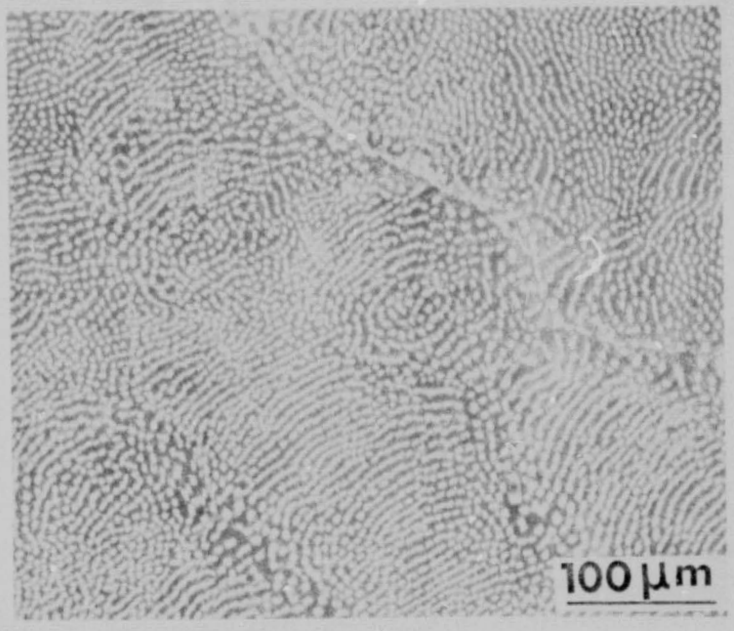

Figure 7-2. Fracture Surface of Room Temperature Tensile Test for γ-M_2Ta Alloy 25

Table 7-4

Stress Rupture Properties of γ-M_2Ta Alloys at 1100 °C in Argon

Alloy	DS Rate (cm/hr)	Stress (MN/m^2)	Life (hr)
25	2	24.0	18.6
25	2	14.0	360.6
25	.64	27.6*	224.0*
26	2	14.0	1009.1
26	.64	34.5	11.89

*Step-loaded, 1546 hrs at 20.7 MN/m^2 and 224 hrs at 27.6 MN/m^2. The parameter is greater than 57.3.

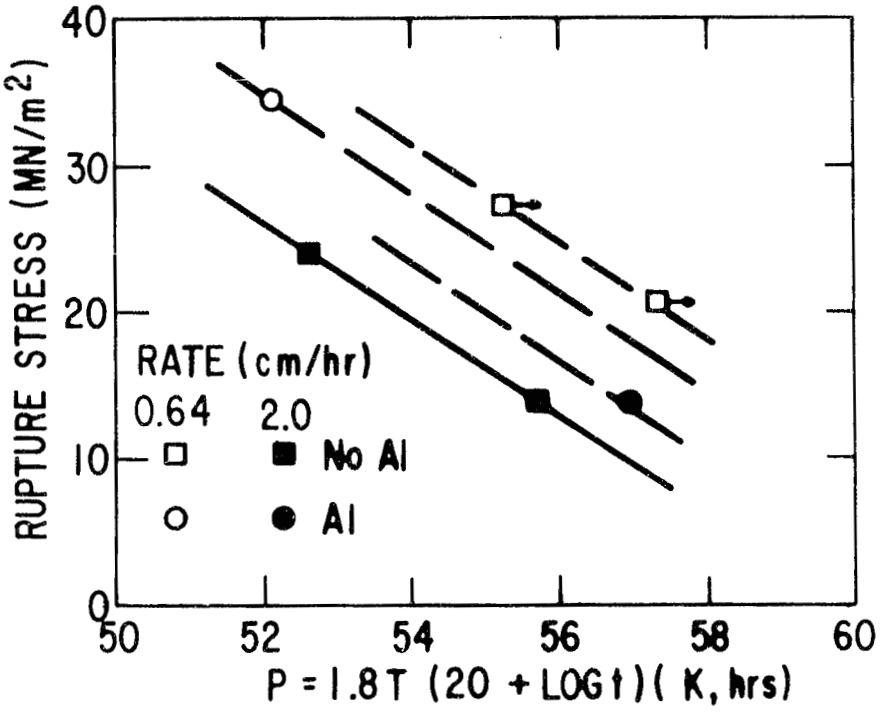

Figure 7-3. Larson-Miller Rupture Parametric Behavior for γ-M_2Ta Eutectics

tensile and stress rupture properties at 1100 °C are disappointing, possibly due to the extreme difficulty of achieving aligned structure.

7.5 Thermal Cycling Resistance

Very limited studies of the thermal cycling resistance of γ-M_2Ta were performed because of the difficulty in achieving aligned growth. Only the

2 cm/hr structure of alloy 25 was cycled. Bars from aligned colonied regions were cycled 150 hours between 425 °C and 1150 °C in a static air furnace. After cycling, substantial M_2Ta agglomeration was noted. This might be expected, since the cellular structure probably consists of γ-M_2Ta interphase interfaces that are far from the low-energy equilibrium configurations. The bars were tested at 1100 °C/14 MN/m^2. One failed at 366.98 hours, and the second at 455.61 hours. No reduction in rupture life relative to uncycled material (360.6 hrs) was noted.

7.6 Cyclic Oxidation

Pins 0.254 cm in diameter were prepared from alloys 25 and 26, each solidified at 0.64 and 2 cm/hr. These pins were subjected to 1-hour cycles in an 1100 °C static air furnace. Table 7-5 lists the weight change data. For both alloys the 0.64 cm/hr material is more resistant to oxidation than is the 2 cm/hr material. Structures for the more resistant 0.64 cm/hr structures are coarser, in that fibers tend to be larger in diameter. However, the cellularity is much less pronounced than in the 2 cm/hr structures, so that the intermetallic phase particles at colony boundaries tend to be much smaller. The Al-containing alloy 26 is more resistant than the Al-free alloy 25. However, the improvement is not nearly as dramatic as is that which results from decreased growth rate.

7.7 Summary

No further work was planned for γ-M_2Ta.

Table 7-5

Weight Change During Exposure to 1100 °C Cyclic Oxidation for γ-M_2Ta Alloys

mg/cm^2 Alloy 25				mg/cm^2 Alloy 26			
Time	DS Rate 0.64 cm/hr	Time	DS Rate 2 cm/hr	Time	DS Rate 0.64 cm/hr	Time	DS Rate 2 cm/hr
7 hrs	- 1.5	144 hrs	- 7.7	6 hrs	+ .02	7 hrs	+ 0.1
14	- 1.5	213	- 46.8	12	- .01	14	- .3
29	- 2.4	307	- 67.3	20	- .4	29	- 1.2
37	- 3.3	407	- 92.3	28	-1.2	37	- 2.4
53	- 5.1	500	-116.0	84	-3.7	53	- 4.6
61	- 6.0	568	-132.4	108	-4.4	61	- 6.2
69	- 7.1			169	-7.0	69	- 7.0
84	- 8.3			240	-9.0	84	- 8.8
117	- 8.9			437	-9.4	117	- 14.1
189	-11.9					189	- 18.6
284	-13.7					284	- 21.0
415	-15.3					415	- 60.0
601	-16.7					601	-145.8
696	-25.9						

8. THE Co-MC SYSTEM (J.L. WALTER)

8.1 Background

Cobalt base TaC eutectics with low Cr contents and high tungsten contents may be directionally solidified at rates in excess of 2.5 cm/hr. Such alloys have stress-rupture lives at 1066 °C and 172 MN/m^2 in excess of 2500 hours, greater than any nickel base directionally solidified eutectic alloy. At lower temperatures and higher stress levels, however, the stress-rupture life is not as great as for nickel base-TaC eutectic alloys. The Co-TaC alloys reported by Bibring et al.[26] generally have nominal compositions as follows: 20 Cr, 10 Ni, 12.7 Ta, 0.75 C, and balance Co. Those examined by Walter and Cline[27] generally contain by weight 15% Cr, 8.5% Ni, 6.0% W, 20% TaC, balance Co. A detailed compilation of Co-TaC alloy properties can be found in Reference 28.

Recently, it has been shown that the stress-rupture life of a simple cobalt base-TaC eutectic, CoTaC-3[29] may be improved by subjecting the directionally solidified alloy to a high temperature solutioning and precipitation anneal. By heating to 1300 °C for 2 hours, quenching, and then aging for 24 hours at 1000 °C, it was possible to form fine carbide precipitates on the order of 0.05μm diameter. Bibring designates this heat-treated alloy CoTaC-33.

This treatment increases the 100 hour stress rupture strength at 900 °C by 20%, at 1000 °C by 34% and at 1070 °C by 40%. At the same stress level and temperature the precipitation treatment increases life by a factor of 10. In prior work at General Electric, alloy modifications have reduced the Cr content and increased the tungsten content, thus increasing the volume fraction of TaC fibers and at the same time, raising the allowable solidification rate to greater than 3 cm/hr before formation of cell or dendrite structures. These latter alloys have stress rupture lives at 1065 °C far in excess of any other alloy. However, in common with all cobalt base alloys, eutectic and non-eutectic, the stress-rupture life at lower temperatures, such as 927 °C, is lower than can be obtained from the best nickel base-TaC eutectic alloys such as NiTaC-13 (300 hours at 927 °C and 280 MN/m^2 for a cobalt base alloy solidified at 2.5 cm/hr versus 1400 hours for NiTaC-13 solidified at 0.6 cm/hr).

8.2 Alloys

Tables 8-1 and 8-2 list the compositions of Co-MC alloys solidified, and Table 8-3 lists the ingot characteristics.

Samples of alloy 28 and alloy 29 were heated for 2 hours at 1300 °C to dissolve some of the TaC phase, and then were water quenched. Next, they were heated at 1000 °C for 24 hours to form fine TaC precipitates in the cobalt base matrix.

Table 8-1

Melt Compositions in the Co-MC System

Atomic Percents

Alloy	Co	Ni	Cr	W	Ta	C
28	63.3	12.7	--	8.1	7.7	8.2
29	55.8	9.4	18.8	2.1	6.7	7.2

Table 8-2

Melt Compositions in the Co-MC System

Weight Percents

Alloy	Co	Ni	Cr	W	Ta	C
28	50	10	--	20	18.67	1.33
29	50.5	8.5	15	6	18.67	1.33

Table 8-3

Characterization of Directionally Solidified Co-MC Ingots

Alloy	DS Rate (cm/hr)	Length of Aligned Structure (cm)
28	2	>4
29	0.64	>4

The precipitates in alloy 28 were studied by transmission electron microscopy and are shown in Figures 8-1 and 8-2. As can be seen, there are regions of no precipitates and regions of high precipitate content. The precipitates are aligned in a fashion parallel to the growth axis of the bar. The dark field analysis shows the precipitates to be small euhedral crystals of TaC with the same lattice constant as the TaC fibers.

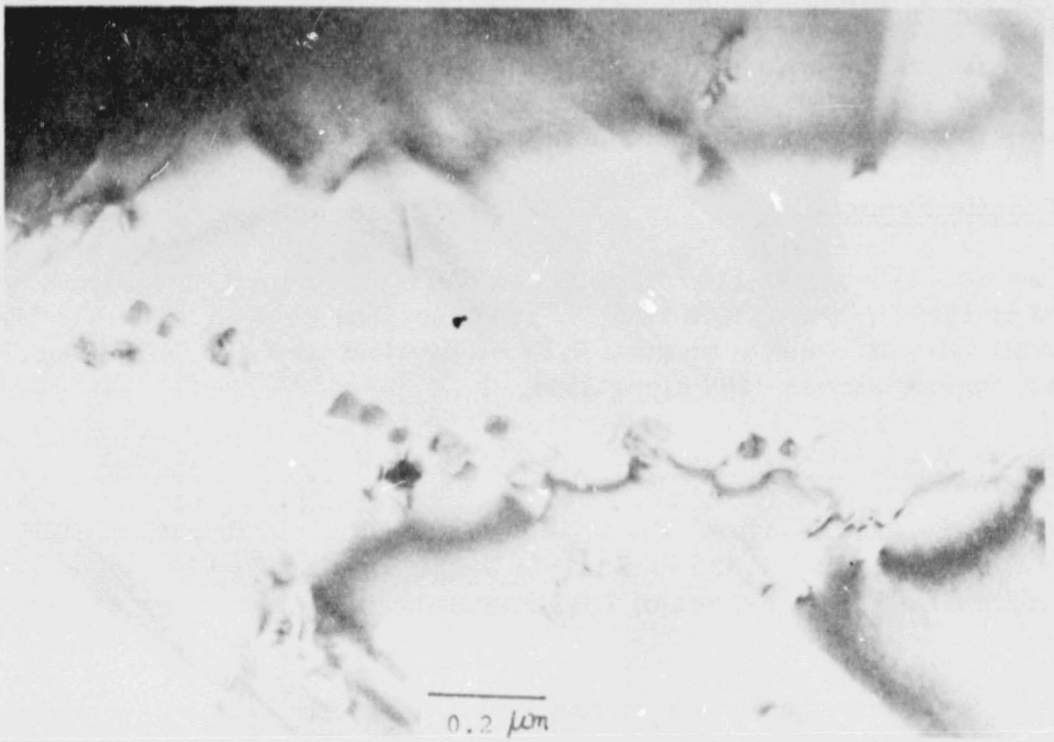

Figure 8-1. Transmission Electron Micrograph of Heat-Treated Alloy 28 Showing TaC Precipitates

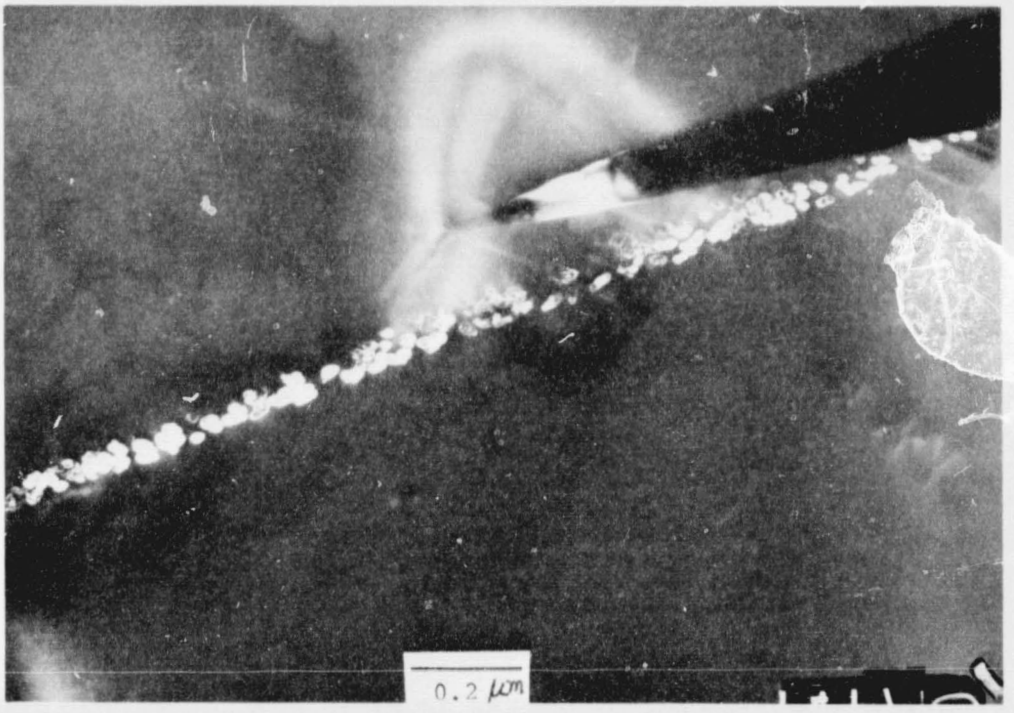

Figure 8-2. Dark Field Electron Micrograph of TaC Fiber and TaC Precipitates in Heat Treated Alloy 28

Based on the observation that precipitation did occur after the 1000 °C anneal, but that the amount of precipitate was low, a second heat treatment was investigated where the solution treatment was changed to 1350 °C for 6 hrs. This was followed by a water quench, an anneal at 1000 °C for 24 hours.

8.3 Tensile Properties

Two tensile tests at 1100 °C in argon were performed on alloy 28 heat treated at 1350 °C/ 6hrs, and 1000 ° C/24 hrs. The results were 413 MN/m^2 (59.9 ksi) ultimate tensile stress, 9.8% elongation; and 406 MN/m^2 (58.9 ksi) ultimate tensile stress, 10% elongation.

8.4 Stress Rupture Resistance

In the as-cast condition, the stress rupture life of alloy 28 at 1066 °C (1950 °F) and 172 MN/m^2 (25 ksi) is 174 hours for the alloy grown at 0.64 cm/hr (0.25 in/hr), and is in excess of 2511 hours for the alloy grown at 2.54 cm/hr (1 in/hr).

Table 8-4 lists the stress rupture resistance of alloy 28 heat treated at 1350 °C/6 hours and 1000 °C/24 hours and of alloy 29 heat treated at 1300 °C/ 2 hours and 1000 °C/24 hours. Figure 8-3 compares the rupture resistance of heat treated and as-cast alloy 28.

Table 8-4

Stress Rupture Resistance of Co-MC Alloys

Alloy	Heat Treatment °C/hours, Quench	Temp. °C	Stress (MN/m^2)	t_f (hrs)	$*P_{20}$
29	As Solidified	1066	206.7	7.8	50.35
29	As Solidified	927	310	5.5	44.80
29	1300/2, HeQ, 1000/24, HeQ	1066	206.1	13.4	50.92
29	1300/2, HeQ, 1000/24, HeQ	927	310	2.4	44.02
28	1350/6, HeQ, 1000/24, HeQ	1100	193	178.8	55.00
28	1350/6, HeQ, 1000/24, HeQ	1100	193	84.5	54.20

$*P_{20} = T(1.8)\ (20 + \log t) \times 10^{-3}$ (K, hr.)

The microstructure of the fracture region of the two rupture specimens of alloy 28 differed considerably. They are shown in Figure 8-4. The shorter lived specimen manifests a shear-like failure. Figure 8-5 shows the fiber fracture area of a tensile specimen.

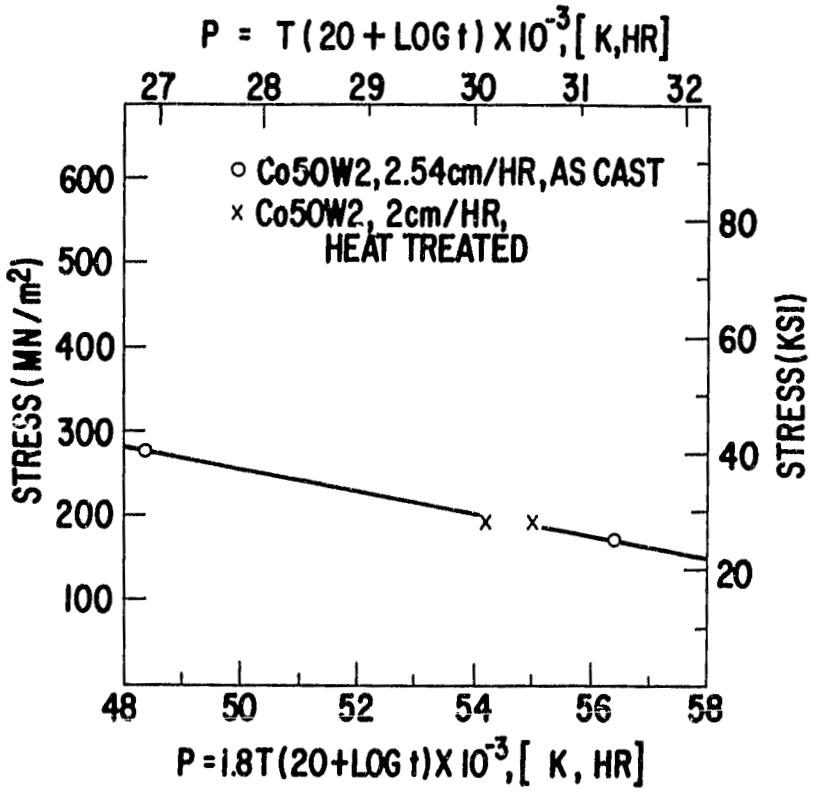

Figure 8-3. Stress Rupture Performance of CoTaC Alloy 28

The carbide fibers in alloy 28 appear to resist dissolution into the matrix, even after a 1350 °C solution anneal. While Co-MC Alloys, whose fibers can be partially dissolved on elevated temperature exposure, can be identified,[28] their lack of thermal cycling resistance precludes their use as base systems.

8.5 Summary

With the potential of other base systems perceived as greater, no further work was performed on the Co-MC system.

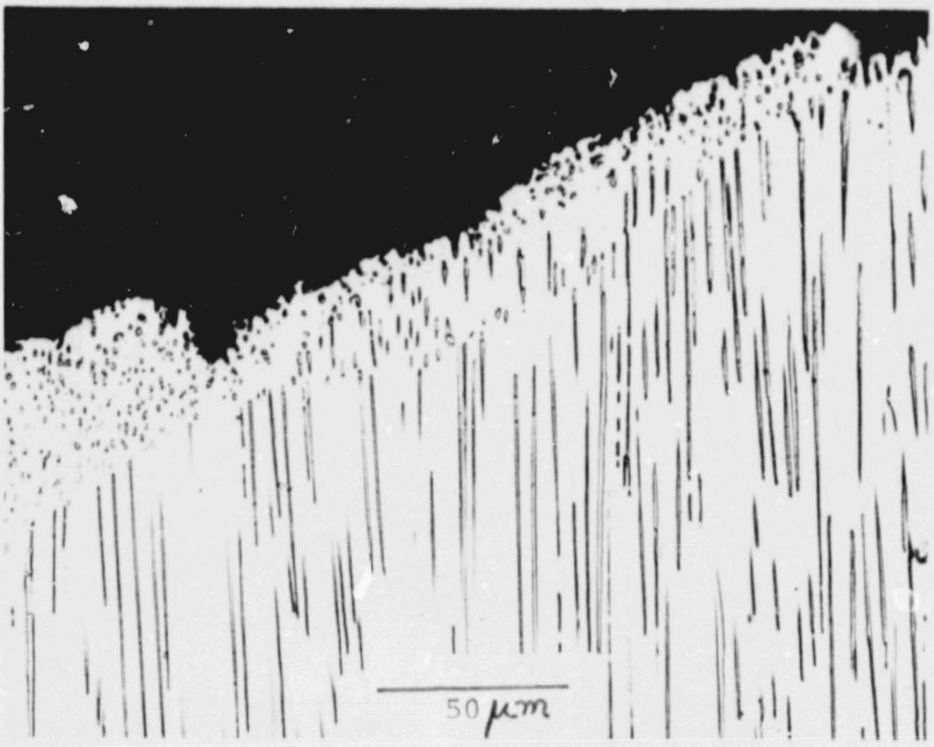

(a)

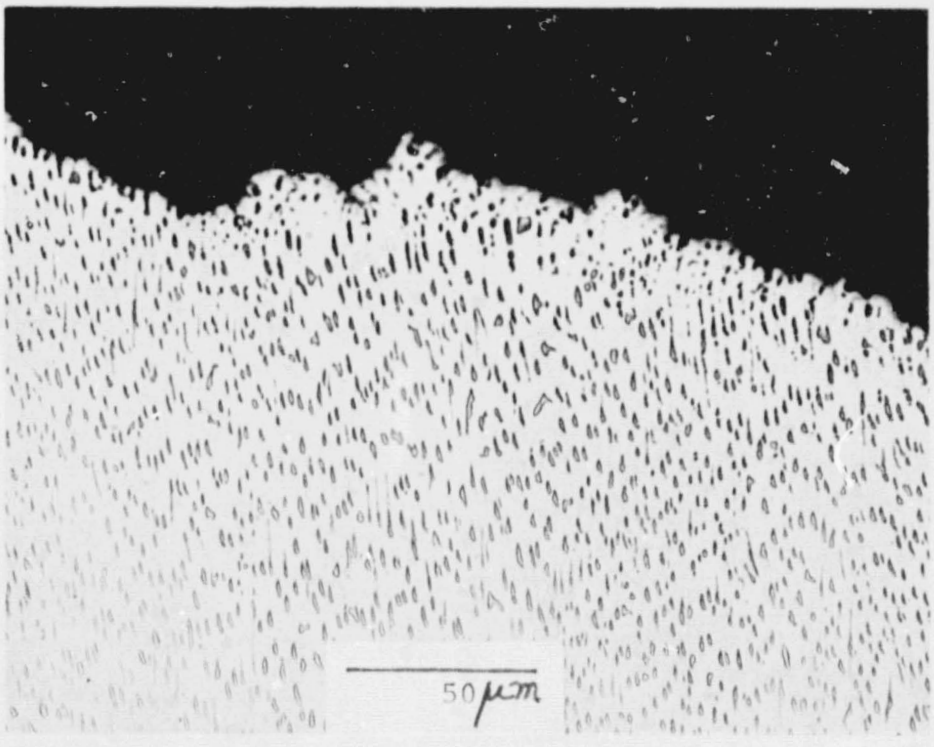

(b)

Figure 8-4. Microstructure of 1100 °C, 193 MPa, Rupture Specimens of CoTaC Alloy 28 at a) 84.5 hours, and b) 178.8 hours

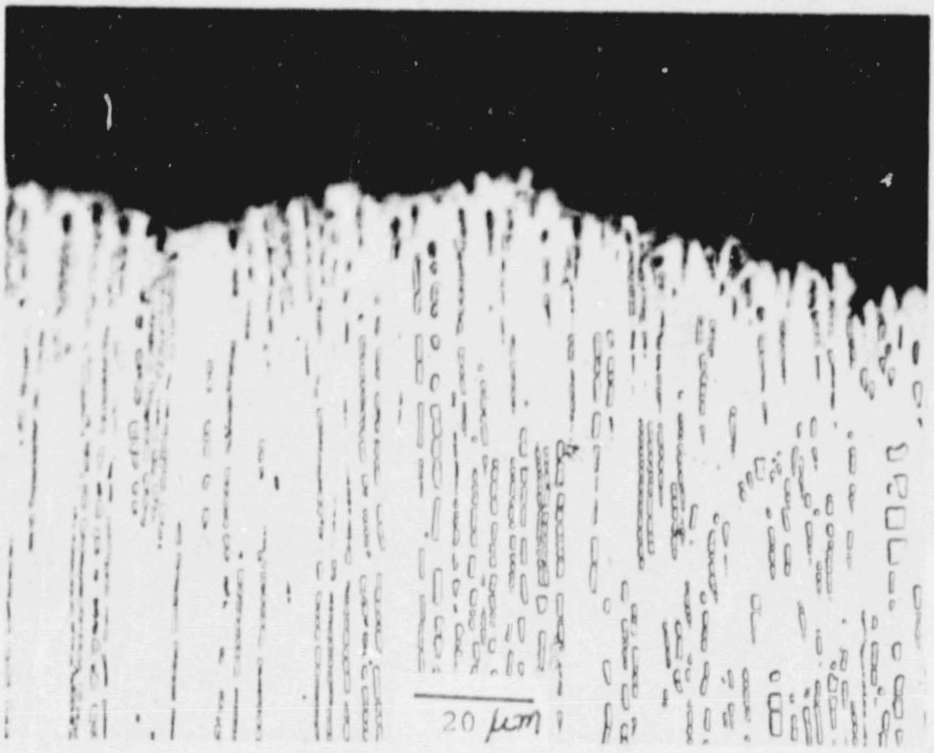

Figure 8-5. Microstructure of CoTaC Alloy 28 Tensile Specimen Fracture

9. THE α-β SYSTEM (J.L. WALTER)

9.1 Background

The basic eutectic consists of 33 a/o Ni, 33 a/o Al, and 34 a/o Cr. This composition may be solidified at rates of up to about 33 cm/hr with continuously increasing tensile strength even though a cell structure occurs at solidification rates below this rate.

The microstructure of the basic system consists of 34% by volume of fine Cr fibers dispersed in a matrix of NiAl.[30,31] The high solidification temperature of the eutectic (1450 °C) provides excellent stability of the structure at temperatures at least up to about 1200 °C and probably at higher temperatures.[32]

The tensile strength at elevated temperatures is respectable. The ultimate tensile strength for a sample solidified at 1.27 cm/hr is 307 MN/m^2 at 1100 °C and 210 MN/m^2 at 1200 °C.[30]

Previous work in this system is well documented in references 30-32. Additions of one or more elements may be made to the basic NiAl-Cr eutectic without destroying the composite structure. Elements such as W, Mo, or V segregate to the Cr phase and, by solid solution, increase the strength of the composite. For instance, the replacement of 5 a/o Cr by 5 a/o Mo increases the tensile strength at 1000 °C by about 40%. Also, the fibrous composite is changed to a lamellar composite with the addition of as little as 0.7 a/o Mo.

Other elements, such as Co and Ti may also be added to partially replace Ni and Al in the NiAl phase. Variations in the ratio of Ni to Al also change the properties and structure of the eutectic. For instance, increasing the Al content relative to the Ni content while maintaining Cr constant, causes the eutectic to be lamellar rather than fibrous.

An interesting result occurs when Fe or Co is added to NiAl-Cr; the microstructure "turns inside out." That is, the NiAl phase, which has very low ductility at temperatures up to about 500 °C, becomes the dispersed rod phase and the ductile CrFe phase becomes the matrix. Such a microstructure, while having the oxidation and corrosion resistance of the original eutectic, should also exhibit improved low temperature ductility compared with the NiAl-Cr system.

9.2 Alloys

Tables 9-1 and 9-2 list the chosen alloy compositions and Table 9-3 describes the ingots solidified.

Table 9-1

Melt Compositions in the α-β System

Atomic Percents

Alloy	Ni	Cr	Al	Fe
30	33	29	33	5
31	31	31.4	31	6.6
32	30.8	31.6	32.7	4.9

Table 9-2

Melt Compositions in the α-β System

Weight Percent

Alloy	Ni	Cr	Al	Fe
30	42	32.7	19.3	6.0
31	39.1	35.0	18.0	7.9
32	39.3	35.6	19.1	6.0

Table 9-3

Characterization of Directionally Solidified α-β Ingots

Alloy	DS Rate (cm/hr)	Length of Aligned Structure (cm)
30	0.64	< 0.3
30	2.0	< 0.3
31	0.64	0.5
32	0.64	1.0
32	2.0	1.0

Alloy 30 was chosen as the base of this system. The composition of the small aligned region of alloy 30 was analyzed by microprobe. This composition was chosen as alloy 31. In a similar manner, the composition of the aligned region of alloy 31 was determined by microprobe analysis and chosen as the composition of alloy 32.

Alloy 32 was directionally solidified at a 2 cm/hr. There is a marked structure improvement over alloy 31. The microstructure shows an initial region, 1 cm in length, of aligned structure, with the remainder of the bar becoming β dendritic.

A second bar of alloy 32 was directionally solidified at 0.64 cm/hr and shows the same microstructure and macrostructure as the bar grown at 2 cm/hr, about 1 cm of aligned structure, and then aligned structure with β-dendrites. Figure 9-1 shows a longitudinal section of the fibrous structure and Figure 9-2, the lamellar structure, 2/3 the length of the ingot.

Figure 9-1. Longitudinal Section of the Fibrous Region in α-β Alloy 32. R = 0.64 cm/hr

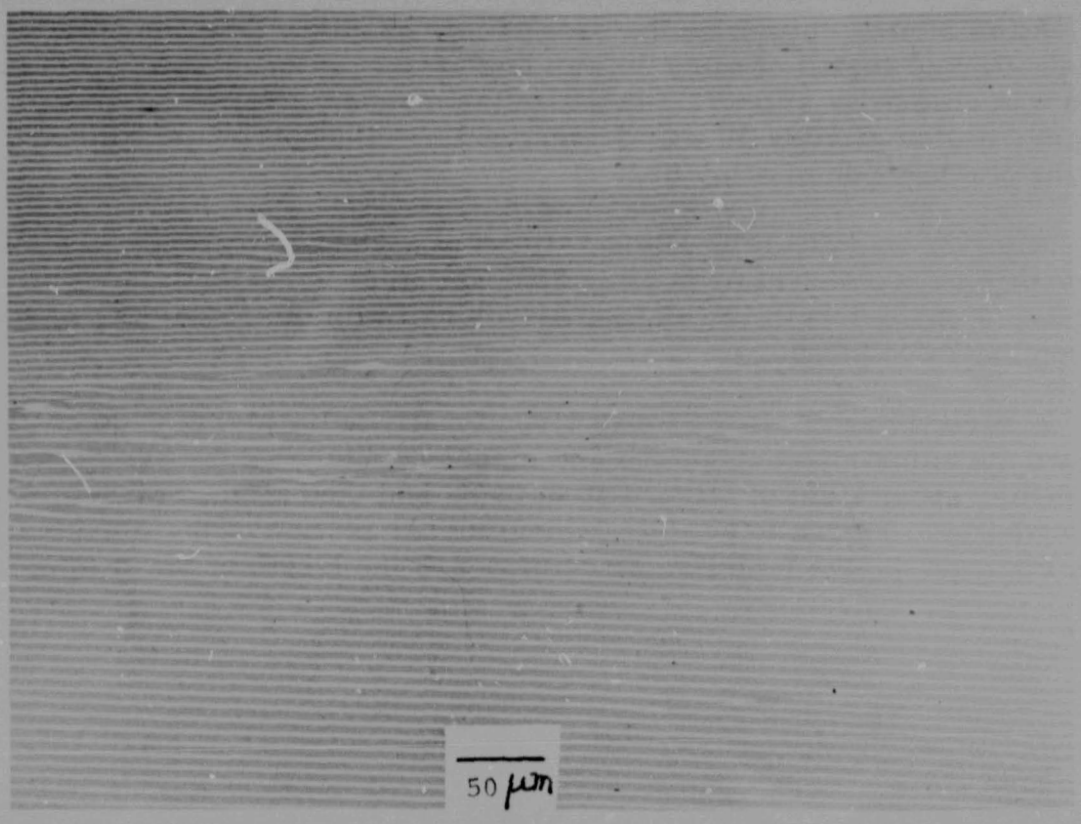

Figure 9-2. Longitudinal Section of the Lamellar Region in α-β Alloy 32. R = 0.64 cm/hr

The development of plate or lamellar regions, rather than the desired rod eutectic, can be due either to:

(1) The high volume fraction of the NiAl rod phase allowing easier diffusion in the solidification process or lamellae, i.e., a rod-lamellar transition due to diffusional kinetics; or

(2) The change in lattice constants of the Cr(Fe) and NiAl phases, which, due to good registry between lamellae, cause this form of growth to be favored.

In either case, the task of producing a fully aligned structure of Cr(Fe) with NiAl rods must not only identify the eutectic point, but also those compositions which minimize the driving forces for lamellar growth.

9.3 Summary

No further alloys were chosen in the α-β system: The Fe additions had not produced sufficient material on which to perform mechanical tests, and had greatly raised the G/R requirement for aligned growth. These conditions combined with the low ductility of the NiAl phase, eliminated the eutectic system as a viable candidate for producing engine components.

An unresolved question is why this system could not be developed with lamellar structures.

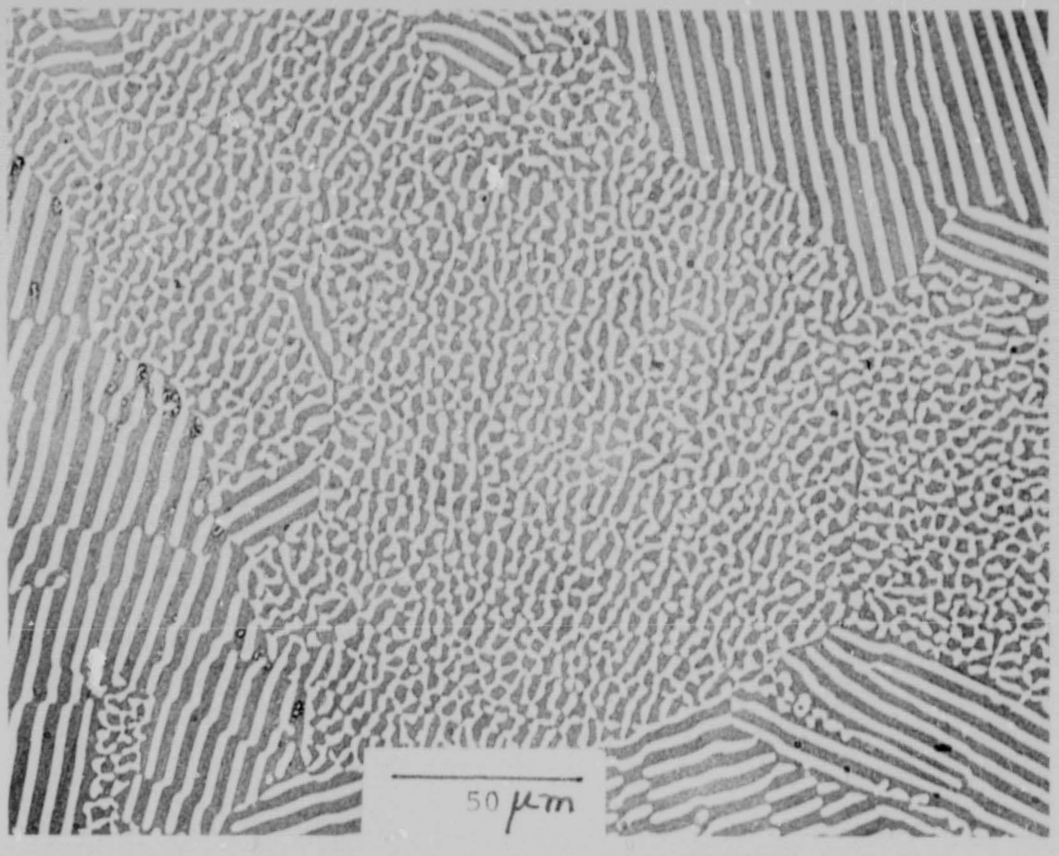

Figure 9-3. Transverse Section of α-β Alloy 32 Showing Fibrous and Lamellar Regions. R = 0.64 cm/hr

10. COMPARISON TO OTHER ALLOYS

Detailed property determinations had been made during the program of alloy 7 (65.8 Ni, 13.2 Al, 21.0 Mo by atomic percents) of the γ/γ'-Mo system, alloy 15 (64.7 Ni, 23.2 Al, 2.8 W, 10.0 Co by atomic percents) of the γ-β system, and alloy 20 (72.0 Ni, 15.0 Al, 4.5 Ta, 5.0 Co, 1.75 V, 0.75 Re, 1.0 W by atomic percents) of the γ/γ' system. These properties were compared with NiTaC-13, a γ/γ' matrix with TaC reinforcing fibers, and γ/γ'-δ, a γ/γ' matrix with Ni_3Nb reinforcing lamellae.

10.1 Background Data for Comparisons

All data on NiTaC-13 are from material grown at 0.64 cm/hr. Data on γ/γ'-δ are from rates as indicated. The tensile data are from reference 15 and unpublished General Electric research for NiTaC-13 and references 33 and 34 for γ/γ'-δ. The longitudinal shear strength data are from unpublished General Electric research for NiTaC-13 and references 34 and 35 for γ/γ'-δ. The stress rupture data are from reference 15 and unpublished General Electric research for NiTaC-13 and from references 33 and 35 for γ/γ'-δ. All cyclic oxidation data are from unpublished General Electric research.

10.2 The γ/γ'-Mo System (M.F. Henry)

Figure 10-1 compares the longitudinal tensile strength of alloy 7 as a function of temperature to γ/γ'-δ and NiTaC-13. The three element γ/γ'-Mo alloy is competitive with those two eutectic alloys up to 900 °C and is slightly weaker at higher temperatures. Two specimens of alloy 7 at 3 cm/hr gave ultimate tensile of 487 and 503 MN/m^2 at 1100 °C. This compares to values of 450 MN/m^2 for alloy 7 at 2 cm/hr, 530 MN/m^2 for NiTaC-13 at 0.64 cm/hr and 550 MN/m^2 for γ/γ'-δ aligned at 3 cm/hr. In this comparison the simple three element γ/γ'-Mo alloy is considered excellent.

Figure 10-2 compares the transverse tensile strength of alloy 7 as a function of temperature to NiTaC-13 and γ/γ'-δ. The γ/γ'-Mo alloy is equivalent to or better than the two other eutectics. To date, only three temperatures have been used for transverse tensile testing on alloy 7. The minimum transverse tensile ductility was 2.8% elongation and 4.7% reduction in area at room temperature.

Figure 10-3 compares the longitudinal shear strength of alloy 7 as a function of temperature to NiTaC-13 and γ/γ'-δ. The longitudinal shear strength of this alloy is probably as good as or better than that of the two other eutectics.

Figure 10-4 compares alloy 7 to NiTaC-13 and γ/γ'-δ on a Larson-Miller parametric plot for longitudinal stress rupture resistance. It is felt that the most appropriate comparison for γ/γ'-δ is to material aligned in blade type gradients, that is 0.64 cm/hr. Alloy 7 at 2 cm/hr is essentially equivalent to γ/γ'-δ in longitudinal stress rupture resistance. In the comparison of longitudinal stress rupture resistance, γ/γ'-Mo is considered excellent because alloy 7 is still a simple three element eutectic.

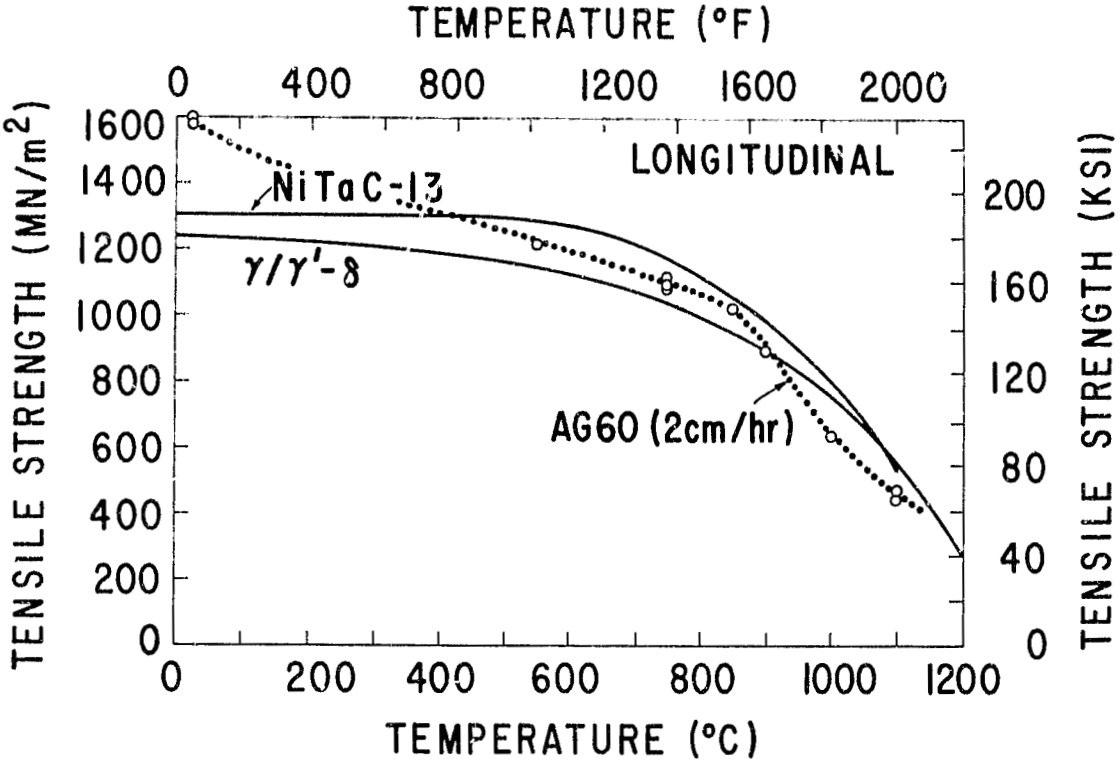

Figure 10-1. Comparison of Longitudinal Tensile Strength of γ/γ'-Mo Alloy 7 (AG60), NiTaC-13 and γ/γ'-δ (3 cm/hr)

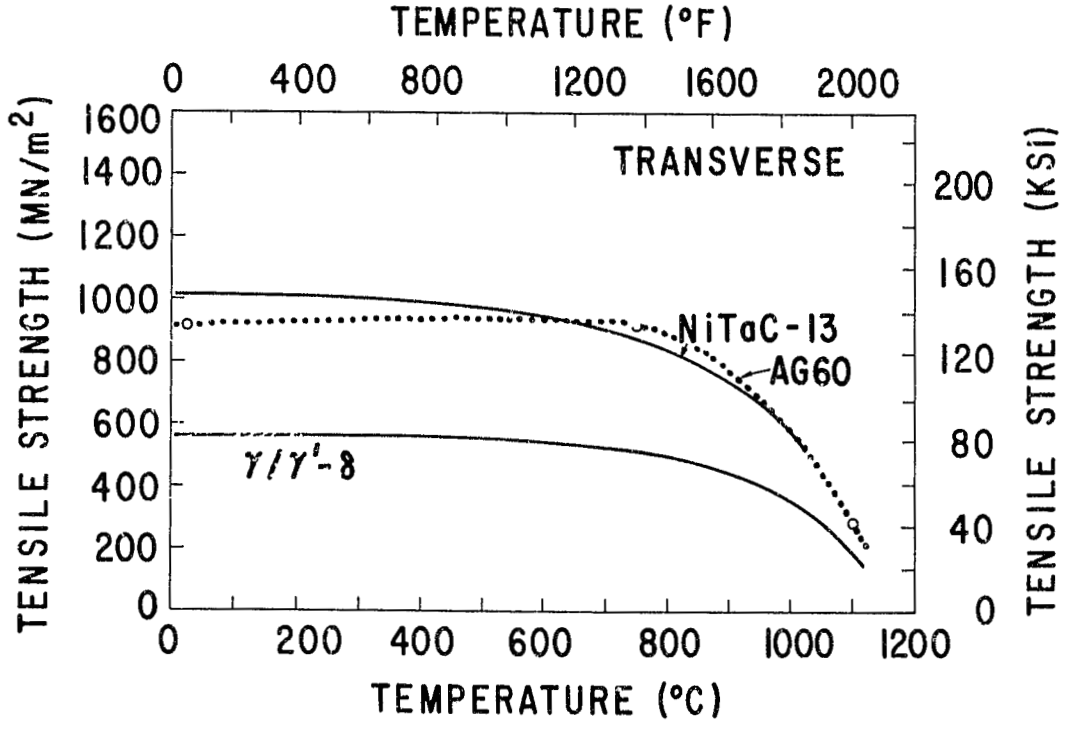

Figure 10-2. Comparison of Transverse Tensile Strength of γ/γ'-Mo Alloy 7 (AG60), NiTaC-13 and γ/γ'-δ (3 cm/hr)

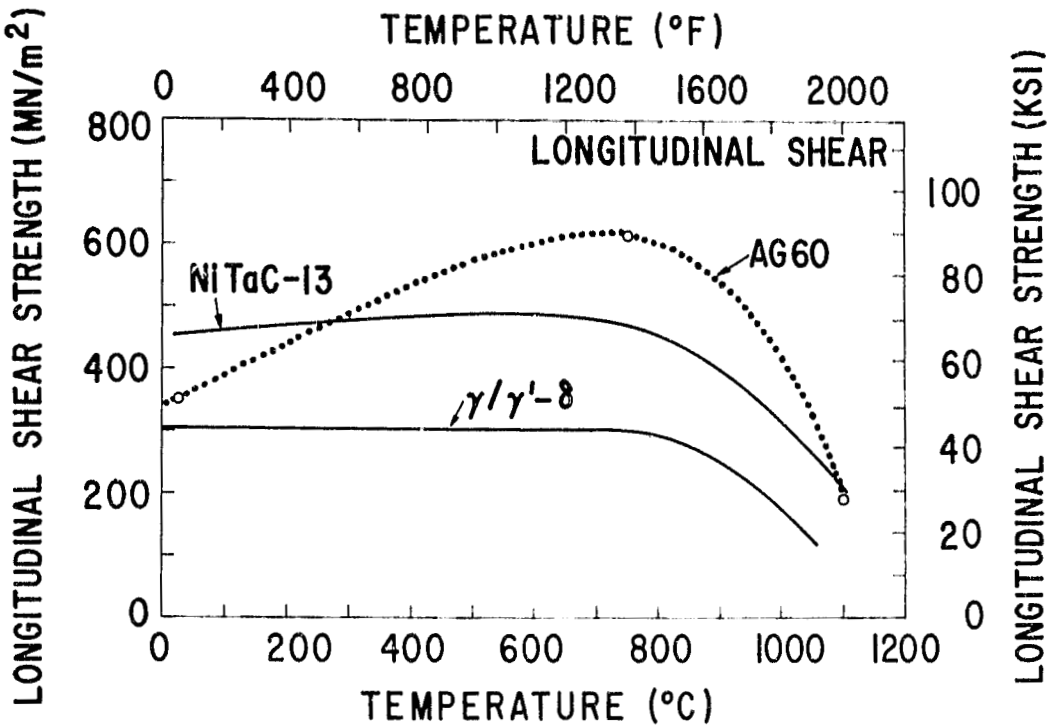

Figure 10-3. Comparison of Longitudinal Shear Strength of γ/γ'-Mo Alloy 7 (AG60), NiTaC-13 and γ/γ'-δ (3 cm/hr)

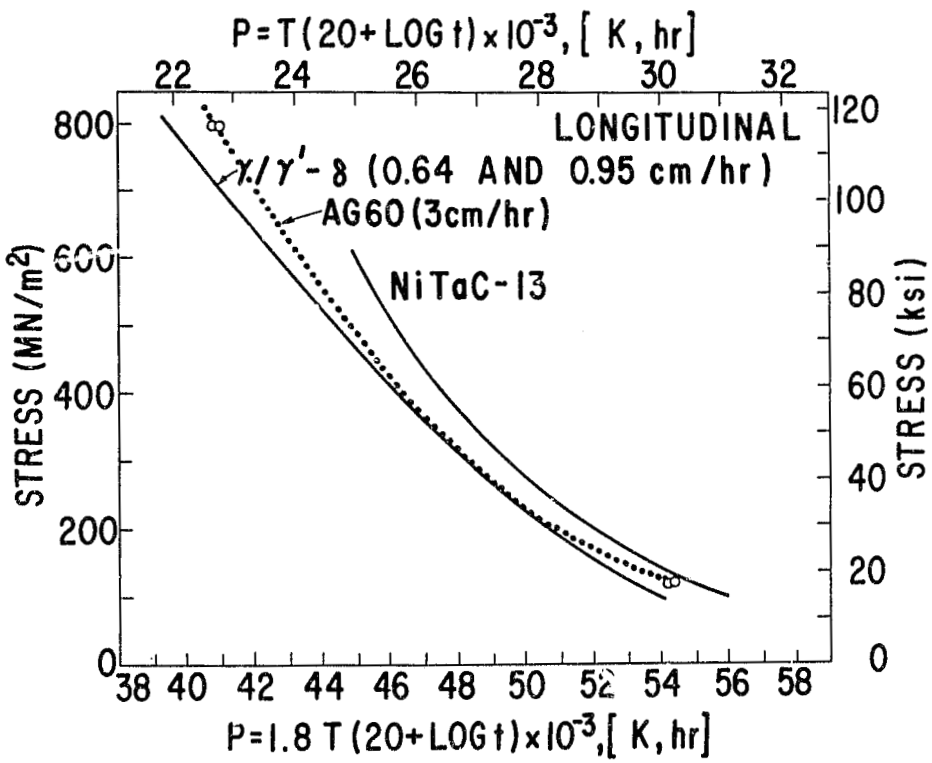

Figure 10-4. Comparison of Longitudinal Stress Rupture Resistance of γ/γ'-Mo Alloy 7 (AG60), Aligned at 2 cm/hr, NiTaC-13 and γ/γ'-δ Aligned at 0.64 and 0.95 cm/hr

Figure 10-5 compares the transverse stress rupture resistance of alloy 7 to NiTaC-13 and γ/γ'-δ on a Larson-Miller parametric plot. The transverse rupture resistance of alloy 7 is superior below 900 °C and competitive above 900 °C.

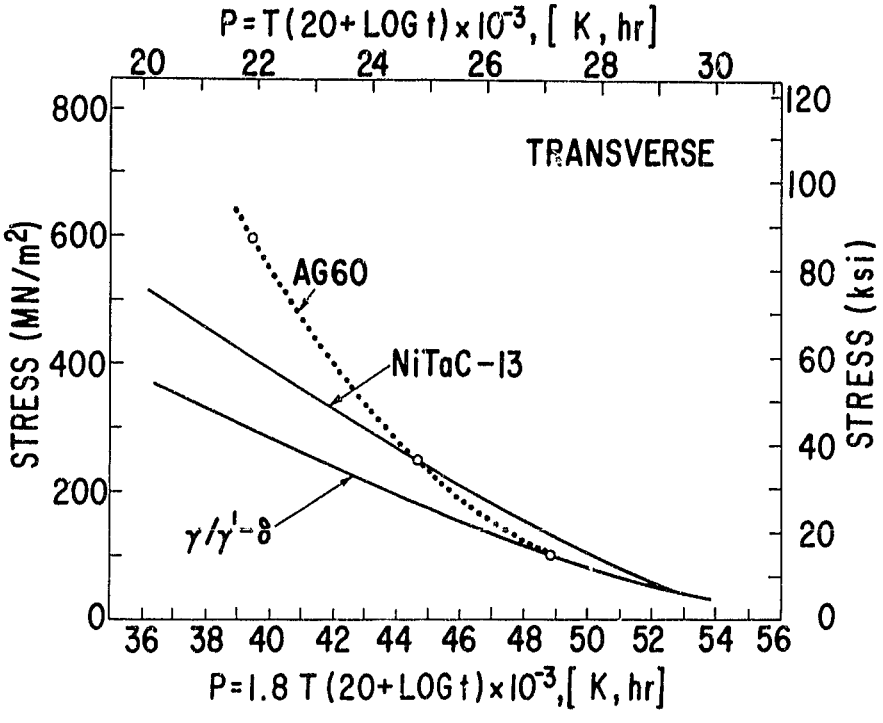

Figure 10-5. Comparison of Transverse Stress Rupture Resistance of γ/γ'-Mo Alloy 7 (AG60), NiTaC-13 and γ/γ'-δ (0.64 and 3 cm/hr)

Figure 10-6 compares the cyclic oxidation resistance of alloy 7 at 1100 °C to NiTaC-13, γ/γ'-δ (6 Cr), René 80, and Hastelloy-X. The alloy is essentially equivalent to NiTaC-13. This is not considered a serious drawback since alloy 7 is a simple three element composition. Unpublished General Electric research has shown that additions of chromium may substantially enhance the cyclic oxidation resistance. Also, coatings would usually be applied to engine parts operating at such elevated temperatures.

10.3 The γ-β System (M. R. Jackson)

Figures 10-7 and 10-8 compare longitudinal and transverse tensile properties of alloy 15 of the γ-β system to γ/γ'-δ and NiTaC-13. For both orientations the γ-β alloys fall well below the comparison systems, but the γ-β system approaches the others more closely as temperature increases. A vane alloy, MARM-509 is also plotted in Figure 10-7 for comparison. The γ-β alloys are much stronger than MARM-509 over the entire range of test temperatures. In regard to the transverse properties, it should be remembered that the data for γ-β plotted are for a lamellar structure. Properties for fibrous γ-β have not been measured in the transverse orientation.

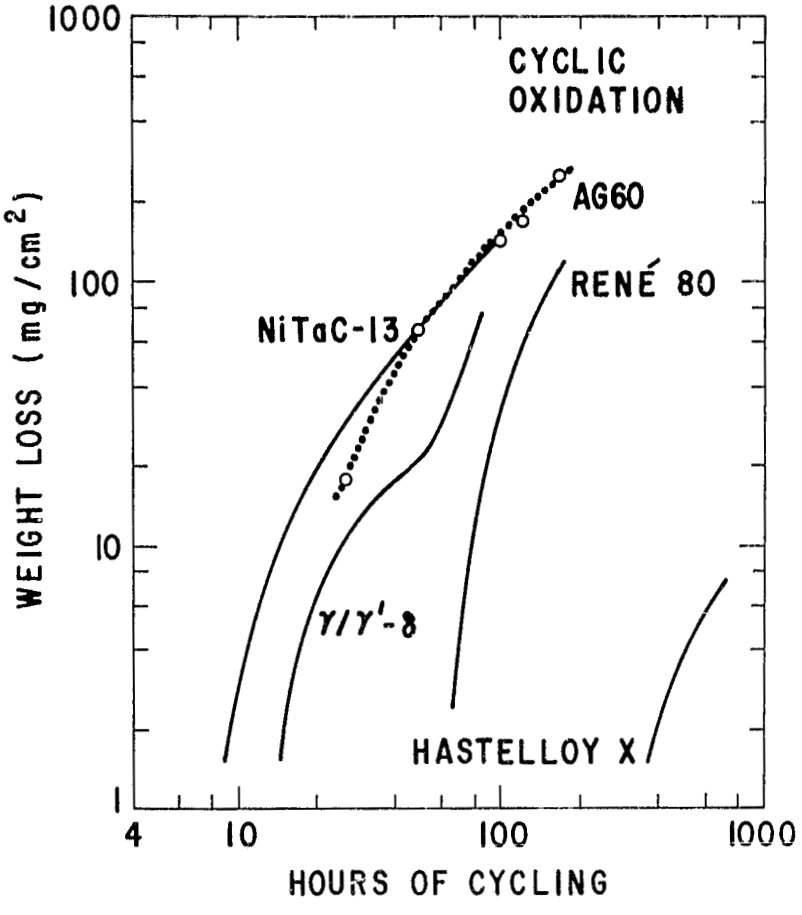

Figure 10-6. Comparison of Cyclic Oxidation Resistance at 1100 °C of γ/γ'-Mo Alloy 7 (AG60) and Several Other Alloys

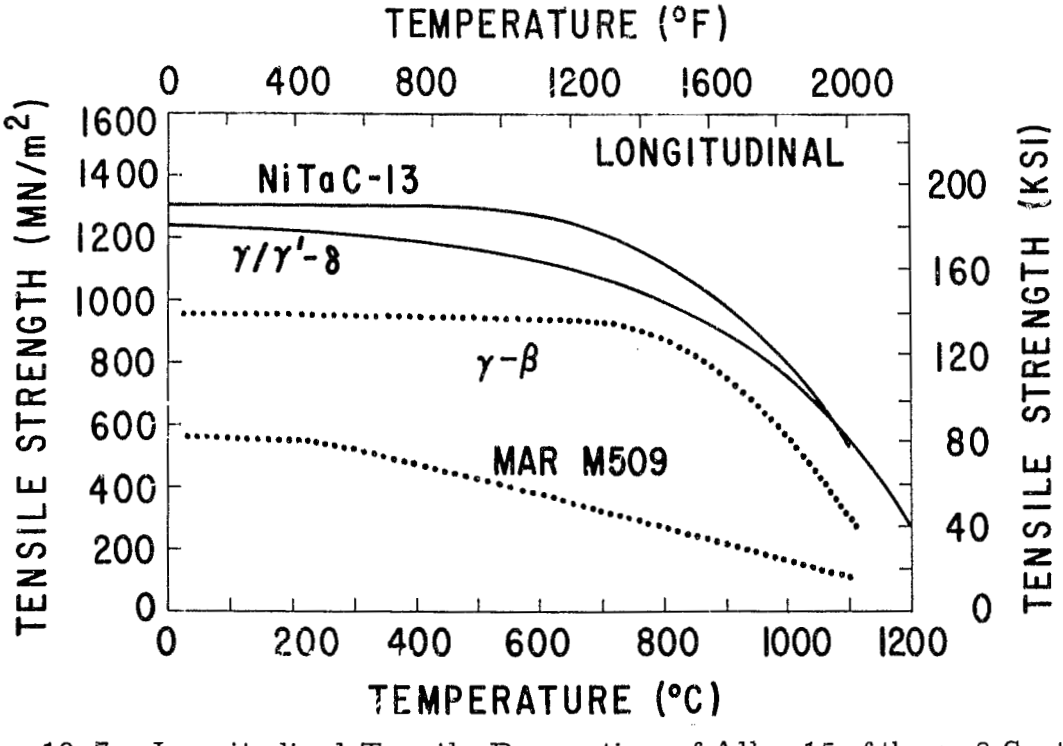

Figure 10-7. Longitudinal Tensile Properties of Alloy 15 of the γ-β System compared to γ/γ'-δ (3 cm/hr), NiTaC-13 and MAR M509

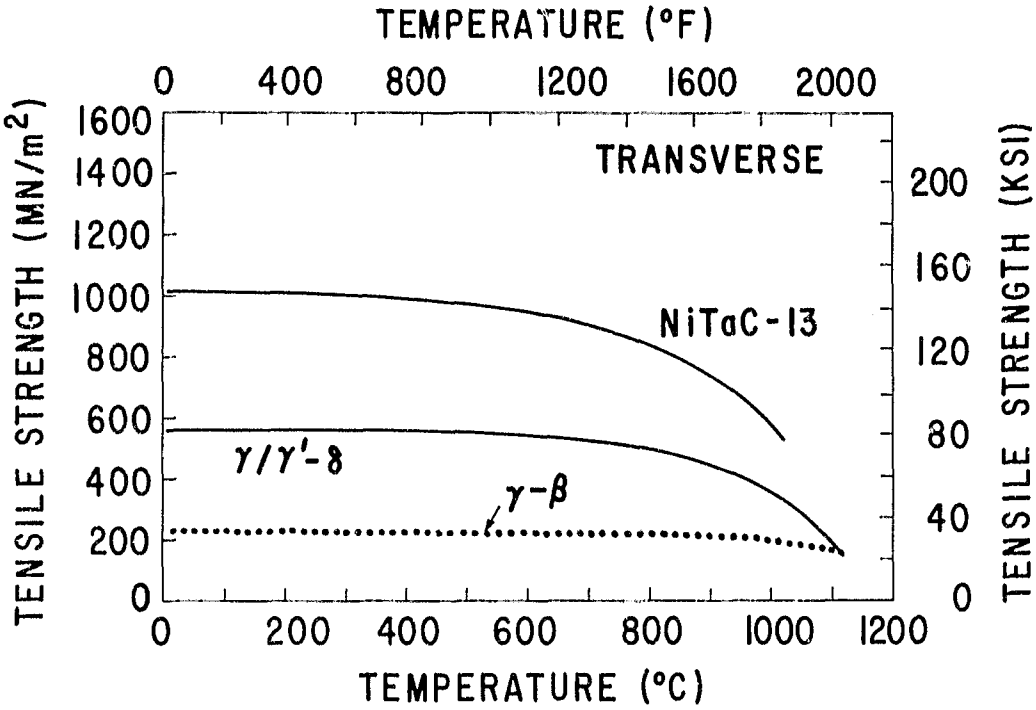

Figure 10-8. Transverse Tensile Properties of Alloy 15 of the γ-β System compared to γ/γ'-δ (3 cm/hr) and NiTaC-13

Figure 10-9 compares the rupture properties of γ-β to those of the γ/γ'-δ and NiTaC-13 eutectics. The lamellar structure falls approximately six parameters below the comparison eutectics, while the fibrous structures are three to four parameters below those systems. The fibrous properties are essentially equivalent to IN-738. Both lamellar and fibrous γ-β are superior to current vane alloys X-40 and MARM-509.

Figure 10-10 illustrates the longitudinal shear strength of the lamellar γ-β alloy compared to γ/γ'-δ and NiTaC-13. The poor behavior of γ-β is a result of the weak grain boundaries in the alloy. No properties have been measured for the fibrous structures.

Figure 10-11 shows oxidation resistance in 1100 °C cyclic exposure. The fibrous alloy number 18, which contains V and Re, is much poorer than the lamellar alloy number 15. However, even the fibrous alloy is much superior to to γ/γ'-δ and NiTaC-13. The lamellar structures are superior to Hastelloy X for times in excess of 400 hours.

The γ-β alloy was much superior to the other alloys in cycling to 1150 °C. An identical ordering of alloys was observed in cyclic oxidation at 1100 °C.

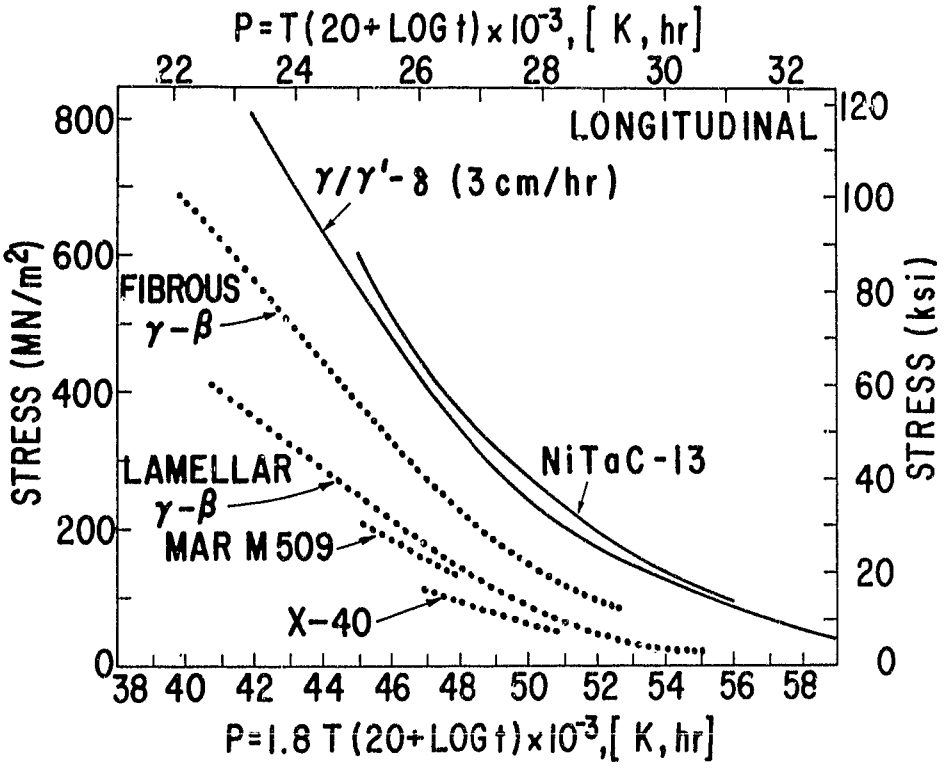

Figure 10-9. Rupture Behavior of the γ-β Alloys (Lamellar = Alloy 15; Fibrous = Alloy 18) Compared to γ/γ'-δ and NiTaC-13, and Two Co-Base Superalloys

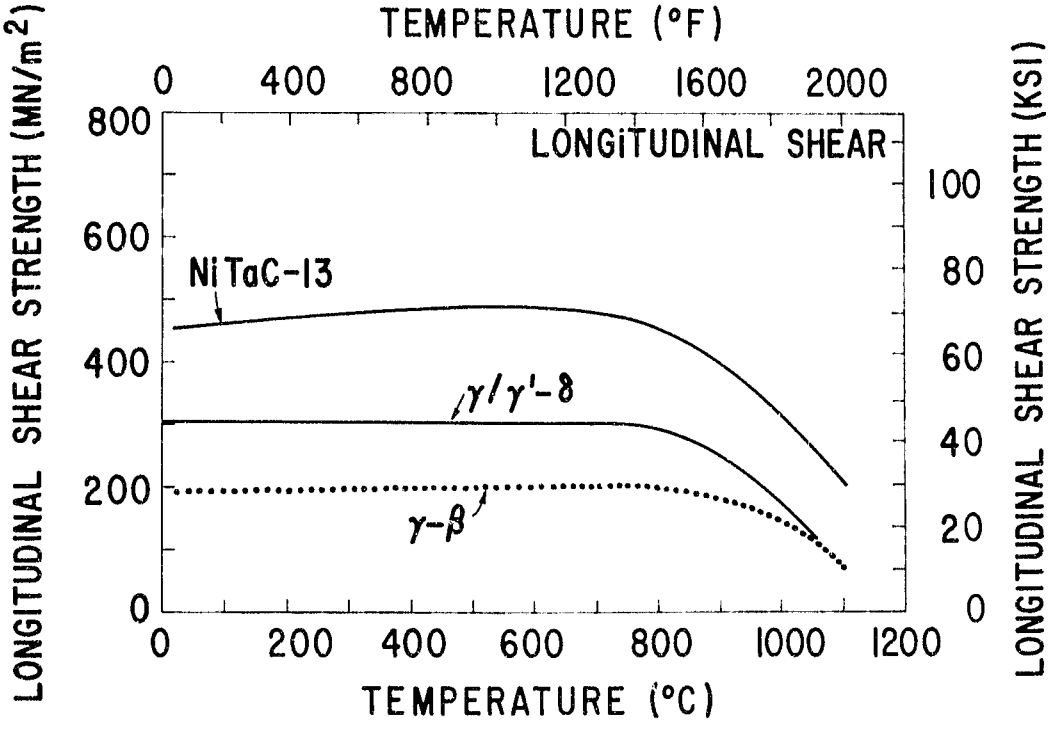

Figure 10-10. Longitudinal Shear Strength of Lamellar γ-β Alloy Number 15 Compared to γ/γ'-δ (3 cm/hr) and NiTaC-13

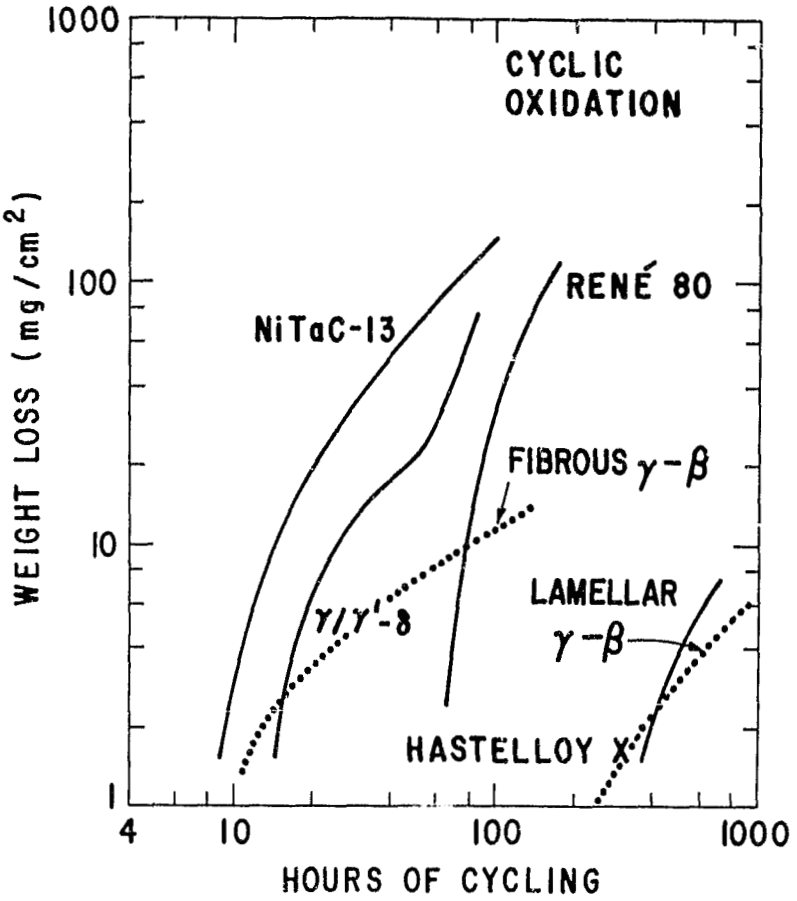

Figure 10-11. Oxidation Resistance in 1100 °C Cyclic Exposure for the γ-β System (Lamellar = Alloy 15; Fibrous = Alloy 18), and Several Other Alloys

10.4 The γ-γ' System (M. R. Jackson)

Figures 10-12 and 10-13, respectively, compare longitudinal and transverse tensile properties of alloy 20 of the γ-γ' system to NiTaC-13 and γ/γ'-δ. In both orientations γ-γ' falls well below the comparison alloys, but the differences become smaller with increasing temperature. Figure 10-14 compares rupture properties. The γ-γ' alloys alloys are about 4-5 parameters below NiTaC-13 and γ/γ'-δ at stresses greater than 200 MN/m^2. However, the stress/parameter relation for γ-γ' becomes very shallow below that stress, and the curve for γ-γ' crosses the comparison alloys at approximately 110 MN/m^2. Figure 10-15 compares longitudinal shear properties for γ-γ', γ/γ'-δ, and NiTaC-13. Properties are much inferior to NiTaC-13 at all temperatures, but are superior to γ/γ'-δ at 1100 °C. In 1100 °C cyclic oxidation (Figure 10-16) γ-γ' is better than NiTaC-13 and γ/γ'-δ, as well as the super-alloy René 80. Oxidation resistance is intermediate between Hastelloy X and René 80, and varies with Al content.

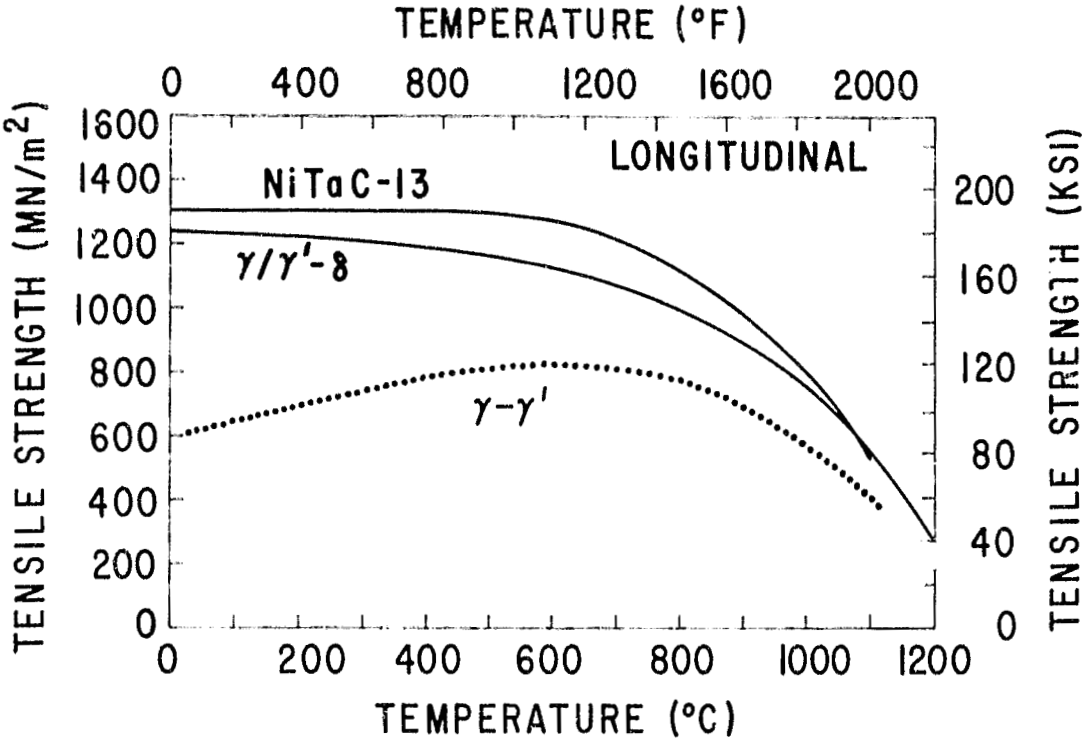

Figure 10-12. Longitudinal Tensile Properties of the γ-γ' Alloy 20 Compared to γ/γ'-δ (3 cm/hr) and NiTaC-13

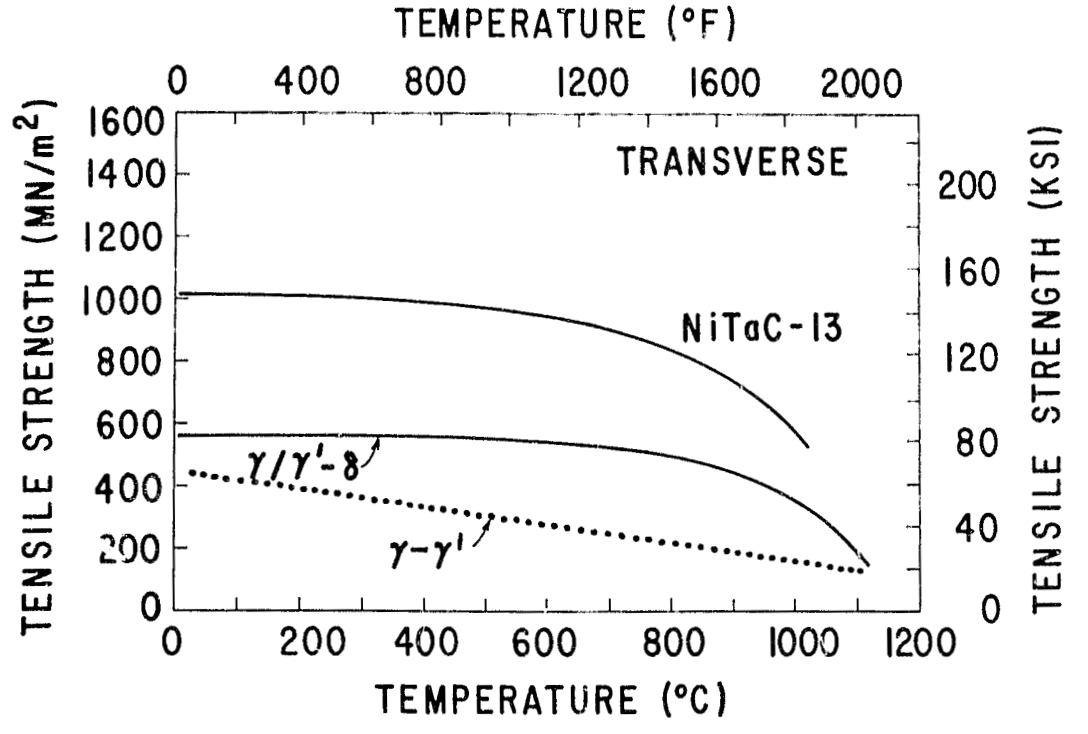

Figure 10-13. Transverse Tensile Properties of the γ-γ' Alloy 20 Compared to γ/γ'-δ (3 cm/hr) and NiTaC-13

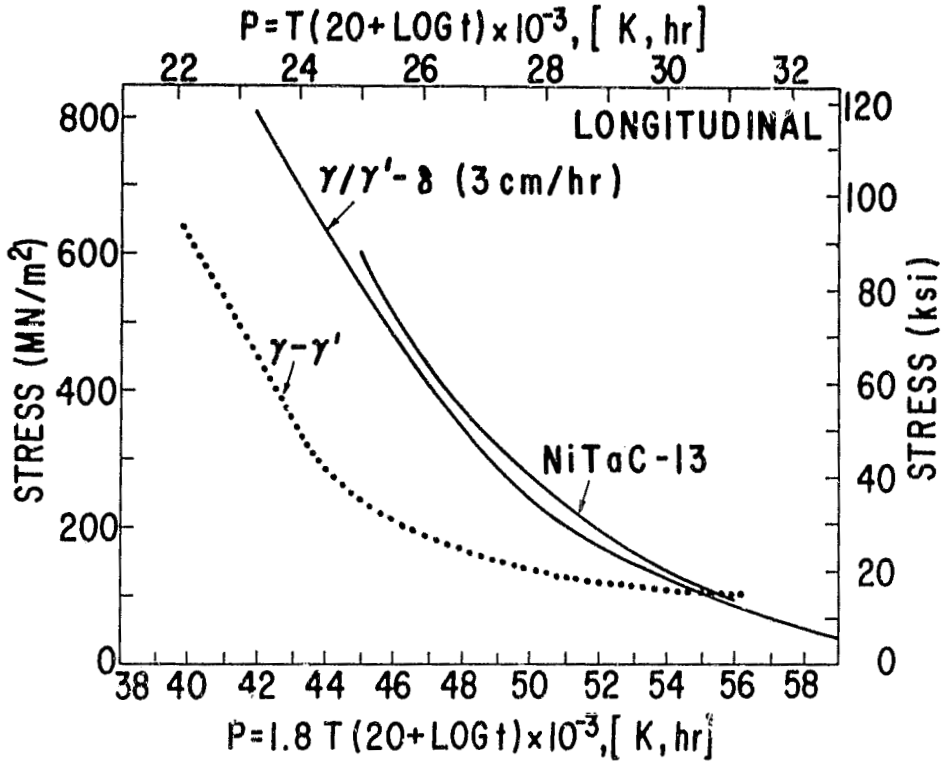

Figure 10-14. Rupture Behavior of the γ-γ' Alloy 20 Compared to γ/γ'-δ and NiTaC-13

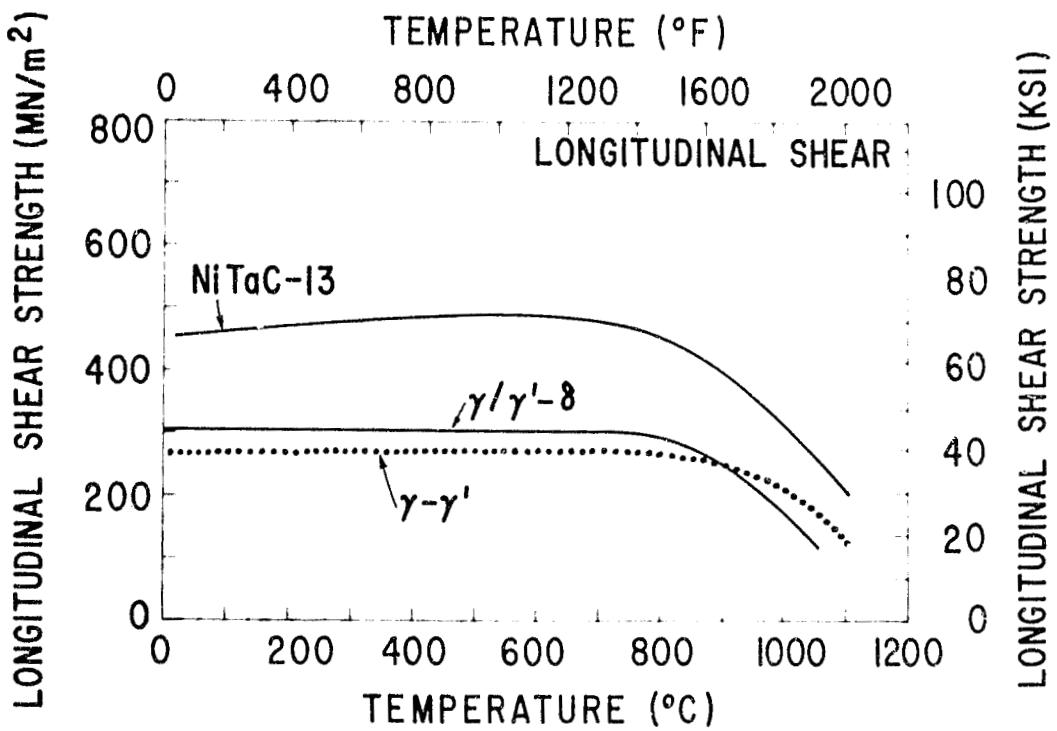

Figure 10-15. Longitudinal Shear Properties of the γ-γ' Alloy 20 Compared to γ/γ'-δ (3 cm/hr) and NiTaC-13

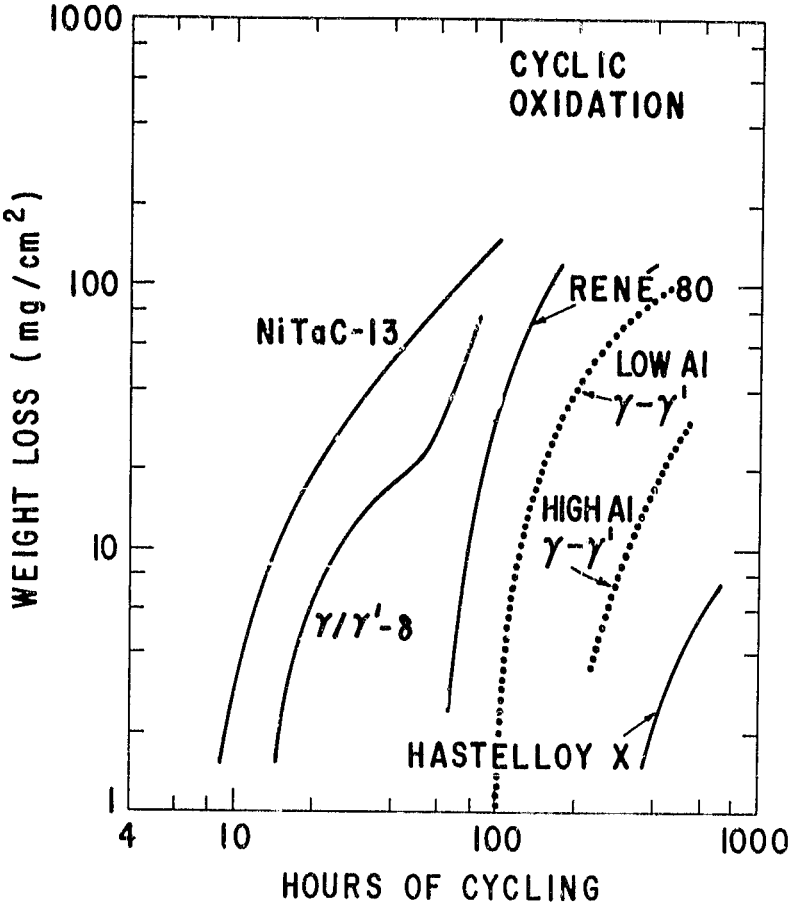

Figure 10-16. Oxidation Resistance in 100 °C Cyclic Exposure for γ-γ' (Low Al = Alloy 20; High Al = Alloy 21), and Several Other Alloys

11. CONCLUSIONS

This program involved an exploratory examination of six high temperature eutectic superalloys systems for application as directionally solidified turbine blades. The objective was to identify at least one new alloy for potential use in jet aircraft engine turbine blades. That objective has been accomplished.

The first phase of this program consisted of exploratory examination of six eutectic alloy system bases, each having at least one ductile phase. Composition and/or processing parameter variations were made and alloys which achieved well aligned structures were tested for density, elevated temperature tensile strength, stress rupture resistance, and thermal cycling resistance. Alloys from the three most promising systems were then subjected to detailed property evaluations which consisted of determining:

- longitudinal tensile strength and ductility
- transverse tensile strength and ductility
- longitudinal shear strength
- longitudinal stress rupture resistance
- transverse stress rupture resistance
- thermal cycling resistance
- cyclic oxidation resistance
- mold/metal reactivity

The three major conclusions of this study are:

1. The γ/γ'-Mo system has potential as a high pressure turbine blade material. Research on this system should continue and should expand from the exploratory nature of this contract to encompass serious alloy development and engineering evaluation.

2. The γ-β system has potential as a vane material. Research on this system should address the critical question of thermal fatigue resistance.

3. The γ-γ' system shows promise for developing into a potential turbine blade material. Exploratory research to evaluate that potential should continue.

The six systems and a brief review of results follow

A. γ/γ'-Mo: a system consisting of a two phase matrix of a face centered cubic Ni-base solid solution γ and an ordered $L1_2$ phase γ' based on Ni_3Al; and body centered cubic α reinforcing fibers, primarily of Mo.

All the alloys examined here have been shown to be γ-Mo eutectics which subsequently undergo γ' precipitation in the γ matrix. The matrix and fibers both solidify with a <100> growth direction. The balance of strength and ductility in the sample alloys examined to date is excellent. The optimum aluminum content for a three element Ni-Al-Mo alloy has been identified for this balance as approximately 13 a/o. Research on this contract and on separate General Electric funded studies have shown that the Ni-Al-Mo system may be alloyed with up to seven additional elements simultaneously and still yield a structure of γ-Mo coupled growth with subsequent γ' precipitation at lower temperatures.

The γ/γ'-Mo system has excellent tensile strength in the longitudinal and transverse directions. The ductilities in the transverse direction are 2% or greater. The longitudinal shear strength of this system is excellent and exceeds 40% of the longitudinal tensile strength over the range of blade operating temperatures.

The stress rupture resistance of the γ/γ'-Mo system lies between that of γ/γ'-δ and NiTaC-13. This is considered very encouraging for the simple three element system. It is felt that the creep resistance can be further enhanced by the addition of elements selected to strengthen all three phases. In comparison to the original NASA goals for this program (1000 hours life at 700 MN/m^2 and 750 °C, and 1000 hours life at 140 MN/m^2 and 1100 °C), the most improvement is needed at high temperature, i.e., the 1100 °C regime. The transverse stress rupture resistance of this system is considered slightly superior to NiTaC-13 and far superior to γ/γ'-δ. The transverse rupture ductility is far superior to γ/γ'-δ or NiTaC-13.

The cyclic oxidation resistance of the simple three element Ni-Al-Mo alloys is essentially equivalent to NiTaC-13 and γ/γ'-δ. The addition of 3 a/o Cr has made the system superior to René 80, but still not as good as Hastelloy X. Preferential oxidation of Mo-fibers did not occur at 750 °C or 1100 °C. It is the current best judgement that this system will need an oxidation resistant coating for operation at 1100 °C (2012 °F).

This system is considered more processable than γ/γ'-δ or NiTaC-13. Values of (G/R)-critical are equal to or better than either of those two systems. Metal ceramic reactivity tests reveal that the current GE Al_2O_3/SiO_2 mold system will probably be adequate for this system.

B. γ-β: a system consisting of a face centered cubic γ solid solution matrix of Ni, Cr, Fe, Co, W, and Al; and a CsCl β structured reinforcing phase of substoichiometric (Ni, Co or Fe)Al.

The alloys of Ni, Al, Co and W have excellent resistance to oxidation at temperatures of 750 and 1150 °C. Mechanical properties are virtually unaltered by cycling to 1150 °C. The tensile and rupture behavior, solidification temperature and densities suggest these materials may be successful

improvements on turbine vane alloys such as X-40 or MAR M-509. The main limitation of the lamellar structure appears to be grain boundary strength, particularly in thermal fatigue. As part of the present program, a fibrous γ-β alloy was prepared. The longitudinal properties are significantly improved over those of the lamellar alloys and of conventional vane materials. Furthermore, the fibrous alloys have good flexibility for further alloy modification, and it may be possible to develop turbine blade properties in these eutectics at solidification rates in excess of 2 cm/hr. It remains to be determined if boundary strengths for the fibrous alloys are sufficient for blade and/or vane applications.

C. γ-γ': a system consisting of a face centered cubic matrix solid solution of Ni, Co, Re, W and V; and reinforcing fibers of an ordered $L1_2$ γ' phase based on Ni_3Al.

Alloys in this system have high temperature mechanical properties comparable to NiTaC-13 and γ/γ'-δ. Oxidation resistance is somewhat better than those eutectics, solidification temperatures are within the range of conventional superalloys, but densities are somewhat higher than desirable. There seems to be little advantage of high Ta to Al ratio alloys in terms of strength, and the high Al alloys are superior in terms of oxidation and density. The alloys are difficult to align at 2 cm/hr., and there are indications that master melt composition control will be more important than for NiTaC-13 and γ/γ'-δ. Grain boundary weakness is the alloy system's most obvious problem. Work is needed to improve grain boundary strength and to determine if this improvement will lead to better intermediate temperature strength. The stability of mechanical properties in thermal cycling to 1150 °C is excellent, and no mold/metal reaction was found in the test conducted.

D. γ-M_2Ta: a system consisting of a face centered cubic γ solid solution matrix of Ni, Fe, Cr and Ta; and a hexagonal M_2Ta reinforcing phase.

This system is capable of exceptional strengths at 23 °C and 750 °C. Oxidation resistance is superior to the γ/γ'-δ and NiTaC-13 alloys. However, the system has many limitations: high density, low solidification temperature, extreme difficulty in achieving fully aligned microstructures in gradients typical of blade casting furnaces, lack of appreciable ductility over a wide temperature range. The probability is low for producing useful alloys in this system.

E. Co-MC: a system consisting of a face centered cubic solid solution matrix phase of Co, Ni and W precipitation strengthened by TaC; and a face centered cubic TaC reinforcing phase.

The high temperature mechanical properties of the base system are excellent. It was anticipated that a precipitation heat treatment by which MC particles were distributed within the matrix would enhance low temperature

mechanical properties. It was found that some slight precipitation could be caused, but its effects on properties were inconclusive. Large scale precipitation of MC was not achieved because the Co-MC alloys have been designed to minimize thermal cycling degradation caused by solutioning and reprecipitation of MC in thermal cycles where the maximum temperature approaches 1100 °C.

F. α-β: a system consisting of a body centered cubic α solid solution matrix of Cr and Fe and a CsCl β structured reinforcing phase based in NiAl.

The α-β system NiAl-Cr has a microstructure of Cr rods in a NiAl matrix. It was anticipated that if the structure was reversed by Fe additions -- NiAl rods in a Cr(Fe) matrix -- improvements in ductility would result. Iron additions resulted in reversed structure region, but a competing microstructure, lamellar, tended to predominate.

ACKNOWLEDGMENTS

The experimental contributions of Arthur J. Peat, P. Bruce Nelson and William E. Rollins were vital to the success of this study.

We are also indebted to the following contributors to this study: S. F. Bartram, W. J. Baxter, M. G. Benz, M. F. Ciccarelli, P. L. Dupree, M. F. X. Gigliotti, M. E. Gill, F. S. Halsey, M. Heiberger, E. F. Koch, M. D. McConnell, W. F. Moore, C. P. Palmer, J. R. Rairden, A. M. Ritter, T. F. Sawyer, G. E. Stebbins, P. S. Svec, and D. A. Woodford.

REFERENCES

1. Hansen, M.; and Anderko, K.: The Constitution of Binary Alloys. McGraw-Hill, New York, New York, 1958.

2. English, J.J.: Binary and Ternary Phase Diagrams of Columbium, Molybdenum, Tantalum, and Tungsten. DMIC Report 183, Defence Materials Information Center, Columbus, 1963.

3. Ashbrook, R.L.: Directionally Solidified Composite Systems under Evaluation. Specialists Meeting on Directionally Solidified In-Situ Composites. E.R. Thompson and P.R. Sahm, eds., AGARD-CP-156, 1974, pp. 93-115.

4. Thompson, E.R.; and Lemkey, F.D.: Directionally Solidified Eutectic Superalloys. M11054-2, United Aircraft Corporation, 1973.

5. Henry, M.F.: Precipitation of γ' in γ-α (Ni-Al-Mo) Eutectics. Scripta Met., vol. 10, 1976, pp. 955-957.

6. Lemkey, F.D.: Development of Directionally Solidified Eutectic Nickel and Cobalt Alloys. NADC-76115-30, 1975.

7. Cline, H.E.: The Mechanical Properties of theCoAl-Co Eutectic. TMS-AIME, vol. 239, 1967, pp. 1906-1916.

8. Hubert, J.C.; Kurz, W.; and Lux, B: Morphologie de l'eutectique orienté Co - CoAl et influence d'une addition de nickel. J. Crystal Growth, vol. 18, 1973, pp. 241-249.

9. Mollard, F.R.; and Lux; B: High Temperature Oxidation Behavior of Directionally solidified Ni_3Al-Ni_3Ta, Ni-Ni_3Al-Ni Ta and (Co, Ni) - (Co, Ni) Al Eutectics. Proceedings of the Second Conference on In-Situ Composites, Xerox Individualized Publishing, 1976, pp. 385-396.

10. Hattersley, B; and Hume-Rothery, W: Constitution of Certain Austenitic Steels. JISI, vol. 204, 1966.

11. Taylor, A., and Floyd, R.W.: The Constitution of Nickel Rich Alloys of the Nickel-Chromium-Aluminum System. J. Inst. Met., vol. 81, 1952-53, pp. 451-464.

12. Taylor, A.: Constitution of Nickel-Rich Quaternary Alloys of the Ni-Cr-Ti-Al System. TMS-AIME, vol. 206, 1956, pp. 1356-1362.

13. Bradley, A.J.: Microscopical Studies on the Iron-Nickel-Aluminum System. JISI, vol. 163, 1949, pp. 19-30.

14. Felten, E. J.; Strangman, T. E.; and Ulion, N. E.: Coatings for Directional Eutectics. NASA CR-134735, 1974.

15. Jackson, M. R.; Rairden, J. R.; and Hampton, L. V.: Coatings for Directional Eutectics. NASA CR-134665, 1974.

16. Grisaffe, S. J.: Coatings and Protection. The Superalloys. C. T. Sims and W. C. Hagel, eds., John Wiley & Sons, Inc., New York, New York, 1972.

17. Jackson, M. R.: The Ni-Cr-Al-Fe (γ-β) Eutectic System. Prodeedings of the Second Conference on In-Situ Composites, Xerox Individualized Publishing, 1976, pp. 67-75.

18. Budberg, P. B.: Study of Alloys of the Ternary System Nickel-Aluminum-Tungsten. Russian Journal of Inorganic Chemistry, vol. 3, no. 3, 1958, pp. 206-213.

19. Kaufman, L.; and Nesor, H.: Calculation of the Ni-Al-W, Ni-Al-Hf and Ni-Hf Systems. Can. Met. Quart., vol. 14, no. 3, 1975, pp. 221-232.

20. Ciccarelli, M. F.: Quan - A Computer Program for Quantitative X-ray Fluorescense Analysis. 77CRD060, General Electric Co., 1977.

21. Giggins, C. S.; Kear, B. H.; Pettit, F. S.; and Tien, J. K.: Factors Affecting Adhesion of Oxide Scales on Alloys. Met. Trans., vol. 5, 1974, pp. 1685-1688.

22. Kubaschewski, O.; and Schneider, A.: Measurements of the Oxidation Resistance of High Melting-Point Alloys. J. Inst. Met., vol. 75, 1948-49, pp. 403, 416.

23. Kubaschewski, O.; and Speidel, H.: Oxidation-Resistance and some Phase Relationships in the System Chromium-Tantalum-Nickel. J. Inst. Met., vol. 75, 1948-49, pp. 417-430.

24. Jaffrey, D.; and Marich, S.: An Fe-Cr-Nb Pseudobinary Eutectic Alloy. Met. Trans., vol. 3, 1972, pp. 551-558.

25. Elliott, R. P.: Constitution of Binary Alloys, First Supplement. McGraw-Hill, New York, p 965.

26. Bibring, H.; Rabinovich, M.; and Seibel, G.: Composites refractaires a fibres, réalisés par cristallisation orientée dans les système Co-Cr-Ta-C et Ni-Cr-Ta-C. C. R. Acad. Sci. Paris, C, vol. 268, pp. 1666-1669.

27. Walter, J.L.; and Cline, H.E.: Structures and Properties of Cobalt Base-TaC Eutectic Alloys. Met. Trans., vol. 4, 1973, pp. 1775-1784.

28. Benz, M.G. et al.: Exploratory Development for Synthesis and Evaluation of Directionally Solidified Composites for High Temperature Application. AFML-TR-73-213, 1973.

29. Trottier, J.P.; et al.: Improvement in the Stress-Rupture Strength of Directionally Solidified COTAC-Type Composites Through Carbide Precipitation. Cobalt, no. 3, 1974, pp. 54-61.

30. Walter, J.L; and Cline, H.E.: The Effect of Solidification Rate on the Structure and High Temperature Strength of the Eutectic NiAl-Cr. Met. Trans., vol. 1, 1970, pp. 1221-1229.

31. Cline, H.E.; and Walter, J.L.: The Effect of Alloy Additions on the Rod-Plate Transition in the Eutectic NiAl-Cr. Met. Trans., vol. 1, 1970, pp. 2907-2917.

32. Walter, J.L.; and Cline, H.E.: Stability of the Directionally Solidified Eutectics NiAl-Cr and NiAl-Mo. Met. Trans., vol. 4, 1973, pp. 33-38.

33. Lemkey, F.D.: Eutectic Superalloys Strengthened by δ, Ni_3Cb Lamellae and γ', Ni_3Al Precipitates. NASA CR-2278, 1973.

34. Lemkey, F.D.; and McCarthy, G.: Quarternary and Quinary Modifications of Eutectic Superalloys Strengthened by δ, Ni_3Cb Lamellae and γ', Ni_3Al Precipitates. NASA CR-134678, 1975.

35. Sheffler, K.D.; Barkalow, R.H.; Jackson, J.J.; and Yuen, A.: Alloy and Structural Optimization of a Directionally Solidified Lamellar Alloy. NASA CR-135000, 1976.